博士論文

Dynamic subcellular compartmentalization of the piRNA pathway in silkworm cells

（カイコ培養細胞におけるpiRNA経路の動的な細胞内区画化）

鍾　沛原

Table of Contents

1. Introduction

1.1. Transposons in metazoan germ line

In eukaryotes, genetic information that supports life is stored in the nucleus as a form of deoxyribonucleic acid (DNA). This set of DNA, called the genome, harbors genes that instruct the cell to produce functional biomolecules which make up the cells themselves and eventually our bodies. First proposed by Francis Crick, it is now universally accepted that information stored on a gene is first transcribed into ribonucleic acid (RNA), RNA then instructs the cell to synthesize proteins. However, sequencing of the human genome revealed that only 2% of our genome code for all the essential proteins we needed for our body (Lander *et al*, 2001). Strikingly, almost half of the remaining human genome is made up of repetitive genes named transposable elements (TEs) or, in short, transposons.

Transposons are gene elements that can duplicate and translocate to a new genomic position spontaneously. These genes are sometimes called "jumping genes" and are highly abundant in the eukaryotic genome. For instance, class I transposons (retrotransposons) make up around 42% of the human genome (Lander *et al*, 2001). It is known that specific proteins like reverse transcriptase and transposases are required for the translocation of various transposons. Same as virtually all other proteins, these transposon-related proteins are translated from RNA, which is transcribed from the transposon genes. An actively translocating transposon is a potential threat to the genome, as it may randomly "jump" into genes that have vital functions, causing mutations and eventually could lead to cell death. Therefore, most harmful transposons are kept inactivated throughout the cell life (Slotkin & Martienssen, 2007).

Unlike all other cells in our body, germ cells are specialized cells that differentiate into gametes that form zygotes upon fertilization. As a result, any gene mutation in germ cells can be easily transmitted to the next generation and causes deleterious consequences. This leads to the evolution of a robust molecular machinery that identify and suppress transposons in germ cells. In metazoan, PIWI-interacting RNAs (piRNAs) represents one of the central components that survey and suppress transposon activity. These germline-specific small RNAs are conserved across the animal kingdom and are crucial to the proper development of germ cells, hence allow the development of an embryo (Malone & Hannon, 2009; Khurana & Theurkauf, 2010; Weick & Miska, 2014).

1.2. piRNA and transposon silencing

piRNAs are ~ 24 to 31-nt small RNAs that are bound by PIWI proteins, a subfamily that belongs to the Argonaute protein family. Similar to the other members in the Argonaute family, PIWI proteins are highly conserved endoribonucleases that consist of 4 domains, known as N, PAZ, MID, and PIWI **(Figure 1-1)**. The PAZ domain and the interface between MID and PIWI domains bind 3′- and 5′-end of the small RNA respectively, resulting in a ribonucleoprotein complex known as the RNA-induced silencing complex, or RISC. The small RNA, now called guide RNA, can search and bind RNAs that bear target sites complementary to its sequence. Subsequent to the successful RNA-RNA pairing, the target RNA is then cleaved by the Mg^{2+}-dependent RNAase H-like catalytic tetrad located in the PIWI domain **(Figure 1-1)** (reviewed in Tolia & Joshua-Tor, 2007; Hutvagner & Simard, 2008). It is of note that some PIWI proteins like Piwi in fruit flies have lost their RNA cleavage activity as evolution proceeds. Instead, these PIWIs are often found located in nuclei, where they target and silence genes via DNA methylation at the epigenetic level (reviewed in Ishizu *et al*, 2012).

Long before the discovery of piRNA in 2006, PIWI subfamily proteins have been identified as essential germ cell factors during some genetic screenings for development defects (Wilson *et al*, 1996; Lin & Spradling, 1997; Williams & Rubin, 2002). After the discovery of piRNA in 2006, the indispensable role of PIWI and piRNAs in transposon silencing has been finally uncovered. (Kalmykova *et al*, 2005; Aravin *et al*, 2006; Grivna *et al*, 2006; Lau *et al*, 2006; Saito *et al*, 2006; Vagin *et al*, 2006; Watanabe *et al*, 2006). Remarkably, the majority of piRNAs were found to be mapped on transposon genes, which suggest that transposons are the primary target of piRNAs (Aravin *et al*, 2006; Saito *et al*, 2006; Vagin *et al*, 2006; Watanabe *et al*, 2006). Depletion of PIWI

proteins or piRNAs has a profound effect on germ cell development, which is caused by the genome-wide de-repression of transposons (Carmell *et al*, 2007; Das *et al*, 2008; Houwing *et al*, 2008). To conclude, piRNA and PIWI proteins work together to assert repression stress on transposon and hence maintain the genome integrity in germ cells.

(a)

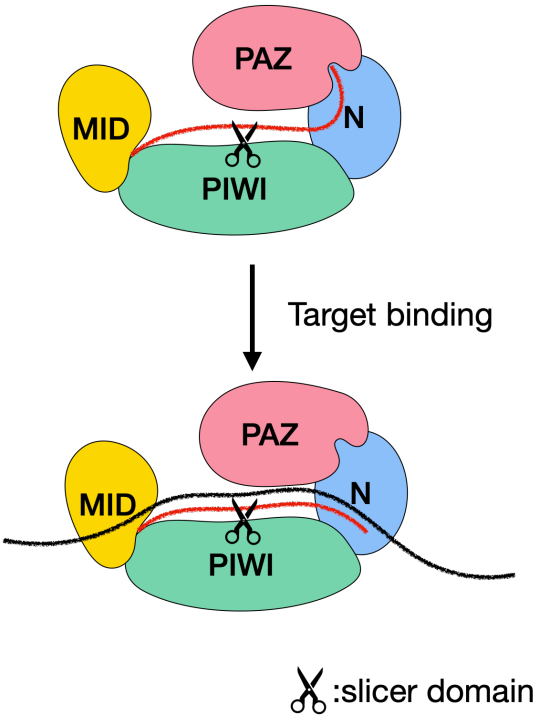

(b)

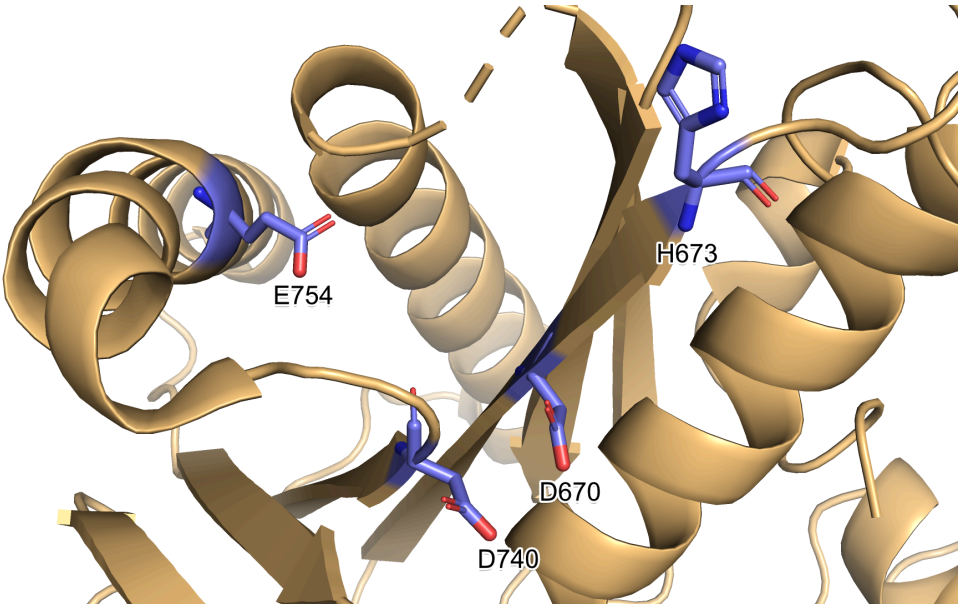

Figure 1-1. Structure of Siwi-RISC
(a) Schematic diagram showing the structure of a Siwi-RISC. The Siwi-bound piRNA, showing as a red line, is bound to MID-PIWI 5′ pocket and PAZ 3′ pocket. Target RNA is shown as a black line.
(b) Detailed structure of the slicer catalytic tetrad in PIWI domain (PDB: 5GUH). D740, E754, D670 and H673 forms the DEDH catalytic tetrad that cleaves target RNA complementary to piRNA.

1.3. Biogenesis of piRNAs

Since the discovery of piRNAs, researchers have been spending efforts on solving the mystery of piRNA biogenesis. While the detailed mechanism alters between species, early day studies using *Drosophila* ovaries as a piRNA model had led to the elucidation of two distinct piRNA biogenesis pathways. In the first pathway, also known as the primary pathway, piRNA precursor transcripts are directly transcribed from specific gene loci named piRNA clusters (Brennecke *et al*, 2007; Vagin *et al*, 2006). These piRNA clusters consist of truncated transposons sequences and can be either uni- or bidirectionally transcribed into long RNAs, which are then subsequently processed into shorter piRNAs. For bidirectionally transcribed piRNA clusters in *Drosophila*, a protein complex called Rhi-Deadlock-Cutoff complex (RDC complex) was reported to recognize and enable the precursor RNA to bypass canonical splicing (Klattenhoff *et al*, 2009; Pane *et al*, 2011; Mohn *et al*, 2014). After exiting the nucleus, the long precursor RNA will then be processed by the mitochondrial-anchored endonuclease Zucchini (Zuc) into shorter piRNAs (Szakmary *et al*, 2009; Saito *et al*, 2010; Nishimasu *et al*, 2012; Ipsaro *et al*, 2012), and subsequently processed by the methyltransferase Hen1, which add a methyl group to the 3′-end of the piRNA (2′-*O*-methylation) (Han *et al*, 2015; Mohn *et al*, 2015). This piRNA is now called mature piRNA and is ready to be bound by the PIWI protein **(Figure 1-2)**.

The secondary pathway, also known as the ping-pong cycle, is an amplification pathway vastly different from the primary pathway. In the ping-pong cycle, once the target RNA is cleaved by a PIWI protein, the 3′ cleavage product is retained inside the RISC and protected by other piRNA factors. These factors then transfer the 3′ cleavage product, which is now a precursor piRNA, to another “empty” PIWI protein, forming a pre-RISC (Brennecke *et al*, 2007; Gunawardane *et al*,

2007). The precursor piRNA will then be shortened by Zucchini or by an exonuclease named Trimmer (Izumi *et al*, 2016; Tang *et al*, 2016; Ding *et al*, 2017; Zhang *et al*, 2017; Nishimura *et al*, 2018). This forms a new mature piRNA that is antisense and partially complementary (up to the cleavage site; ten base pairs) to the original piRNA. The antisense piRNA then undergoes the same fate as its counterpart, closing up the cycle and generates more sense piRNAs (Brennecke *et al*, 2007; Gunawardane *et al*, 2007) **(Figure 1-2)**. In *Drosophila*, ping-pong piRNAs that are loaded into Aubergine (Aub) have a strong preference for uracil at their 5′-end nucleotide (Brennecke *et al*, 2007; Gunawardane *et al*, 2007). In contrast, the 10th nucleotide of piRNAs loaded into Argonaute-3 (Ago3), which is complementary to the 1st nucleotide in Aub piRNA, has a bias for adenine (Brennecke *et al*, 2007; Gunawardane *et al*, 2007). Ping-pong cycle and the hallmarks for ping-pong piRNAs are widely conserved in most, if not all, animals, including mice (Aravin *et al*, 2008; Fazio *et al*, 2011), zebrafishs (Houwing *et al*, 2007), and silkworms (Kawaoka *et al*, 2009). It has been believed that this feed-forward mechanism is responsible to generate most of the piRNA in some of these organisms, thus counteracting the exponential proliferation of active transposons (Siomi *et al*, 2011; Czech & Hannon, 2016; Ozata *et al*, 2019).

Notably, a recent study proposed a new "unified" model for primary and secondary piRNA pathways (Gainetdinov *et al*, 2018) **(Figure 1-3)**. In 2015, two groups reported that phased piRNA production, which was previously believed to be independent of the ping-pong cycle, can be initiated by ping-pong piRNAs (Han *et al*, 2015; Mohn *et al*, 2015). In the ping-pong cycle, the PIWI-cleaved RNA fragment will be handed to the counterpart PIWI for amplification of piRNAs. In the new model, the loading of this fragment triggered the production of phased (primary) piRNAs directly downstream of the putative ping-pong piRNA by positioning an endonuclease

downstream of the RISC that bound to the 3′ cleavage product (Han *et al*, 2015; Mohn *et al*, 2015; Gainetdinov *et al*, 2018). This allows the endonuclease to cleave the precursor transcript right before a uridine residue, which will create the 3′-end of the upstream piRNA precursor and generate the 5′-end of the downstream piRNA simultaneously. The choice of this endonuclease could vary between species, wherein silkworm it was found that both the PIWIs and Zucchini are responsible for the cut, depending on the sequence context (Izumi *et al*, 2020). The new model makes sense as PIWI proteins localize to a specialized membrane-less ribonucleoprotein (RNP) condensate called nuage, which has been reported to frequently contacts mitochondria (Mahowald, 1962, 1968).

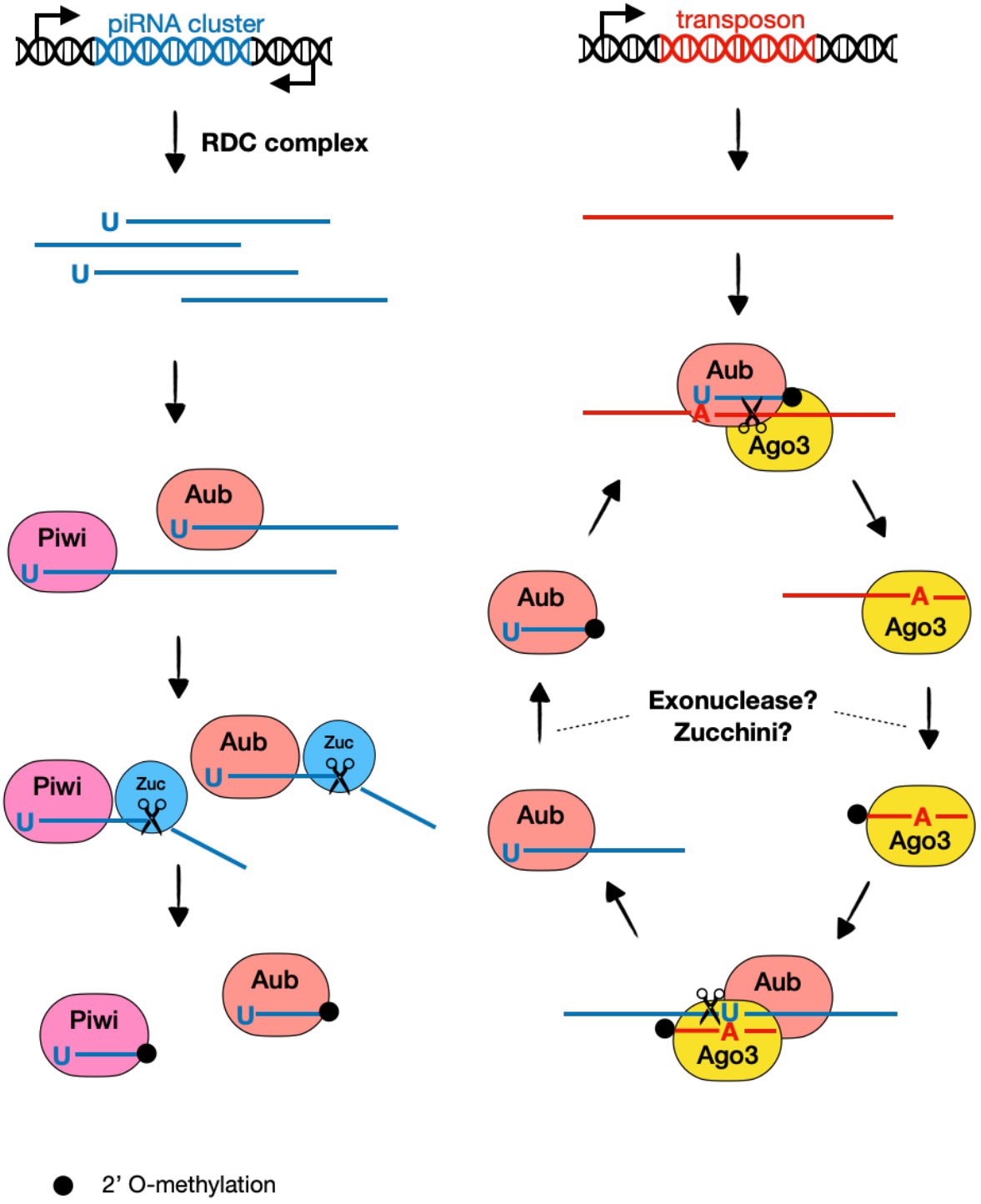

Figure 1-2. General model of piRNA biogenesis pathways in *D. Melanogaster*
piRNA cluster driven by endogenous promoters generates antisense piRNAs that are specifically loaded into empty Piwi and Aub. In secondary piRNA biogenesis, or ping-pong cycle, Aub cleaves transposon RNA and Ago3 cleaves antisense transcript by their slicer catalytic domains. Their cleavage products are loaded to corresponding partners and processed into mature piRNAs, coupling piRNA amplification to transposon silencing.

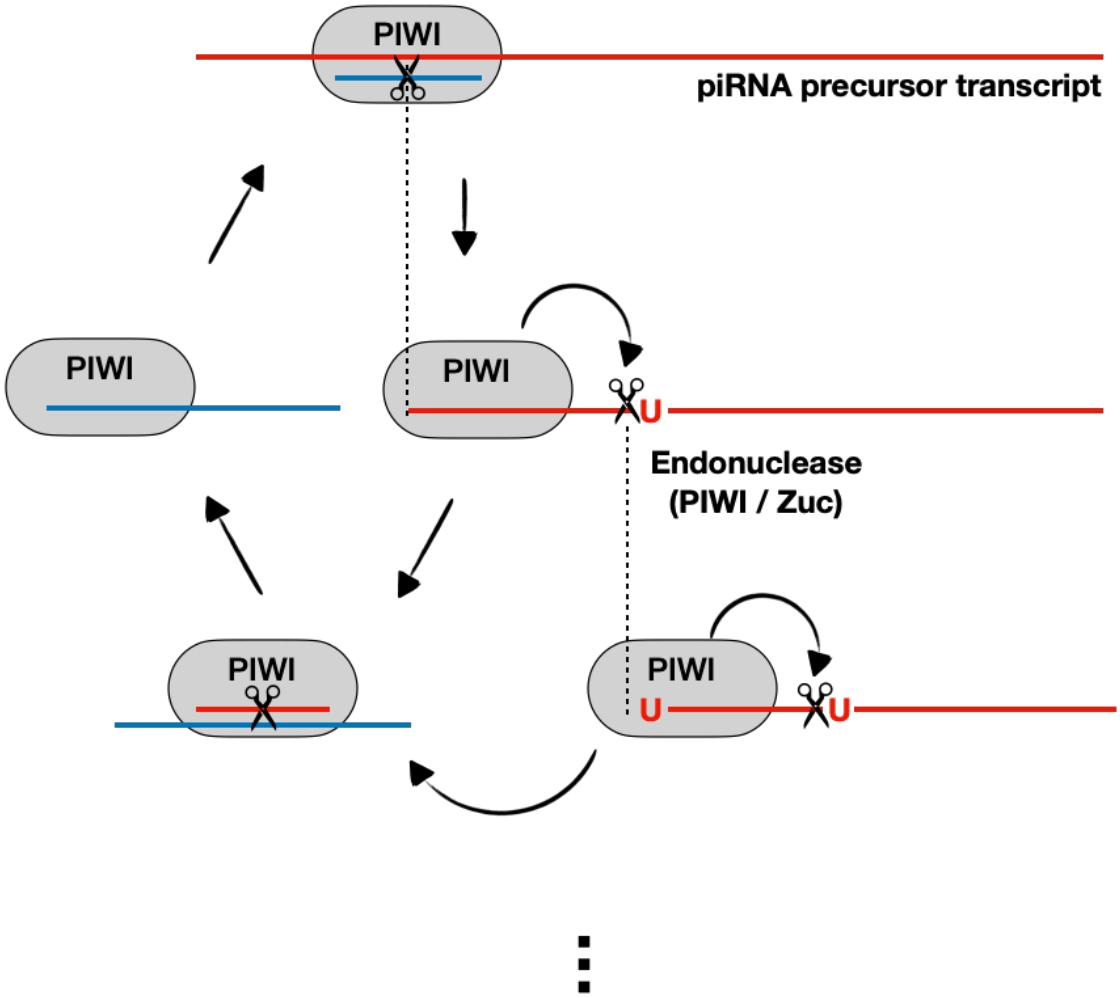

Figure 1-3. A unified model for piRNA biogenesis
Proposed by Gainetdinov et al in 2018, the new model demonstrated the ability of a secondary piRNA to trigger production of phased piRNA downstream via positioning a endonuclease, likely Zucchini or PIWIs. This unified the two current models and explained the variation of piRNA biogenesis in different species.

1.4. Germ granules and piRNA pathway

Nuage, the aforementioned membrane-less RNP condensates, is a subcategory of germ granules. Germ granules are electron-dense granules found specifically in germ cells and are conserved in over 80 metazoans investigated (Hegner, 1912; Huettner, 1923; Rabinowitz, 1941; Eddy, 1975). Early attempts to characterize germ plasm granules provided valuable information on their size, architecture, localization, rich RNA contents, and mitochondrial attachment in *Drosophila melanogaster* late-stage oocytes and early embryos (Counce, 1963; Mahowald, 1962, 1968, 1971). In mid 1980s, groups of researchers identified several essential genes, namely *oskar*, *vasa*, *tudor*, *staufen* and *valois*, encode proteins that reside in germ granules at the posterior pole of *Drosophila* embryo and developing oocytes (Boswell & Mahowald, 1985; Lehmann & Nüsslein-Volhard, 1986; Nüsslein-Volhard *et al*, 1987). Soon, the gene *vasa* was identified to encode an ATP-dependent DEAD-box RNA helicase, which was found to be the antigen of a well-established germ polar granule specific antibody (Lasko & Ashburner, 1988; Hay *et al*, 1988b). Following this discovery, perinuclear nuage in *Drosophila* nurse cells were identified to contain Vasa. Nuage was therefore considered the precursor of germ granules that accumulated at the anterior germ plasm (Mahowald, 1971; Hay *et al*, 1988a; Liang *et al*, 1994). Later studies, however, argued against the precursor theory and suggested that nuage functions in post-transcriptional gene silencing instead (Snee & Macdonald, 2004).

The *Drosophila* PIWI *Aub* and *Piwi* were first identified in the late 1990s as genes that are essential for germline development, and later as core nuage factors (Lin & Spradling, 1997; Harris & Macdonald, 2001). The molecular function of PIWI proteins has remained elusive until the discovery of piRNAs in 2006. Since then, other nuage components including Maelstorm, Krimper,

and Spindle-E were quickly identified as essential factors to produce this new class of small RNAs as well (Lim & Kai, 2007). Furthermore, it has been well-documented that nuage and its derivative germ granules are often found in contact with the mitochondrial outer surface (Mahowald, 1962, 1968). Subsequent studies also confirmed the involvement of mitochondrial surface proteins in piRNA biogenesis in flies (Pane *et al*, 2007; Ipsaro *et al*, 2012; Nishimasu *et al*, 2012; Handler *et al*, 2013), in mice (Ma *et al*, 2009; Watanabe *et al*, 2011; Shiromoto *et al*, 2013; Nishimura *et al*, 2018), and in silkworms (Liu *et al*, 2011; Honda *et al*, 2013; Izumi *et al*, 2016, 2020). These studies together point to a cooperative relationship between nuage components and outer mitochondrial surface proteins in piRNA biogenesis. Examples include the previously mentioned Trimmer and Zucchini nucleases, Tudor domain protein Papi (Liu *et al*, 2011; Izumi *et al*, 2016), and RNA helicase Armitage (explained in chapter 1.6).

To summarize, nuage is a subtype of germ granule that locates in the perinuclear region, physically contacting with mitochondria, and harbors piRNA factors as well as transposon RNAs. How nuage is assembled is currently unclear, but there is an emerging focus on a process named phase separation, which might provide the answer to parts of the question.

1.5. Phase separation and germ granules

A study published in 2009 described the *C. elegans* P-granule as "liquid-like", as these granules display liquid-like physical characteristics like fusion, dripping and wetting (Brangwynne *et al*, 2009). This has sparked great interest in a process called "liquid-liquid phase separation", or LLPS in short, as it potentially underlies the assembly mechanism of membrane-less condensates. LLPS is a common process that can be found in our daily life (for example, oil droplets separating from water is a form of LLPS). By definition, LLPS describes the process of a homogenous liquid demix into two liquid phases, but in biological scenarios, the separation happens between liquid-like substances that consist of the cytosol and biomolecules, such as low-complexity protein domains and RNAs. Similar to *in vitro* LLPS droplets, membrane-less condensates are mostly spherical, readily fuse together and have a high molecule exchange rate as suggested by photobleaching experiments (Brangwynne *et al*, 2009; Sheth *et al*, 2010). Remarkably, key factors of germ granule formation were found to form phase-separated condensates *in vitro* and in Hela cells when ectopically expressed (Nott *et al*, 2015). All these properties suggested a role of LLPS in membrane-less condensate formation, which creates a new field in cell biology and kick-started an intense investigation into the molecular mechanism that underlies LLPS *in vivo*.

The formation and properties of LLPS condensates are highly sensitive to environmental factors such as temperature, pH and concentration of molecules that facilitate condensation (reviewed in Dodson & Kennedy, 2020). In cells, LLPS is also proposed to be regulated by an array of biomolecules, with the list starting with intrinsically disordered proteins (Molliex *et al*, 2015; Nott *et al*, 2015; Elbaum-Garfinkle *et al*, 2015; Burke *et al*, 2015), RNA (Molliex *et al*, 2015; Elbaum-Garfinkle *et al*, 2015; Zhang *et al*, 2015) and post-translational modifications

(Wang *et al*, 2014; Nott *et al*, 2015). For instance, human DDX4 (homolog of *Drosophila* Vasa gene, a core nuage helicase and a piRNA factor) contains an N-terminal disordered domain, in which the purified form of this domain can nucleate LLPS condensation *in vitro* on its own (Nott *et al*, 2015). Of note, the region contains stretches of amino acid repeats (RGG motif, in particular) that are both involved in RNA interaction and post-translational modification, or arginine methylation, to be specific. Arginine methylation at RGG motifs caused destabilization of the DDX4 condensates (Nott *et al*, 2015), which is intriguing because many piRNA factors are Tudor-domain containing proteins, and the Tudor domain specifically recognizes symmetrical dimethylated arginine (sDMA) sites (Kirino *et al*, 2009; Nishida *et al*, 2009; Vagin *et al*, 2009; Reuter *et al*, 2009; Chen *et al*, 2009; Wang *et al*, 2009; Honda *et al*, 2013). This suggested a complex interplay between traditional protein-protein interaction (PPI) and the regulatory mechanism of phase separation in the event of nuage assembly.

To make matters more complicated, DDX4 itself is an RNA helicase that engages in RNA remodeling. BmVasa (silkworm homolog of DDX4) is reported to release cleaved target RNA from Siwi, one of the silkworm PIWI proteins (Xiol *et al*, 2014; Nishida *et al*, 2015). The changes in RNA local concentration, RNA length and RNA secondary structures may further affect the LLPS process that was proposed to underlie nuage assembly. It is therefore not surprising that germ granules alter their physical properties, composition, and localization along the cascade of developmental events, where switching of transcriptional activity constantly happens.

1.6. Subcellular spatial regulations of piRNA biogenesis

piRNA factors are tightly regulated for their localization and translocation between nuage and mitochondrial surface for their proper functions. The regulation is a result of an orchestrated protein-protein or protein-RNA interactions by some highly conserved protein domains, such as Tudor domains and RNA helicases. At a larger scale, piRNA factors could possibly transit through compartments, hinting at the existence of an organelle-level regulatory system. Here is a brief introduction of the key mechanisms that have been reported to regulate subcellular localization and functions of piRNA factors.

(i) Tudor-domain proteins

Germ granule assembly in *Drosophila* requires a gene named *tud*. It was found to encode an ~280 kDa protein with 11 repeating motifs, and thus give the name Tudor to these motifs (Boswell & Mahowald, 1985). Tudor motif is around 60 residues long and is found in more than 200 proteins in eukaryotes, where 10 of 26 in mice were assigned as the Tud-domain containing (TDRD) family (reviewed in Siomi *et al*, 2010). These proteins and their homologs in piRNA model animals are commonly found to be required for germ granule assembly and piRNA biosynthesis. Examples include TDRD5, TDRD7, Qin/Kumo (with 5 Tudor domains) and SpnE (with 1 Tudor domain). Tudor has a β-barrel like structure with 4 β-strands and 1 α-helix, which possess the ability to bind specifically to sDMA (symmetric dimethyl arginine) residues in proteins (reviewed in Lasko, 2010). Consistent with the biological significance of Tdrd family proteins in the piRNA biogenesis, abolishing their interaction with PIWIs through sDMA site mutation, TDRD proteins or PRMT5 (a methyltransferase responsible for generating sDMA) depletion impairs PIWI localization and piRNA biogenesis in flies (Kirino *et al*, 2009; Nishida *et al*, 2009),

mice (Vagin *et al*, 2009; Reuter *et al*, 2009; Chen *et al*, 2009; Wang *et al*, 2009) and silkworms (Honda *et al*, 2013). In addition, Vasa homologs in african clawed frogs and mice were also reported to contain N-terminal sDMA sites, which are required for their interactions with TDRD proteins and/or PIWIs (Kirino *et al*, 2010). It is therefore believed that Tudor-sDMA association is responsible for nuage assembly and is required for proper biogenesis of piRNAs. How Tudor family proteins attain their specificity towards PIWIs among numerous sDMA modified proteins remains to be investigated.

(ii) RNA helicases

Originally reported by Xiol et al in 2014, an ATPase mutant of silkworm Vasa homolog BmVasa was shown to accumulate a multiprotein complex called Amplifier complex with two silkworm PIWI proteins Siwi (homolog of Aub), BmAgo3 (homolog of Ago3) and BmQin (Homolog of Qin/Kumo) in silkworm ovary derived BmN4 cells (Xiol *et al*, 2014). The group generated the mutant by substituting only one single amino acid conserved in D-E-A-D consensus (at motif II) into D-Q-A-D, and by resolving its crystal structure they found that the mutation abolished ADP-Pi and RNA release. The mutant, named $Vasa^{DQAD}$, forms a large aggregate with the mutant binding to sense transposon RNA, suggesting that Vasa ATPase activity facilitates piRNA precursor handover from Siwi to BmAgo3 during the ping-pong cycle (Xiol *et al*, 2014). Proteins that reside in the aggregate lost their molecular dynamics, most likely due to the irreversible binding of RNA. Based on these results, the group proposed a model with ATP-bound Vasa helicase domains acting as the scaffold for Ping-pong proteins (Xiol *et al*, 2014). The study represents the first attempt to capture the rapid and volatile function of an RNA helicase at the subcellular level and demonstrated the central roles of RNA helicases in piRNA biology.

Recently, another RNA helicase named Armitage was reported to connect piRNA production on mitochondria surface to piRNA biogenesis in *Drosophila* nuage (Ge *et al*, 2019; Ishizu *et al*, 2019). Armitage is an ATP-dependent 5′-to-3′ helicase required for mRNA silencing (Tomari *et al*, 2004; Cook *et al*, 2004) and for the production of primary piRNA (Saito *et al*, 2010; Haase *et al*, 2010; Olivieri *et al*, 2010). It was found that Armitage localizes to both nuage and mitochondria (Ge *et al*, 2019), in which the helicase utilizes ATP to selectively bind pre-piRNA precursors (pre-pre-piRNAs) (Ge *et al*, 2019; Ishizu *et al*, 2019). Given that Zucchini-dependent piRNA production happens on the mitochondrial surface, it is therefore believed that Armitage escorts the pre-pre-piRNAs from nuage (or Yb body in *Drosophila* ovarian somatic cells) to mitochondria outer membrane (Ge *et al*, 2019; Ishizu *et al*, 2019). The discovery of piRNA material exchange between compartments is profound, but Armitage likely represents one among the many undiscovered routes of how nuage communicates with the mitochondria outer membrane and beyond.

(iii) Subcellular compartmentalization at the organelle level

In addition to the nuage-mitochondria compartmentalization, there is an early report suggested that multiple species of nuage derivative could co-exist in a single cell, where these compartments may regulate piRNA biogenesis by physically separating key biochemical reactions. It was found that in mouse gonocytes, in addition to pi-body (also known as intermitochondrial cement; nuage-equivalent RNP granule), an additional perinuclear granule named piP-body contains piRNA factors (Aravin *et al*, 2009). The two granules were found to frequently contacting with each other but seldom overlap **(Figure 1-4)**. While both granules contain MVH, the mouse

Vasa homolog, each of them accommodates a distinct mouse PIWI protein, accompanied by a set of their specific interacting factors. Strikingly, piP-body was found to contain core Processing body (P-body) proteins involved in mRNA decay and miRNA pathways. P-body is a species of membrane-less RNP condensate that mostly consists of protein factors from the siRNA/microRNA pathways and mRNA decay pathways, including Dcp1/2 (mRNA Decapping enzyme), DDX6 (RNA helicase), AGO1/2 (Argonaute that binds miRNA or siRNA), XRN1 (exonuclease) etc. Recent reports suggested that instead of actively degrading mRNAs, P-bodies may function to store translationally-repressed mRNPs (Hubstenberger *et al*, 2017).

As proof of the functional linkage between the two granules, Aravin *et al* found that upon depletion of MAEL (Maelstrom homolog; piRNA factor localized in piP-body), both MILI (one of the three mouse PIWIs) localization in pi-body and the ping-pong amplification were both disrupted (Aravin *et al*, 2009). This suggested an organelle-level regulation of piRNA biogenesis, where piRNA factors actively sort themselves into two distinct granules for particular steps in the ping-pong cycle. Nevertheless, this pi-body/piP-body compartmentalization was only reported in mice but not in fruit flies, which greatly hindered efforts in resolving the biological significance of this process.

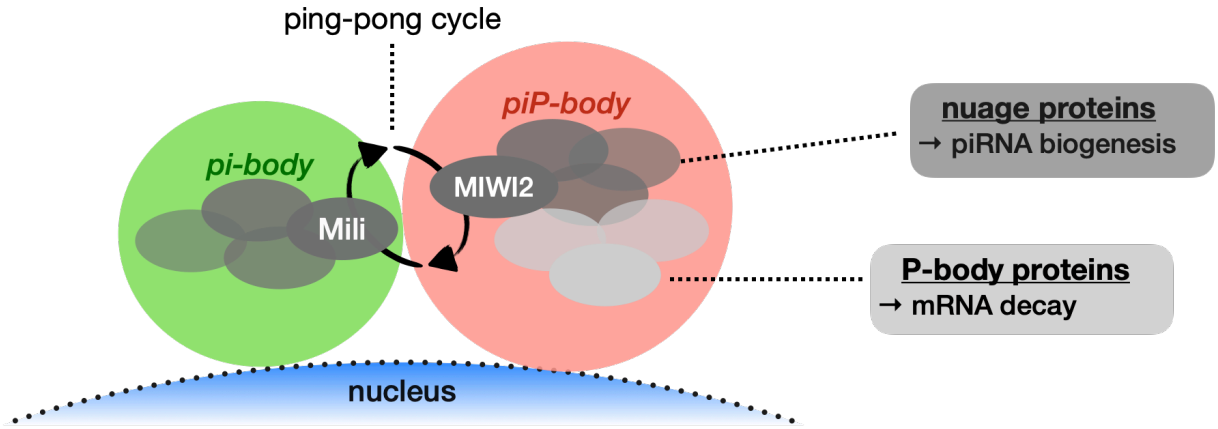

Figure 1-4. Subcellualar compartmentalization of the mouse piRNA pathway
In mouse gonocytes, perinuclear germ granules may include pi-body (where Mili resides) and piP-body (where MIWI2 and P-body proteins resides).The two granules were frequently contacting, while an active ping-pong cycle happening across the granules.

1.7. Research purpose and overview

Recent advances in small RNA biology have led to the discovery of piRNAs, PIWI proteins and a battery of piRNA factors. We now know that their orchestrated interactions at germline RNP granules are a prerequisite for transposon silencing and germline development. These orchestrated interactions result in the assembly of nuage, an RNP condensate widely regarded as the production site of piRNAs. It is however unclear how nuage assembly is regulated, especially in cases like mouse gonocytes where multiple nuage-like condensates co-exist. The distinct RNP contents and hierarchal organization of co-existing nuage-like condensates hinted the presence of a new layer of regulation on piRNA biogenesis at the organelle level, but it was largely unexplored.

Interestingly, a recent study revealed that in silkworm BmN4 cells, Siwi-complexes were divided into two distinct protein complexes, one contains BmVasa and the other contains BmSpnE. Given that these two RNA helicases excluded each other while actively participating in piRNA biogenesis, this partition is likely to have a role in maintaining piRNA biogenesis and harbor Siwi protein at different stages. Therefore, I set to study the contents of the two Siwi-complexes by characterizing the localization of prominent piRNA factors in BmN4 cells. By using live cultured cells and an epitope-tagged protein expression system that allows robust mutagenesis, I envisaged that this colocalization study will yield valuable insights on the functions of the key catalytic activities on protein localization, and hence the functional separation of the Siwi-complexes. In addition to the microscopy experiments, my study also included deep sequencing of piRNAs, which will enable in-depth analysis of the effect of mis-localized piRNA factors on the global piRNA profiles. This will help to solve the bigger question – the unknown function of the subcellular compartmentalization of the piRNA pathway.

In this thesis, I reported the colocalization relations between several known silkworm piRNA factors including Siwi, BmAgo3, BmVasa, BmSpnE and BmQin. For the first time, I confirmed the nuage/P-body subcellular compartmentalization in the silkworm piRNA pathway (Chung *et al*, 2021), which is largely distinct from fly oocytes but shared similarity with the case of mouse gonocytes. I also conducted a comprehensive investigation on the effect of piRNA factors depletion at the subcellular level, which uncovered the dependency of proper P-body localization of piRNA factors on the presence of nuage piRNA factors. I further explored the interplay between nuage and P-body by introducing catalytic mutants of piRNA factors to the cells, which disrupted the nuage/P-body partition of piRNA factors and thus enabled the analysis of small RNA profiles when piRNA factors were mislocalized. This revealed that when multiple piRNA factors were trapped in P-bodies, piRNA derived from self-mRNAs are promiscuously produced. These results together demonstrated that proper spatial regulation of piRNA factors by partitioning themselves into distinct granules is essential to preserve fidelity during piRNA biogenesis.

2. Results

2.1. Localization of silkworm piRNA factors

To examine the spatial regulations of silkworm piRNA factors, I first checked the subcellular localization of core piRNA biogenesis factors in BmN4 cells. These factors, including the two PIWIs (Siwi and BmAgo3), BmVasa, BmSpnE and BmQin were previously characterized by genetic and biochemistry methods as essential piRNA factors (Xiol *et al*, 2014; Nishida *et al*, 2015). In addition to these factors, BmDcp2 (a core P-body protein) was also included in this experiment to mark the P-bodies (Franks & Lykke-Andersen, 2008; Zhu *et al*, 2013). Recombinant fluorescence proteins (FPs) AcGFP and mCherry were cloned into the pIZ vectors and the open-reading frames (ORF) of the piRNA factors were subsequently inserted into the carboxy-terminal of fluorescence protein ORFs by removing the stop codons. These plasmids were then transfected to BmN4 cells and incubated for 4 days for the expression of FP-tagged piRNA factors, which were each driven by an OpIE2 baculovirus promoter. The transfected, living cells were then observed by deconvolution microscopy at day 4 post-transfection.

I found that FP-tagged BmVasa and BmAgo3 localized to spherical granules that restricted to the perinuclear region of the cytoplasm of BmN4 cells **(Figure 2-1-1)**, which share the same pattern with the immunofluorescence experiments performed directly on endogenous BmVasa and BmAgo3 previously (Nishida *et al*, 2015). FP-tagged Siwi showed a significantly dispersed localization at cytoplasm but were also accumulated in nuage-like granules **(Figure 2-1-1)**, which is concurrent with the previously reported localization pattern of endogenous Siwi (Nishida *et al*, 2015).

In contrast, FP-tagged BmDcp2 and BmQin were accumulated in cytoplasmic granules that were not restricted to the perinuclear region, but instead spread over the whole cytoplasm **(Figure 2-1-1)**. FP-tagged BmSpnE was largely dispersed but with a few puncta in the non-perinuclear part of the cytoplasm **(Figure 2-1-1)**. BmQin and BmSpnE were previously reported to form a distinct cytoplasmic focus which is independent of BmVasa-containing nuage, which could partly explain the non-perinuclear localization observed here. To further confirm these findings, colocalization experiments were performed and will be explained in the following chapter.

Live cell imaging also enables time lapse observation of foci. I found that BmVasa foci, which is commonly defined as nuage, were often highly mobile at the perinuclear region. While these foci do not move in a zigzag pattern – typical for free diffusing foci – it is not clear what kind of forces drove their displacement. Time-lapse observation further demonstrated the constant fusion and division of BmVasa foci, suggesting that they possess the characteristic of LLPS condensates and are highly dynamic **(Figure 2-1-2)**.

It was previously shown that when rescuing the *ago3* null mutant, slicer activity of Ago3 was required for nuage localization of Aub and nucleus localization of Piwi (Wang *et al*, 2015), suggesting that slicer activities not only cleave target RNA but may also regulate the localization of piRNA factors. To interrupt the slicer-regulated localization of piRNA factors, I generated slicer mutants of each PIWI by substituting their conserved aspartate residue at their slicer catalytic tetrad (D670A in Siwi and D697A in BmAgo3) to alanine, resulting in Siwi-D670A and BmAgo3-D697A. I then examined the localization of these mutants. Strikingly, Siwi-D670A mutant appeared to be less dispersed and more often found in non-perinuclear region than its wildtype

counterpart **(Figure 2-1-3)**. In contrast, BmAgo3-D697A displayed a similar localization pattern with wildtype BmAgo3 **(Figure 2-1-3)**. This suggested that the slicer activity of Siwi but not BmAgo3 is required for its correct subcellular localization.

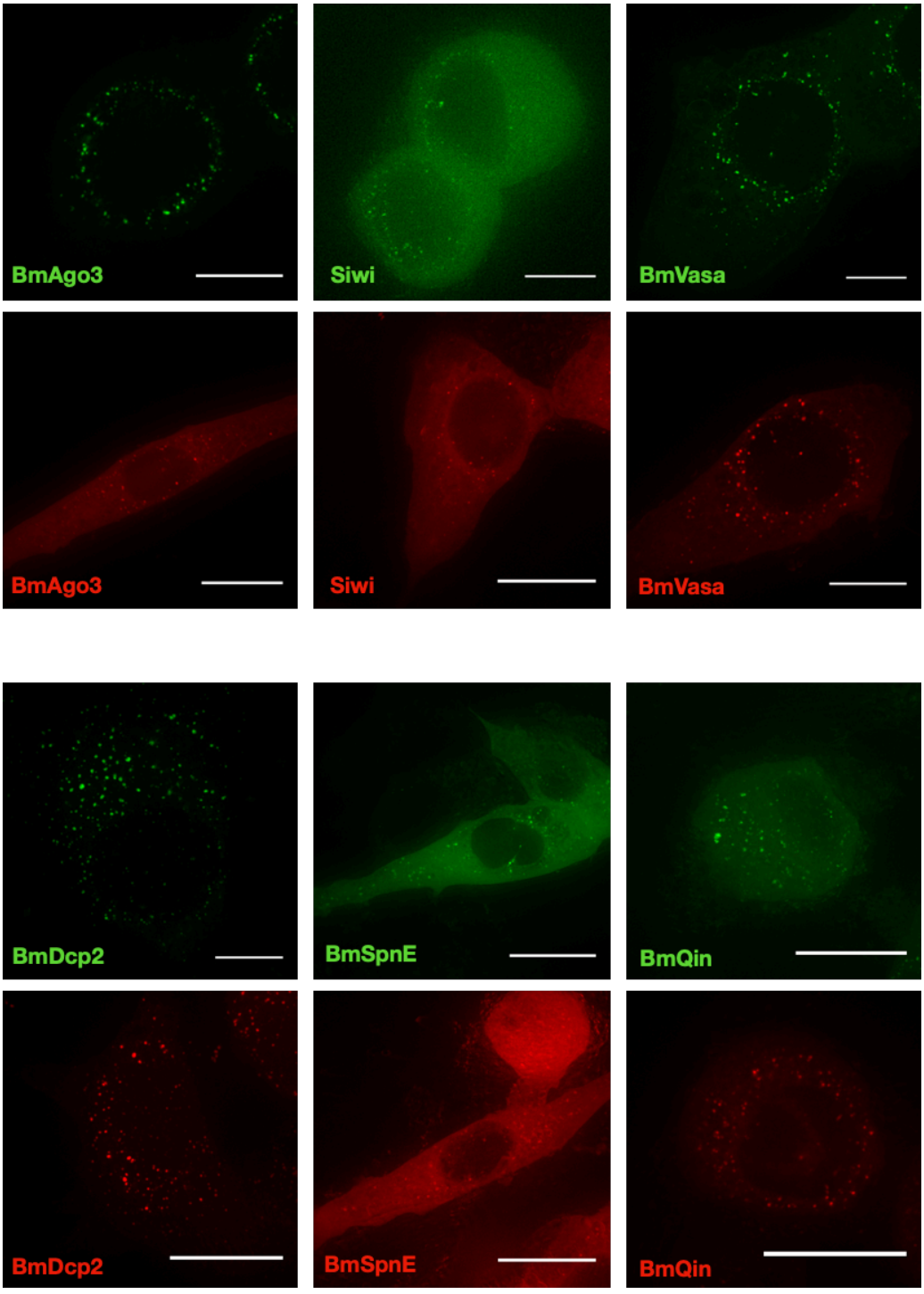

Figure 2-1-1. Subcellualar localization of FP-tagged piRNA factors and P-body marker
Deconvolution microscopy of BmN4 expressing FP-tagged piRNA factors (BmAgo3, Siwi, BmVasa, BmDcp2, BmSpnE) and P-body marker BmDcp2. Scale bar 10 μm.

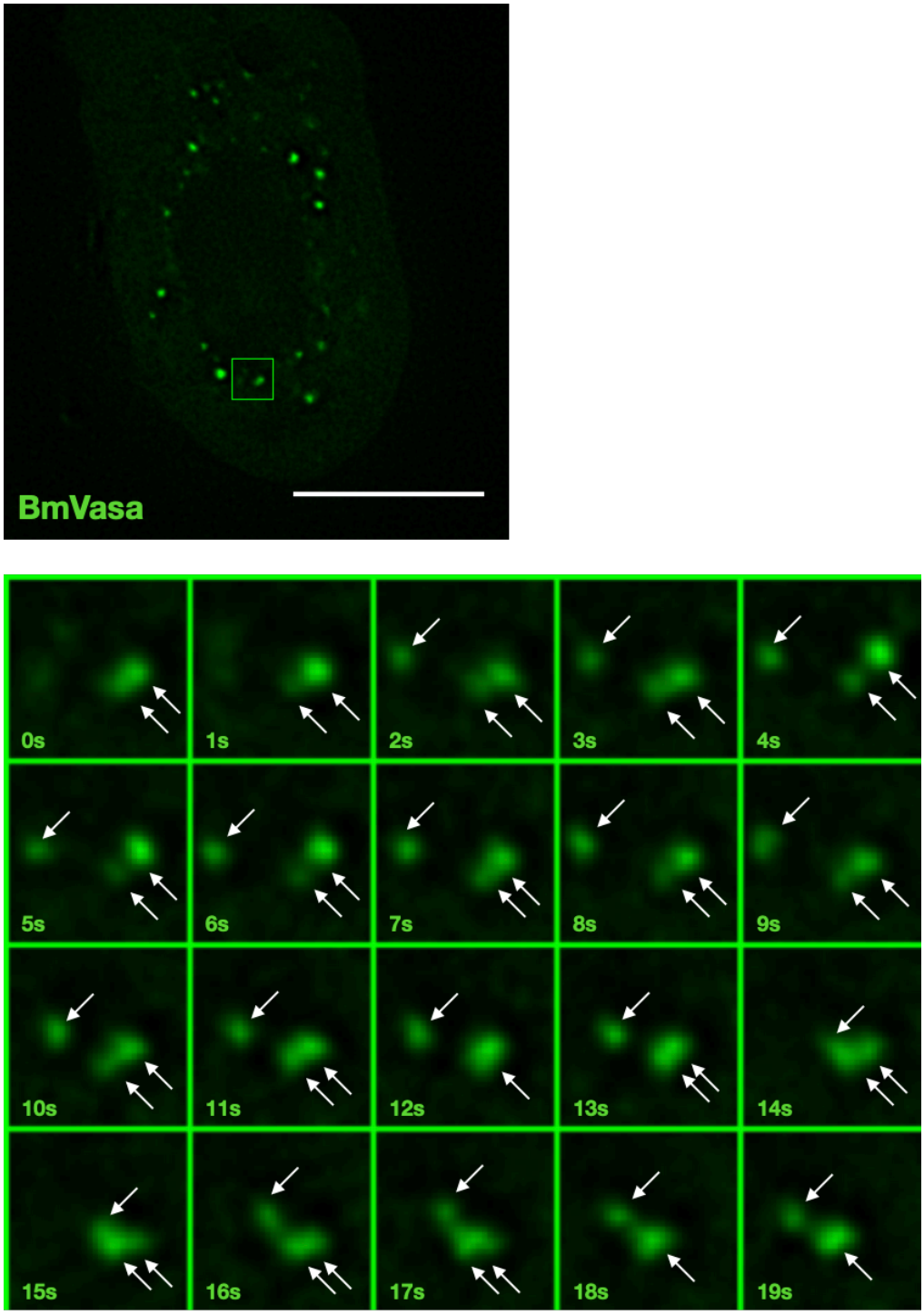

Figure 2-1-2. Fusion and division of BmVasa-containing nuage RNP granules
Time lapse by deconvolution microscopy of BmN4 expressing AcGFP-tagged BmVasa. BmVasa-containing nuage displayed liquid-like properties as they spontaneously fuse and divide. Upper panel shows the wide-field image and the lower panel showed the time lapse series for 20 frames (1 frame per second) in the green box marked. Time frame is marked at bottom-left corner of each frame. Scale bar 10 μm.

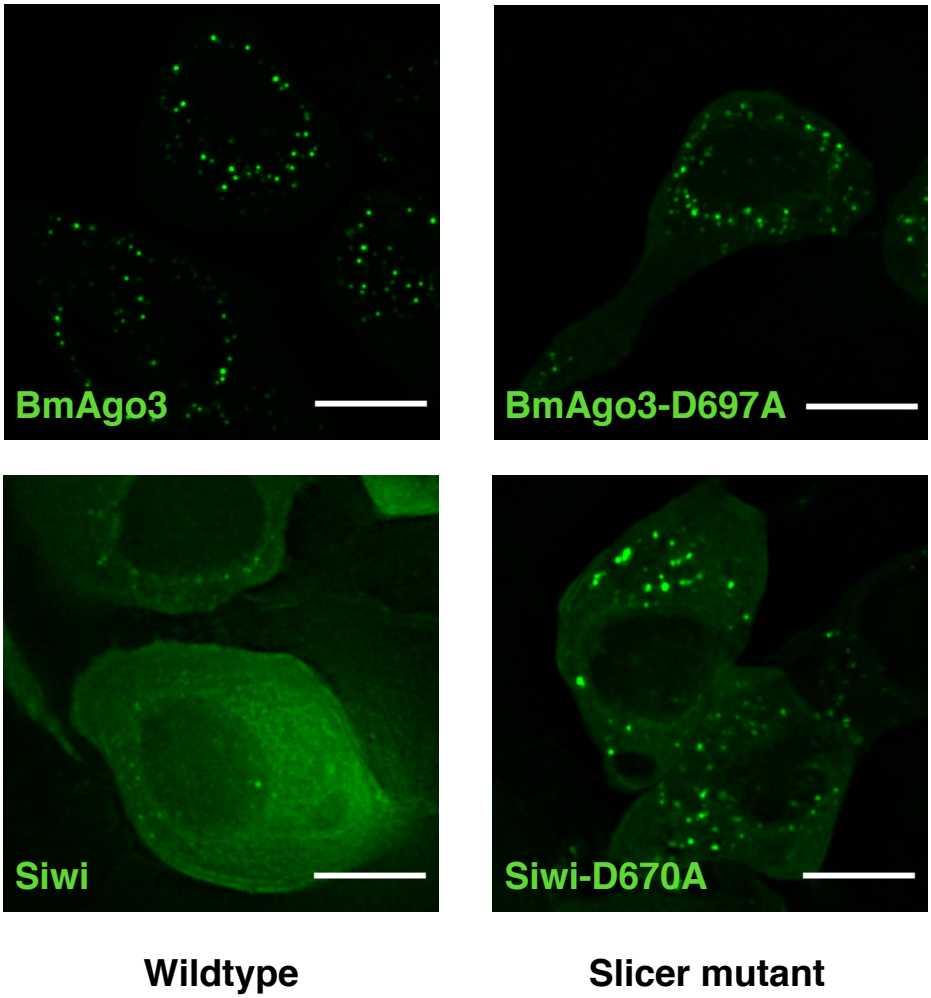

Figure 2-1-3. Subcellular localization of silkworm PIWIs and their slicer mutants in BmN4
Deconvolution microscopy of BmN4 expressing AcGFP-tagged BmAgo3, BmAgo3-D697A, Siwi and Siwi-D670A. Scale bar 5 μm.

2.2. Cytoplasmic compartmentalization of the silkworm piRNA pathway

In order to characterize the colocalization relations between silkworm piRNA factors, I checked all co-expression combinations between any two factors among BmAgo3, BmAgo3-D697A, Siwi, Siwi-D670A, BmVasa, BmSpnE, BmQin, and BmDcp2 for their colocalization patterns in three-dimensional Z-stacks. I first confirmed that when the wildtype PIWIs were co-expressed with BmVasa, they colocalized well in perinuclear, spherical foci that resemble nuage **(Figure 2-2-1)**. As expected, Siwi-D670A lost its colocalization with BmVasa. In contrast, BmAgo3-D697A remained in nuage **(Figure 2-2-1)**. While both PIWIs did not colocalize with BmDcp2, the slicer mutant Siwi-D670A now clearly overlapped with BmDcp2 foci **(Figure 2-2-2)**, suggesting a shift of its localization pattern from nuage to P-body. As a control, BmAgo3-D697A did not overlap with BmDcp2 **(Figure 2-2-2)**. These results demonstrated that the slicer activity of Siwi but not BmAgo3 is required for its proper nuage accumulation.

Given that Siwi slicer mutant accumulated in P-bodies, I speculated that silkworm P-bodies may contain additional piRNA factors. To answer this question, I analyzed the remaining co-expression combinations and quantified the colocalization ratio by counting granule-like particles with the ImageJ plugin Comdet. The result is plotted as a heatmap, which clearly showed that BmAgo3, Siwi and BmVasa colocalized as a nuage cluster at the top-left corner **(Figure 2-2-3)**. The piRNA factor BmQin and BmSpnE were both excluded from the nuage cluster but enriched in the P-body cluster which was marked by Siwi-D670A and BmDcp2 **(Figure 2-2-3)**. While microscopic images show significant overlap between BmSpnE and BmDcp2 loci, a closer examination of BmQin revealed that BmDcp2 and BmQin did not overlap perfectly with each other but instead formed sub-regions in P-bodies **(Figure 2-2-4)**. Of note, Siwi-D670A but not

wildtype Siwi overlapped with BmDcp2, BmSpnE and BmQin **(Figure 2-2-4)**. It is noted that BmSpnE and BmQin have a marked difference in terms of their localization with previous studies in *Drosophila*, where both SpnE and Qin were found localized in perinuclear nuage (Lim & Kai, 2007; Zhang *et al*, 2014). Instead, the localization of silkworm piRNA factors resembles the mouse gonocyte model, where the homolog of BmSpnE in mouse (TDRD9) was found localized to piP-body (Aravin *et al*, 2009).

Since all these FP-tagged proteins were expressed by the baculovirus OpIE2 promoter, I suspected that overexpression of piRNA factors may alter their co-localization pattern, which could cause false-positive results. To validate the results, I replaced the OpIE2 promoter with a Tet-On inducible promoter (Gossen & Bujard, 1992). With an inducible promoter, a low expression level that is comparable or even lower than the endogenous protein can be activated by titrating the concentration of the inducing drug (in this case, doxycycline). A side-by-side comparison was performed between Tet-On plasmids (pTet) and OpIE2 plasmids (pIZ), where the same amount of DNA was transfected to BmN4 cells and 100 ng/mL doxycycline was applied. The results showed that the expression level of FP-tagged proteins was greatly reduced in bulk when checked with Western blotting **(Figure 2-2-5)** and whole cell fluorescence quantification **(Figure 2-2-6)**. Since the expression drop in bulk does not take count of the transfection efficiency, and therefore does not necessarily reflects an expression reduction at the single cell level, I further validated the expression drop by using flow cytometry. The result suggested that most of the transfected cells to have > 30-folds cut in fluorescence intensity **(Figure 2-2-7)**, which, by quantifying the protein band intensity from the Western blotting experiment, suggests that pTet-expressed Siwi was around 12-folds less abundant than endogenous Siwi (see also Materials and

Methods). I then validated several key colocalization findings by replacing one of the transfected pIZ plasmids with pTet plasmid. The result demonstrated that even at low expression background, Siwi-D670A, BmSpnE and BmQin colocalized with BmDcp2 **(Figure 2-2-8)**. With these results, it is not likely that an overexpression artifact could cause the mislocalization of piRNA factors to P-bodies.

In mouse gonocytes, the piRNA factor MAEL is identified as the core component of piP-body (Aravin *et al*, 2009). For this reason, I cloned BmMael (homolog of MAEL) into both pIZ and pTet plasmids. With the help of Dr. Natsuko Izumi, I found that endogenous BmMael was partially colocalized with BmDcp2, the P-body marker **(Figure 2-2-9)**. BmMael also colocalized with Siwi in nuage, and extensively colocalized with Siwi-D670A in P-body **(Figure 2-2-9)**. These results revealed the dual localization pattern of BmMael, which is somewhat different than MAEL in mice.

Armitage is an RNA helicase that shuttles between nuage and mitochondrial outer membrane in *Drosophila* to facilitate piRNA production (Ge *et al*, 2019; Ishizu *et al*, 2019). In *Drosophila*, Armitage is known to physically associate with both nuage and mitochondrial piRNA factors, especially PIWI proteins (Ge *et al*, 2019). Since Armitage was reported to bind long piRNA precursors (or, pre-piRNA precursor) along with PIWI proteins, it is tempting to believe that Armitage may also follow Siwi-D670A to enter silkworm P-bodies. Indeed, by using a previously established GFP-BmArmi stable cell-line (Izumi *et al*, 2020), we found that BmArmi partially colocalized with Siwi-D670A in P-bodies **(Figure 2-2-10)**. For wildtype Siwi, BmArmi was instead localized in nuage with Siwi, consistent with previous reports in *Drosophila* (Ge *et al*,

2019; Ishizu *et al*, 2019). This result further strengthened the presence of silkworm piRNA factors in P-bodies and suggested the relocation of piRNA factors to P-bodies when Siwi-D670A is present.

To conclude this chapter, I found that BmSpnE, BmQin and BmMael are enriched in silkworm P-bodies but not in nuage, where BmVasa resides. While both wildtype PIWIs could be readily found in nuage, slicer-defective Siwi but not BmAgo3 was found accumulated in P-bodies and colocalizing with BmSpnE, BmQin and BmMael. The mitochondria-nuage helicase BmArmi was found in Siwi-D670A foci, suggesting that a portion of the piRNA factors was relocated to P-bodies when Siwi-D670A is expressed. These results have been validated at protein expression levels comparable to or lower than the endogenous level, which was achieved by replacing the Baculovirus OpIE2 promoter with an inducible Tet-On promoter. These data all together confirmed the subcellular compartmentalization of the piRNA pathway in silkworm BmN4 cells, a phenomenon documented in mouse gonocytes but not in the fly ovary. In courtesy of the mouse study, BmN4 P-bodies are herein referred to as “piP-bodies”.

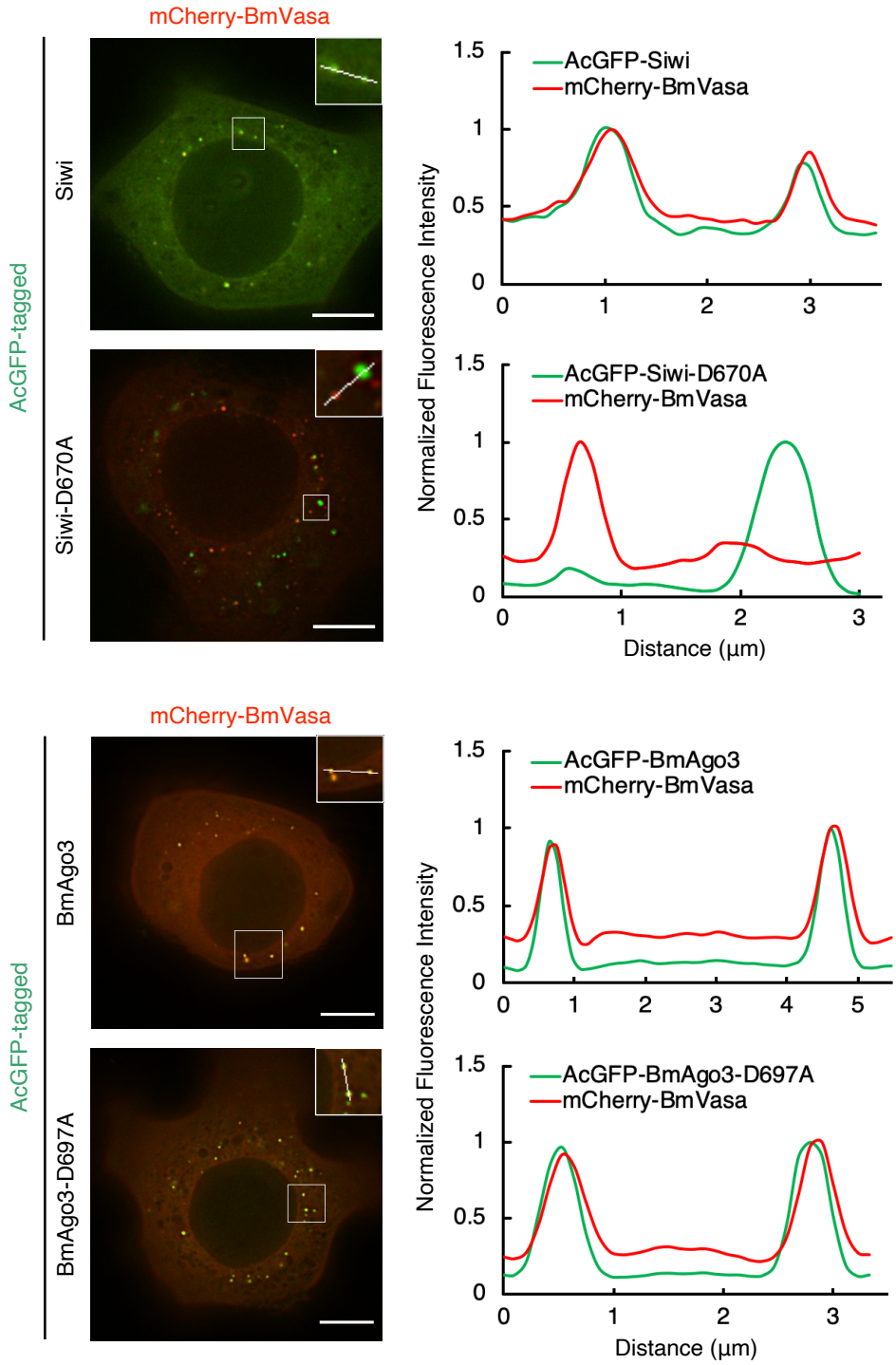

Figure 2-2-1. Colocalization of Siwi, BmAgo3 and BmVasa in BmN4
Line scans (performed along the white line shown in the enlarged region) show that Siwi-D670A mutant but not BmAgo3-D697A mutant lost its colocalization with nuage marker BmVasa. Line scan values were normalized to the highest value. Scale bar, 8 μm.

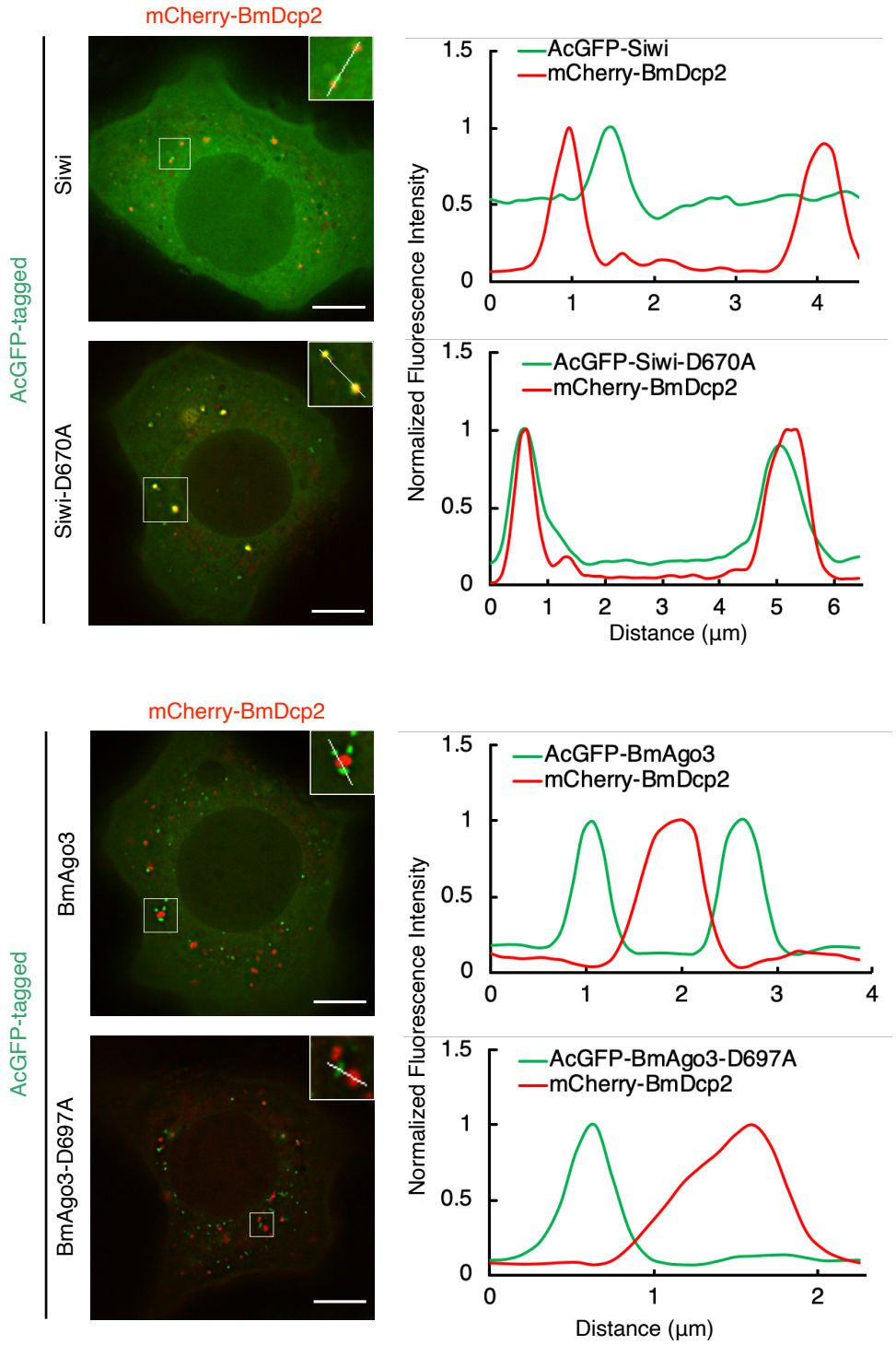

Figure 2-2-2. Colocalization of Siwi, BmAgo3 and BmDcp2 in BmN4
Line scans (performed along the white line shown in the enlarged region) show that Siwi-D670A mutant but not BmAgo3-D697A mutant colocalized with P-body marker BmDcp2. Line scan values were normalized to the highest value. Scale bar, 8 μm.

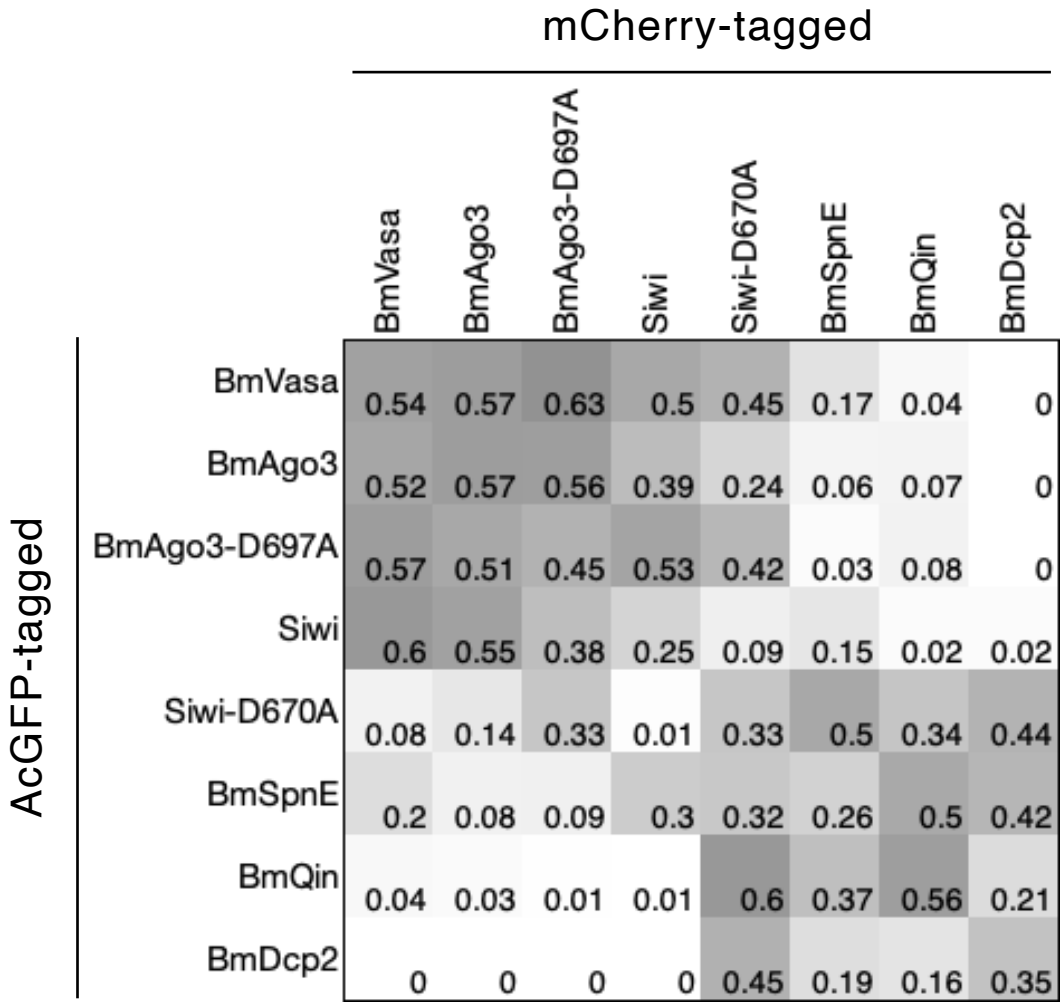

Figure 2-2-3. Colocalization heatmap between FP-tagged piRNA factors.
Colocalization ratio is quantified by using Comdet (see Materials and Methods) and depicted as a mean value from *n*=3 independent z-stacks. Nuage proteins (BmVasa, BmAgo3, Siwi) form a cluster at the top-left corner, while Siwi-D670A mutant, but not BmAgo3-D697A, clusters with BmSpnE, BmQin and BmDcp2 at the bottom-right corner.

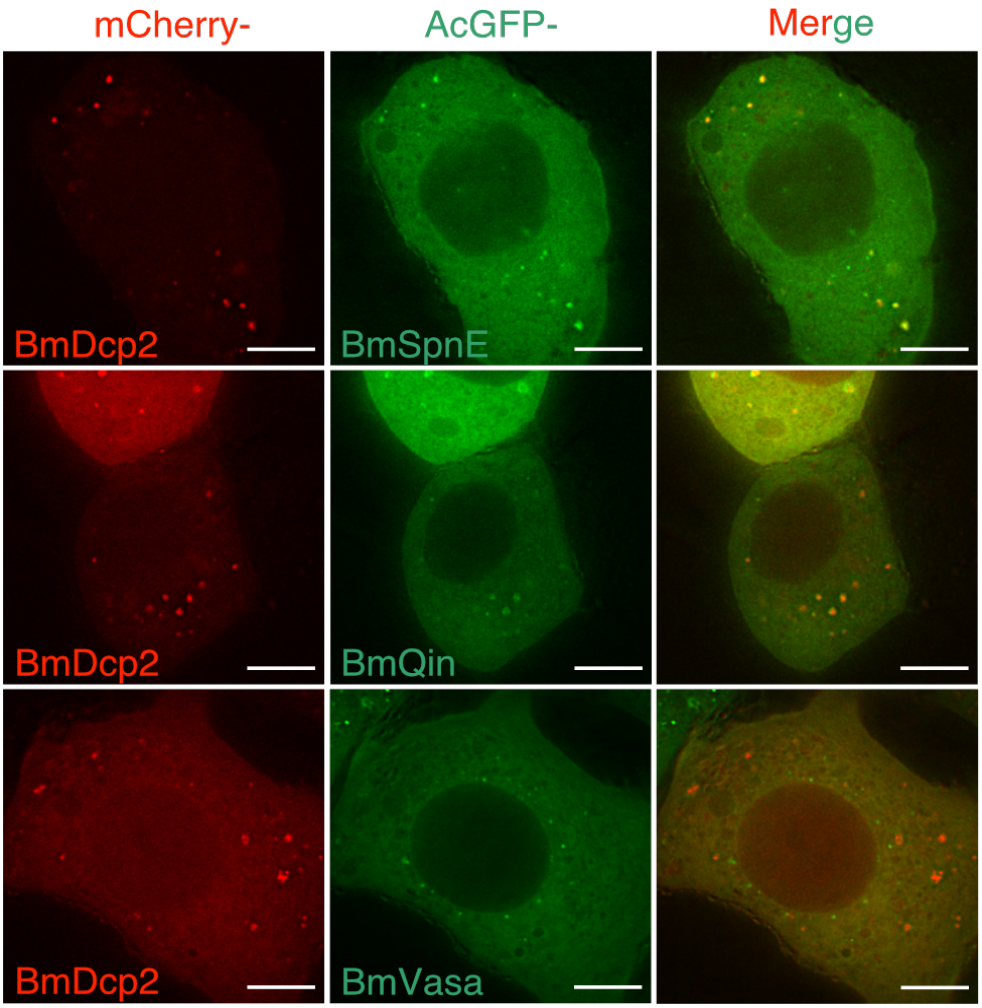

Figure 2-2-4. Colocalization of silkworm piRNA factors with BmDcp2 in P-bodies.
Both BmSpnE and BmQin are localized in BmDcp2 foci, representing P-bodies. Nuage marker BmVasa did not colocalized with BmDcp2. Scale bar 8 μm.

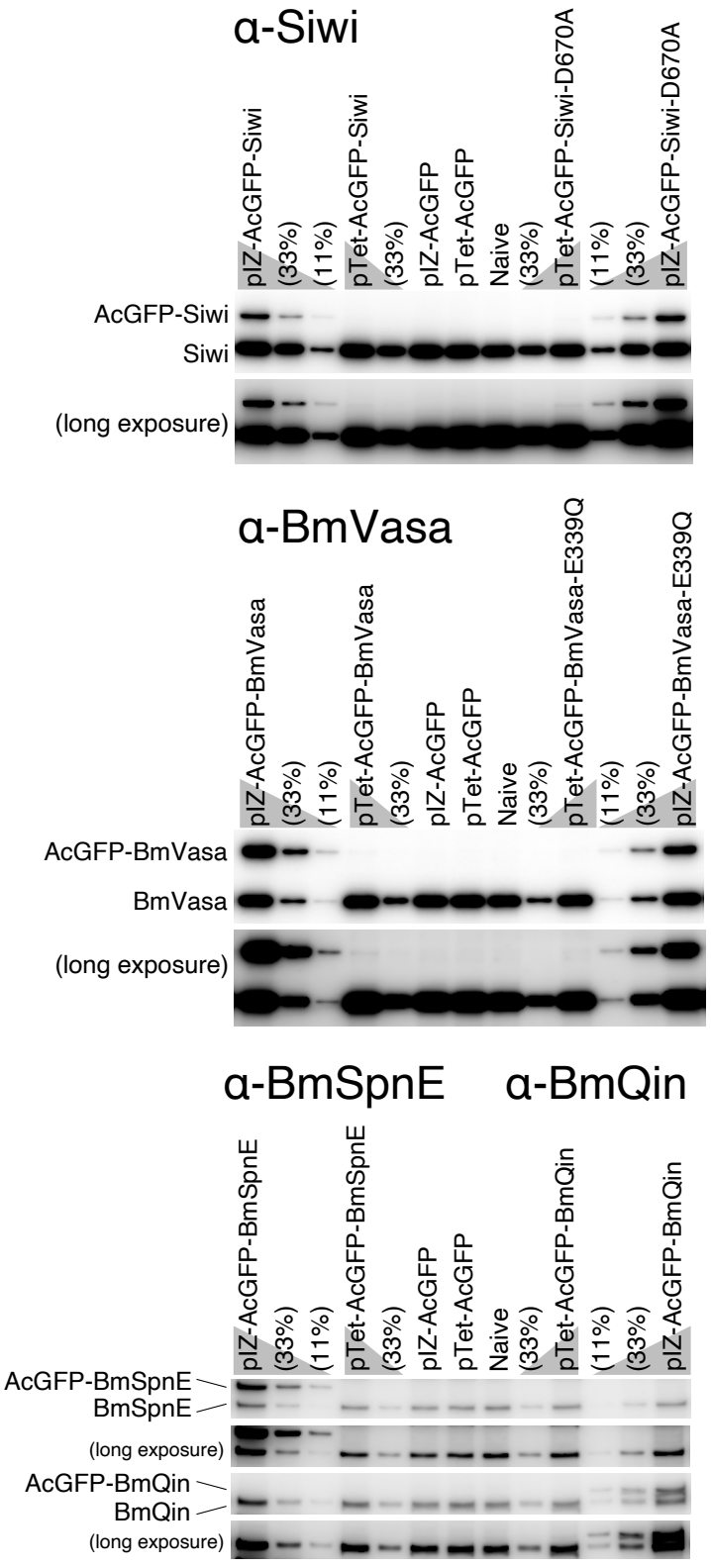

Figure 2-2-5. Western blotting of endogenous piRNA factors and their epitope-tagged counterparts expressed by an OpIE2 promoter (pIZ) or a Tet-On system (pTet)
The expression level of epitope-tagged proteins (upper bands) were mostly comparable to the endogenous counterparts (lower bands). When replaced by a Tet-On system, piRNA factors in general were expressed at significantly lower levels than their endogenous counterparts.

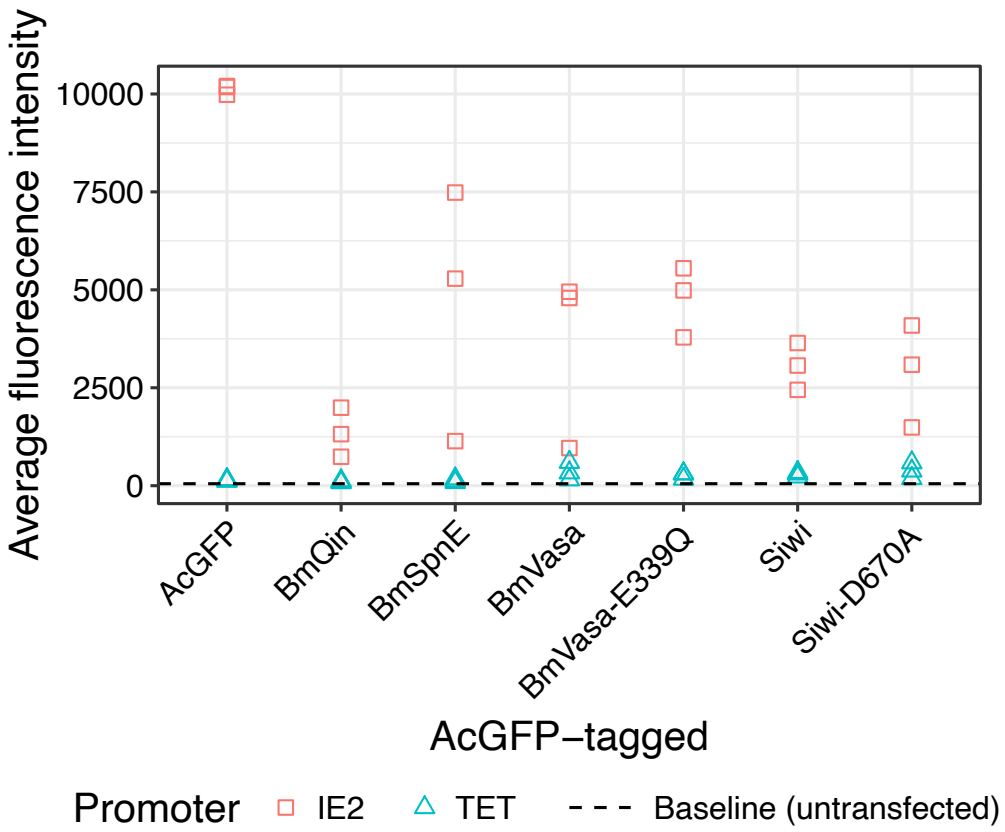

Figure 2-2-6. Relative whole cell fluorescence intensity of AcGFP-tagged piRNA factors expressed by an OpIE2 promoter (pIZ) or a Tet-On system (pTet)

Fluorescence intensity of every Z-stacks was quantified layer by layer and the average value of all Z planes among a Z-stack was showed as a single data point. Baseline value was obtained with untransfected, naive BmN4 cells.

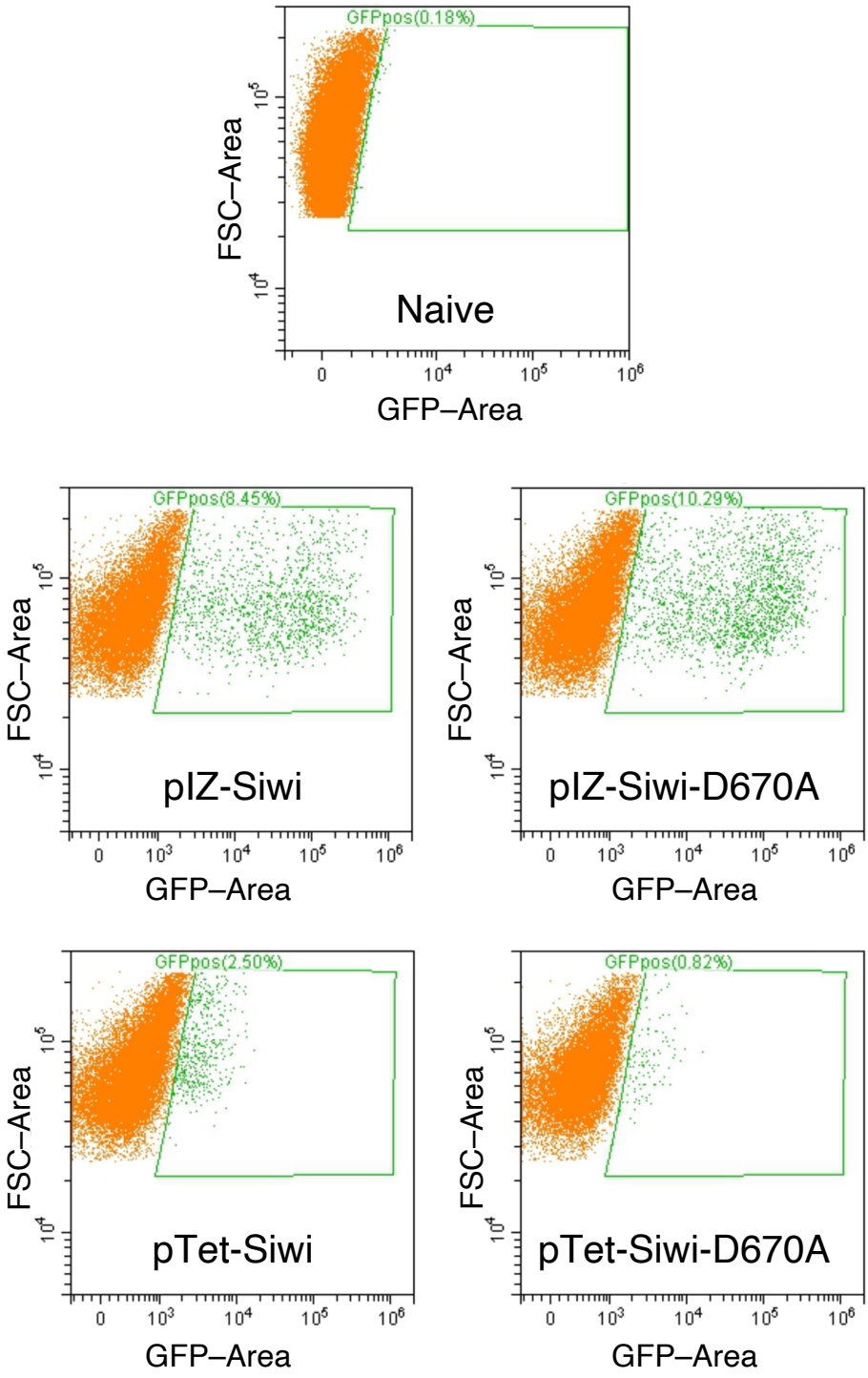

Figure 2-2-7. Flow cytometry analysis of pIZ- or pTet-AcGFP-Siwi expressing BmN4 cells
Naive BmN4 was used as a negative control to define gate "GFPpos", which detects GFP positive cells. pIZ constructs had 8.45% and 10.29% GFPpos cells, while pTet had 2.5% and 0.82% GFPpos cells that were about > 30 folds dimmer than pIZ GFPpos. FSC: Forward scatter.

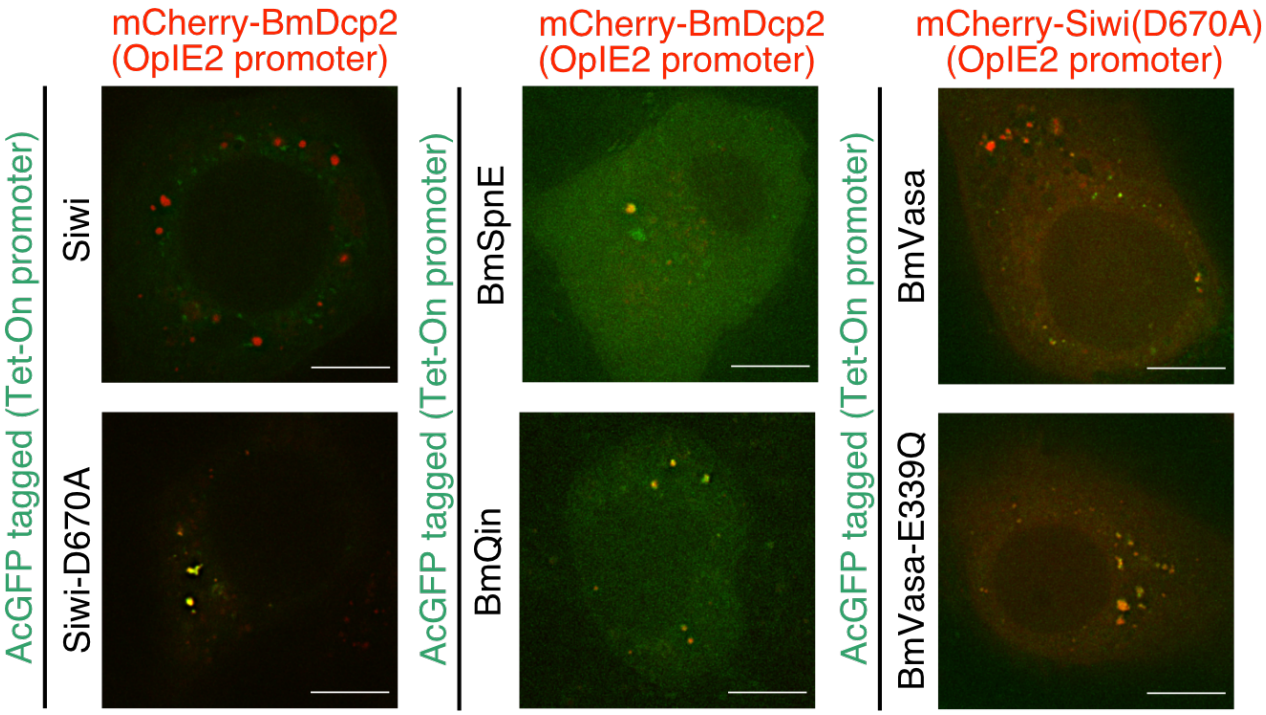

Figure 2-2-8. Colocalizations of pTet-expressed Siwi-D670A, BmSpnE and BmQin with BmDcp2 or with BmVasa-E339Q at low protein expression level

pTet-expressed AcGFP-tagged proteins were co-expressed with pIZ-expressed mCherry-BmDcp2 or Siwi-D670A. Scale bar 10 μm.

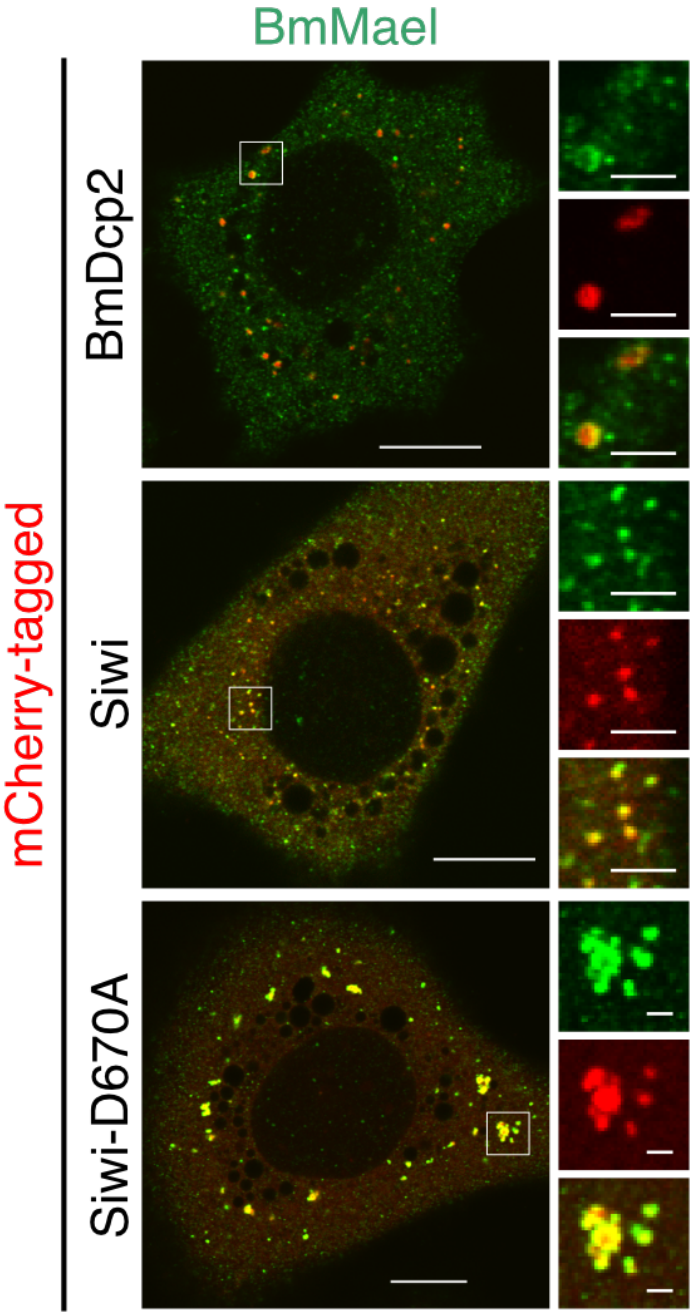

Figure 2-2-9. Colocalization of endogenous BmMael with BmDcp2, Siwi and Siwi-D670A
Endogenous BmMael is localized to the peripheral region of BmDcp2 foci and is strongly colocalized with wild-type and Siwi-D670A in nuage and P-bodies, respectively. Scale bar 10 μm (cell), 2 μm (foci, enlarged region from the white box).

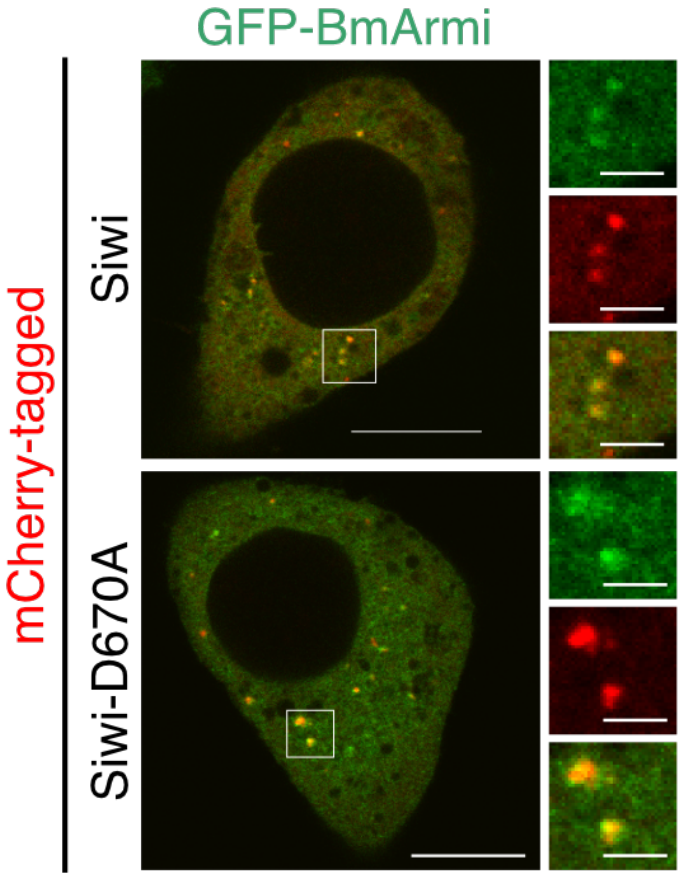

Figure 2-2-10. Colocalization of stably expressed GFP-BmArmi with Siwi and Siwi-D670A
Stably expressed GFP-BmArmi is partially localized to both Siwi and Siwi-D670A foci, representing nuage and P-bodies respectively. Scale bar 10 μm (cell), 2 μm (foci, enlarged region from the white box).

2.3. Siwi slicer mutant forms solid-like aggregates with piRNA factors in piP-bodies

The slicer defective Siwi-D670A is known to retain its ability to bind piRNA, but not its cleavage activity (Matsumoto et al., 2016). This raised the possibility that the mutant Siwi can irreversibly bind to a target RNA as a "frozen" pre-cleavage complex, which incorporates BmSpnE, BmQin and BmMael. To test this hypothesis, I performed photobleaching experiments (Fluorescence-Recovery After Photobleaching; FRAP) on wildtype Siwi and Siwi-D670A foci. I found that when in nuage, wildtype Siwi is highly dynamic and readily exchange contents with the cytoplasm **(Figure 2-3-1)**. This is in line with previous reports on the dynamic nature of nuage (Nagao *et al*, 2008; Nott *et al*, 2015; Webster *et al*, 2015). Importantly, I found that Siwi-D670A foci have a markedly reduced recovery rate after photobleaching, which suggests that Siwi-D670A has a low molecule exchange rate **(Figure 2-3-1)**.

To further test the molecule dynamic inside Siwi-D670A foci, I treated Siwi-D670A expressing cells with aliphatic alcohol named 1,6-Hexanediol. This alcohol was frequently emerged as an LLPS suppressant in cells through weakening hydrophobic interactions (Patel *et al*, 2007; Kroschwald *et al*, 2015, 2017). It was reported that 1,6-Hexanediol can dissolve liquid-like condensates but not amyloid condensates (Kroschwald *et al*, 2015; Peskett *et al*, 2018). Treating Siwi-expressing BmN4 cells with 5% 1,6-Hexanediol for 30 minutes at room temperature dissolved all nuage-like foci **(Figure 2-3-2)**. Nevertheless, the same treatment did not dissolve Siwi-D670A foci, which agrees with the finding with FRAP experiments. These results together demonstrated that Siwi-D670A foci are largely static and, likely an aggregate. It should be noted, however, that 1,6-Hexanediol treatment could potentially affect membrane permeability (Kroschwald *et al*, 2017; Alberti *et al*, 2019), thus make the interpretation of whether the observed

foci are LLPS condensates or not difficult. After all, the same effect asserted on Siwi foci by 1,6-Hexanediol did not applies to Siwi-D670A, which is still valuable evidence to argue for the changing of physical properties in Siwi-D670A foci.

Next, I checked whether the accumulation of pre-cleavage Siwi-D670A in piP-bodies will enhance piP-bodies localization of piRNA factors. This hypothesis is justified as Siwi is known to co-immunoprecipitate with BmSpnE and BmQin (Nishida *et al*, 2015). Indeed, in Siwi-D670A-expressing cells, I found that the granule-to-cell intensity ratios of BmSpnE, BmQin were both significantly increased, meaning that piP-body foci were brighter and less disperse than Siwi-expressing cells **(Figure 2-3-3)**. As a control, western blotting suggested that the expression level of BmSpnE or BmQin was not increased by co-expression of Siwi-D670A **(Figure 2-3-4)**. This suggested that Siwi-D670A, when trapped in piP-bodies, co-aggregated with BmSpnE and BmQin as the pre-cleavage complex.

There is a chance that the piP-body accumulation of Siwi-D670A can result from a change in the protein structure, but not from a "frozen" pre-cleavage state. However, the chance is slim, given that the structure of Siwi resolved by X-ray crystallography indicates that the catalytic tetrad (slicer) forms only after extensive guide-target base pairing and does not involve in piRNA loading (Matsumoto *et al*, 2016). To test this hypothesis, I generated a piRNA loading mutant by replacing Siwi Tyr607 into glutamate (Y607E mutant; Kawaoka *et al*, 2011). As expected, the Y607E mutant was found largely dispersed, not even accumulates in perinuclear granules **(Figure 2-3-5)**. Introduction of Y607E mutation to Siwi-D670A slicer mutant results in a double mutant (Siwi-Y607E-D670A; Siwi-YE-DA), which abolished its piP-body localization completely **(Figure 2-**

3-6). This proves that the localization of Siwi-D670A to piP-body requires piRNA loading, most likely in a form with the slicer catalytic tetrad in place but then stalled because of lacking an Asp670 residue.

Still, it is unclear whether the aggregation of Siwi-D670A and piRNA factors was caused by reduced turnover of protein-protein interaction due to the stalled pre-cleavage conformation of Siwi-D670A, or by RNA-mediated accumulation. In the latter case, slicer defective Siwi can instead "protect" the target RNA by irreversibly binding to the piRNA target sites. This could impair shortening as well as degradation of these target RNAs, and it is likely that multiple Siwi-D670A pre-cleavage complexes will bind to a single, long RNA in piP-bodies. Since direct apply of RNase to piP-body is technically challenging, I performed immunoprecipitation (IP) of Siwi-D670A with or without RNase treatment. Oriole staining of immunoprecipitated proteins revealed that Siwi-D670A was co-purified with various unidentified protein bands which were not found within wildtype Siwi co-precipitant **(Figure 2-3-7)**. Such a "dirty" background was disappeared after treatment with RNase A **(Figure 2-3-7)**, suggesting that RNA has a role in the co-aggregation between Siwi-D670A and other protein interactors.

In summary, I found that when Siwi-D670A is expressed, multiple piRNA factors including BmSpnE and BmQin co-aggregated in piP-body. Siwi-D670A aggregate in piP-body has a lower molecular exchange rate with the cytoplasm, suggesting an irreversible target RNA binding caused by the point mutation at catalytic tetrad of slicer domain. Supporting this statement, I confirmed that Siwi-D670A aggregation requires loading of piRNA. Finally, treating Siwi-

D670A-overexpressed lysates with RNase wiped out multiple protein bands from the Siwi-D670A co-precipitates, suggesting that irreversible target RNA binding might promote such aggregation.

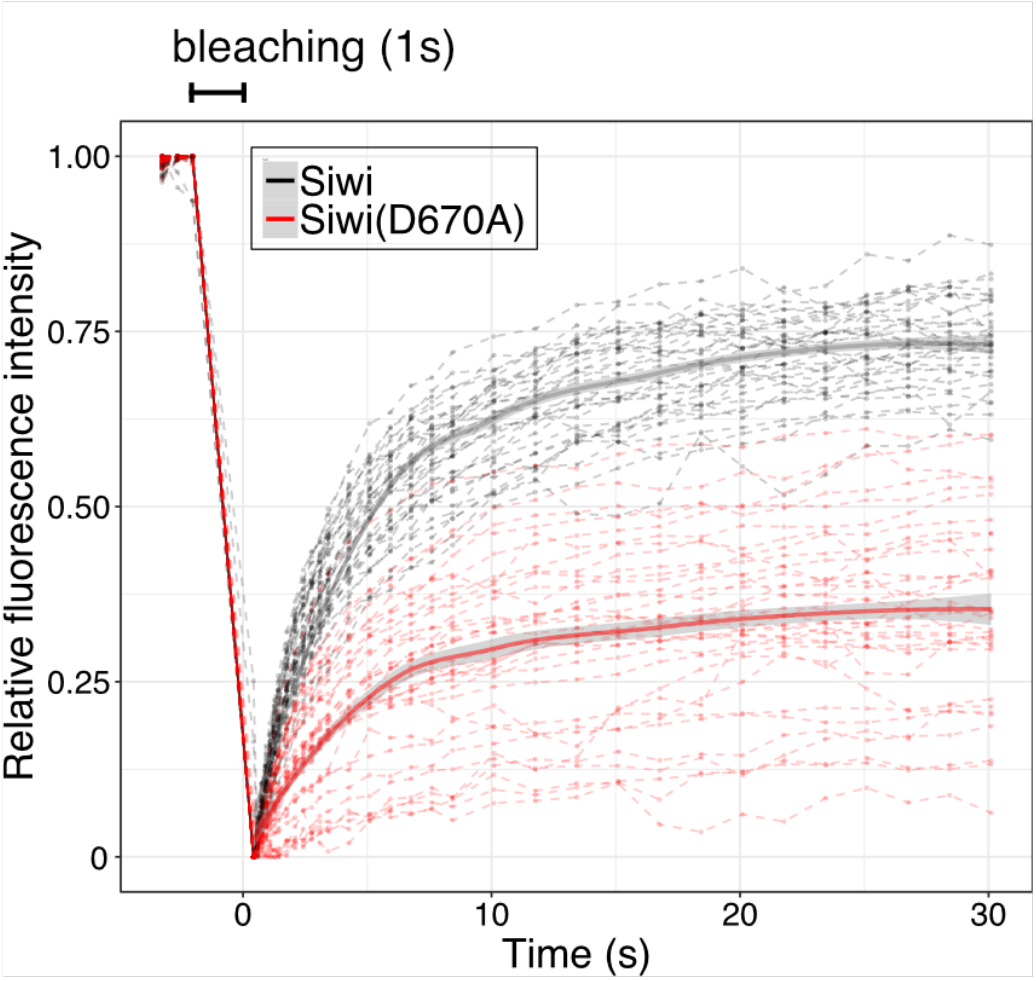

Figure 2-3-1. Photobleaching experiment on AcGFP-Siwi and AcGFP-Siwi-D670A
Relative fluorescence intensity of Siwi-D670A foci (*n*=36) and Siwi foci (*n*=36) after photobleaching was depicted as red and black dotted lines, respectively. Solid lines represent locally estimated scatterplot smoothing (LOESS) curve and the grey areas represent 95% confidence level interval. Fluorescence intensity is double-normalized to minimum and maximum to neglect differences in foci brightnesses and bleaching efficiency.

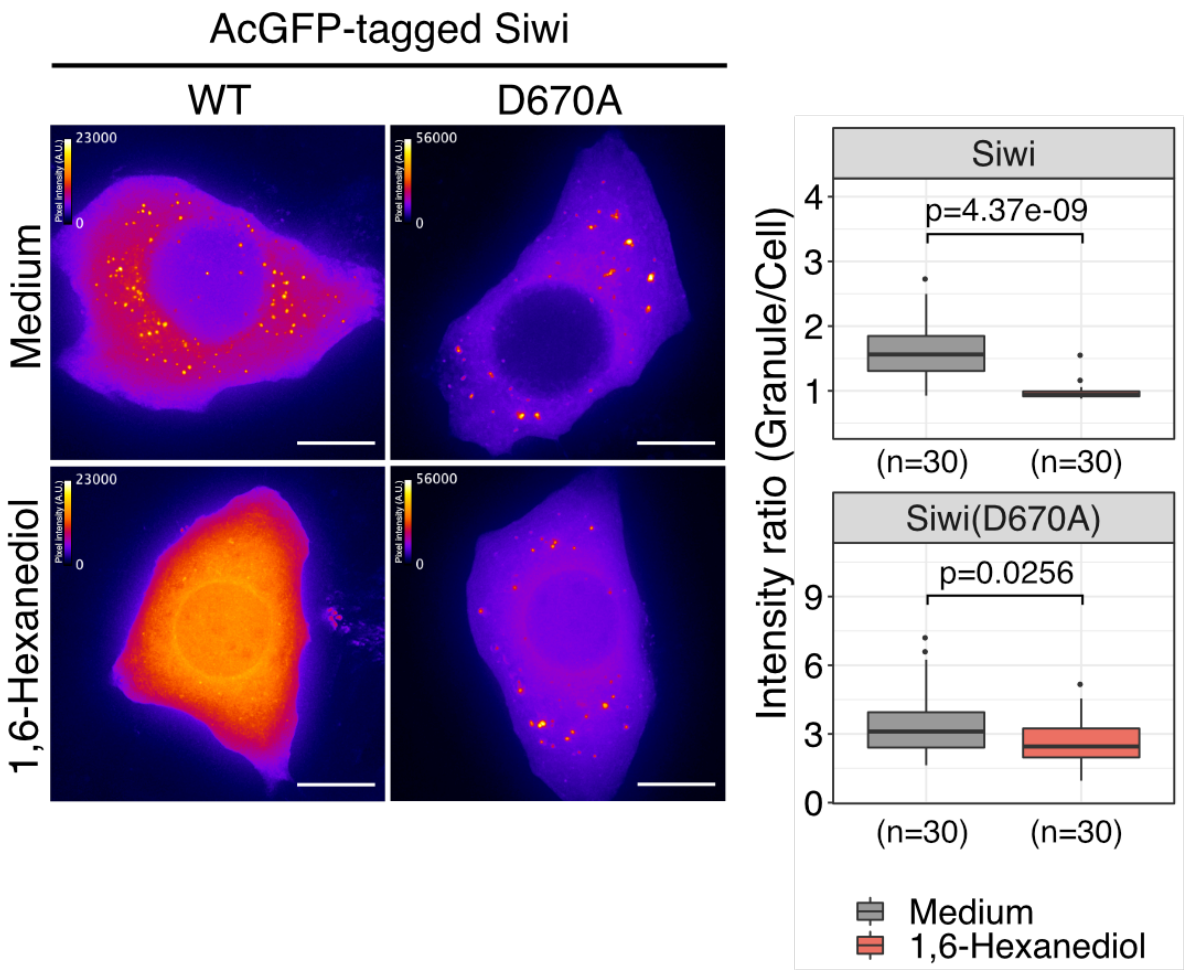

Figure 2-3-2. 1,6-Hexanediol treatment on AcGFP-Siwi and AcGFP-Siwi-D670A foci
(Left) Z-stacks were performed prior to the treatment of 1,6-Hexanediol and once more after 30 minutes of incubation at RT. Z-stacks are projected and normalized and pseudo-colored with Fire LUT to show the foci intensity. Scale bar 10 μm. Color scales represent pixel intensity in arbitrary units (A.U.)
(Right) Granule/cell intensity ratio of Siwi-D670A foci persists after 1,6-Hexanediol treatment, while the Siwi foci record a significant decrease. Representative data from $N = 3$ independent experiments are shown. P-values are calculated by Asymptotic Wilcoxon rank sum test.

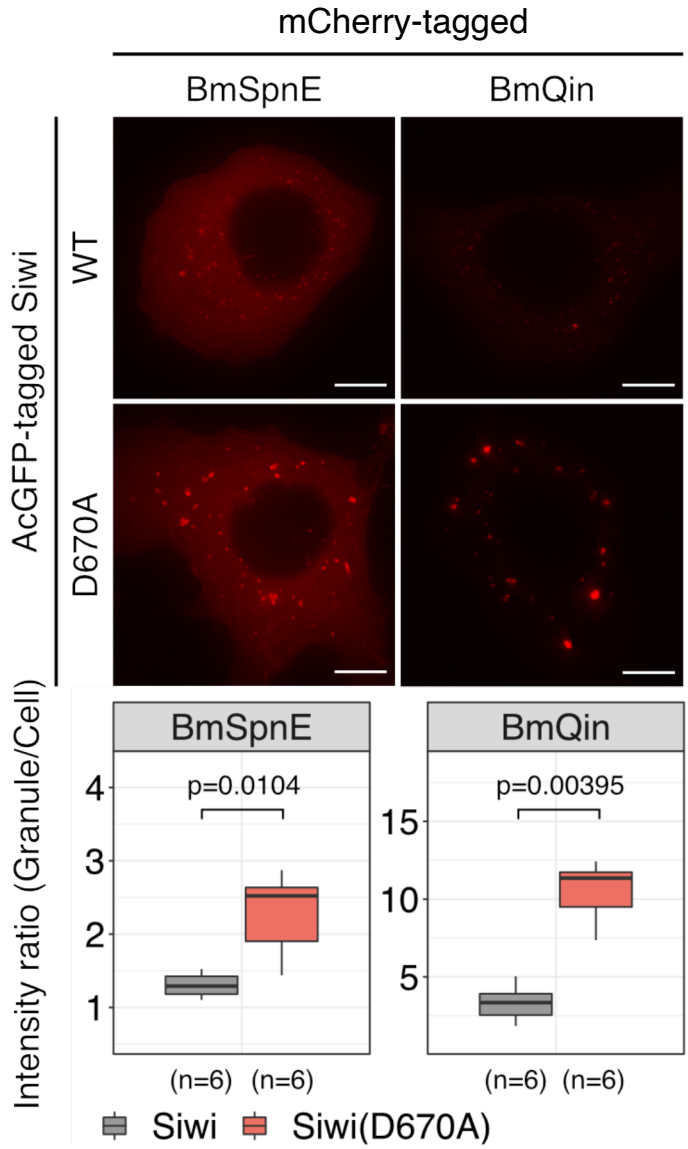

Figure 2-3-3. Co-expression of Siwi-D670A elevates granule-to-cell intensity ratio of BmSpnE and BmQin foci

(Upper) Z-stack projection (maximum intensity) of mCherry-BmSpnE and mCherry-BmQin foci. AcGFP-Siwi or AcGFP-Siwi-D670A foci from the green channel is not shown. Scale bar 8 μm.

(Bottom) Intensity ratio averaged from Z-stacks (n=6 per set) depicted as box plots. Representative data from $N \geq 3$ independent experiments are shown. P-values are calculated by Asymptotic Wilcoxon rank sum test.

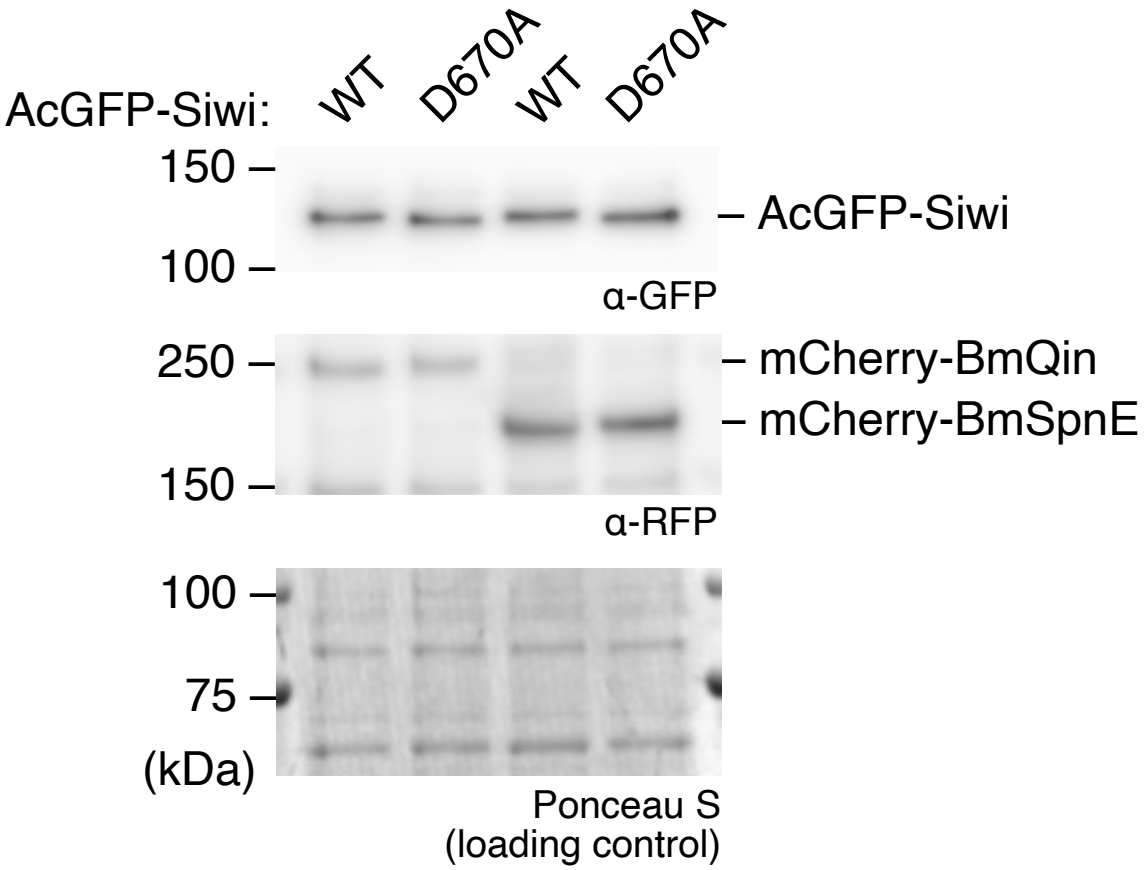

Figure 2-3-4. Western blotting of AcGFP-Siwi, AcGFP-Siwi-D670A and the co-expressed mCherry-BmQin or mCherry-BmSpnE

The expression levels of BmQin and BmSpnE were not affected by Siwi or Siwi-D670A co-expression.

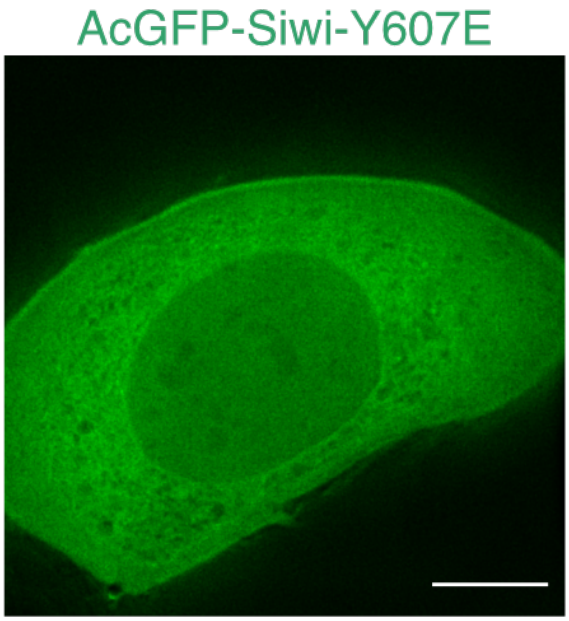

Figure 2-3-5. Localization of Siwi piRNA loading mutant (Y607E) in BmN4 cells
Siwi-Y607E is largely dispersed in the cytoplasm. Scale bar 8 μm.

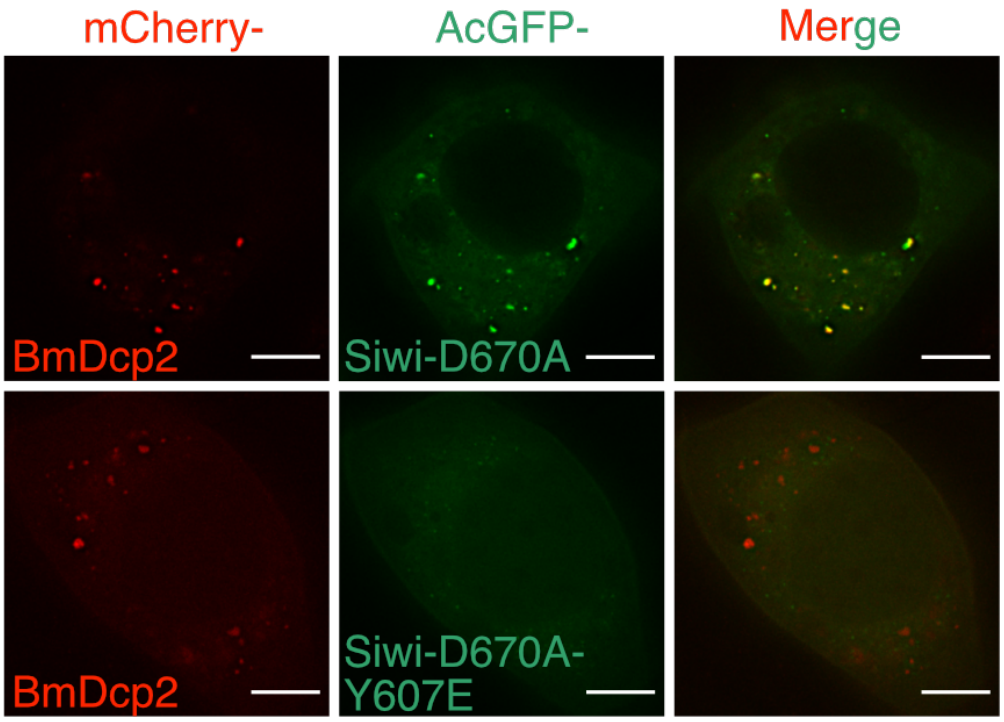

Figure 2-3-6. Colocalization of Siwi-D670A or Siwi-D670A-Y607E double mutant with BmDcp2

Y607E mutation that prevent piRNA being loaded severely compromised the colocalization between Siwi-D670A and BmDcp2. Scale bar 8 μm.

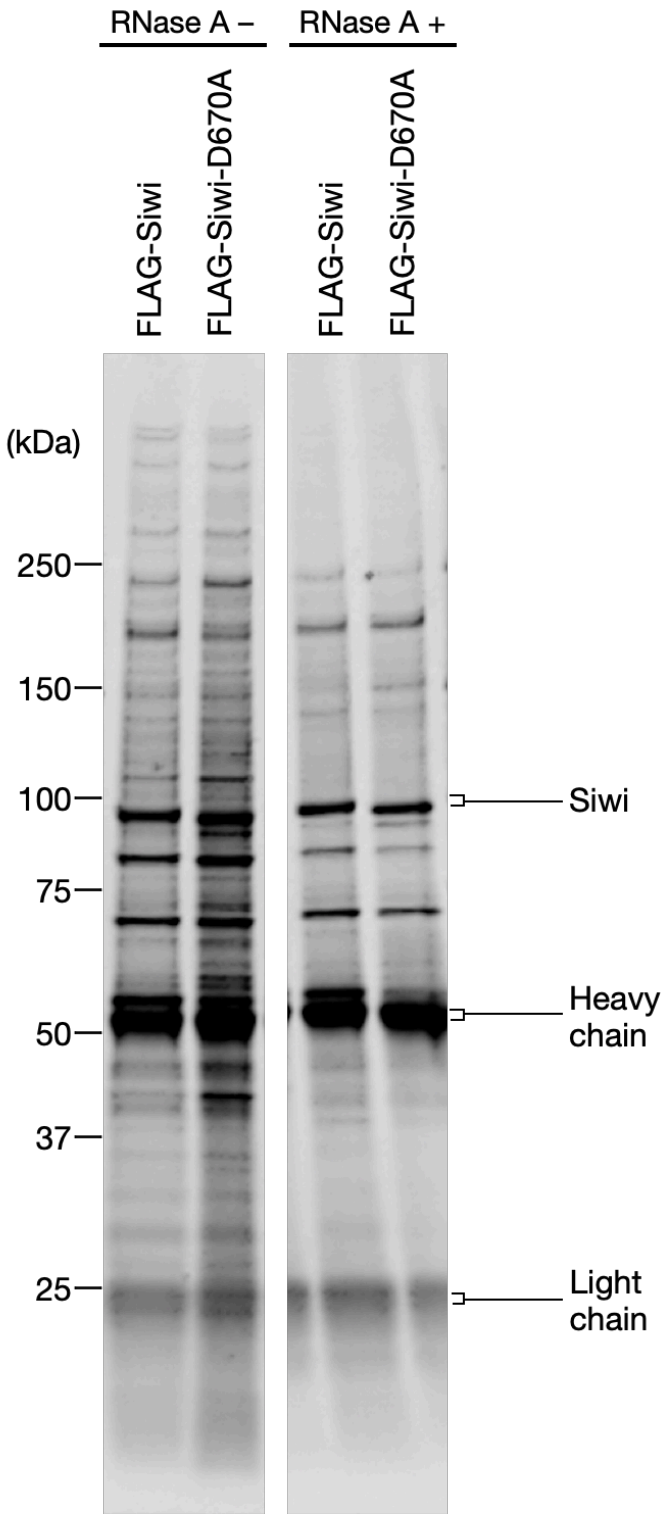

Figure 2-3-7. Oriole fluorescent gel staining of proteins co-immunoprecipitated with FLAG-Siwi and FLAG-Siwi-D670A, with or without RNase A treatment

RNase A treatment prior to the immunoprecipitation step removed multiple co-immunoprecipiated protein bands in both FLAG-Siwi and FLAG-Siwi-D670A immunoprecipitations.

2.4. Nuage proteins are required for proper piP-body assembly

It is remained to answer why and how Siwi-D670A aggregated in piP-bodies but not in other compartments such as mitochondrial surface or nuage. Given that BmSpnE and BmQin reside in piP-bodies even without the presence of Siwi-D670A **(Figure 2-2-4)**, it is likely that these piP-body proteins make piP-body the more favorable subcellular compartment to harbor Siwi-D670A.

To test this hypothesis, I performed knock-down experiments on BmSpnE and BmQin by transfecting the cells with double-stranded RNA (dsRNA), which specifically deplete the target protein through endogenous siRNA pathway (Fujita *et al*, 2009; Tanaka *et al*, 2009). The depletion of target proteins was verified for the endogenous protein **(Figure 2-4-1)** as well as the epitope-tagged, transiently expressed protein **(Figure 2-4-2)**. By depleting BmSpnE or BmQin, I found that the colocalization ratio between Siwi-D670A and piP-body marker BmDcp2 was significantly reduced when compared to the control knockdown (dsRLuc) **(Figure 2-4-3)**. Instead, Siwi-D670A foci were mostly in contact but did not overlap with BmDcp2 when BmSpnE or BmQin was absent **(Figure 2-4-3)**. This result suggested that while Siwi-D670A can form granule-like aggregates in the cytoplasm without BmSpnE and BmQin, both piP-body factors have non-redundant roles in recruiting Siwi-D670A to piP-bodies.

The next question is obvious: what would be the case when endogenous Siwi was depleted instead? Wildtype Siwi co-precipitated with BmSpnE and BmQin (Nishida et al., 2015) but did not colocalize with both factors **(Figure 2-2-3)**. It is possible that Siwi, partly dispersed in the vast cytoplasm, interacts with these piP-body factors while diffusing freely, but this also raised the possibility that wildtype Siwi may transit through the piP-bodies and interact with BmSpnE and

BmQin inside. To answer this question, I depleted Siwi **(Figure 2-4-2)** and evaluated the colocalization between piP-body marker BmDcp2 and BmSpnE or BmQin. The result shows that when Siwi was absent, the colocalization ratio between BmDcp and both piP-body factors was markedly reduced **(Figure 2-4-4, Figure 2-4-5)**. Instead of diffusing across the vast cytoplasm, BmSpnE is now re-located to distinct foci which appear to be some bright, densely packed condensates. These foci were found to contain BmVasa **(Figure 2-4-6)**, which is reasonable since both BmSpnE are Tutor-domain proteins and homologs of Vasa as well as the silkworm PIWIs are targets of sDMA modifications (Kirino *et al*, 2010; Honda *et al*, 2013; Izumi *et al*, 2016).

The above data suggest that Siwi can contribute to the assembly of piP-body while enriched in nuage. Since nuage are highly dynamic **(Figure 2-3-1)** and Siwi are partially dispersed **(Figure 2-1-1)**, it is expected that Siwi will, at some stages of the ping-pong cycle, leave nuage and travel to a new subcellular compartment. On some occasions, Siwi is likely to enter piP-body and interacts with BmSpnE and BmQin, but only in a transient way. Disabling the ability to cleave the bounded target RNA stalled the departure of Siwi from piP-bodies, thus visualized the transient interaction as an aggregate.

To validate the above-proposed model, there is a need to visualize the translocation of wildtype Siwi from nuage to piP-body. When nuage is present in BmN4 cells, Siwi presumably localizes in nuage together with BmAgo3 and BmVasa. I reasoned that disruption of nuage could render wildtype Siwi accumulate in other piRNA-related compartments, just like how BmSpnE behaves when piP-body was disrupted by Siwi depletion. To disrupt nuage, I first depleted BmVasa **(Figure 2-4-1, 2-4-2)** and quantified the colocalization ratio between Siwi and BmAgo3.

As expected, depletion of BmVasa caused Siwi to dislodge from BmAgo3 foci **(Figure 2-4-7)**. Surprisingly, Siwi in BmVasa-depleted cells still formed puncta that resemble RNP granules. I therefore checked the colocalization between Siwi and BmDcp2 in cells where BmVasa was depleted. Remarkably, Siwi now forms concatenated aggregates with BmDcp2, as both foci were contacting each other but did not overlap **(Figure 2-4-8)**. This resembles the sub-regions of piP-bodies observed when co-expressing BmQin and BmDcp2 **(Figure 2-2-4)**.

In conclusion, by depleting endogenous piRNA factors, I found that assembly of piP-body requires Siwi, despite its apparent absence from piP-bodies. Since piP-body factors physically bind wildtype Siwi and recruit Siwi-D670A to piP-body, wildtype Siwi is expected to transiently enter piP-body for its biological functions. Disruption of nuage causes wildtype Siwi to relocate from nuage to piP-body, which suggests that Siwi dynamically changes its interactors and shuttles between the two RNP condensates – nuage and piP-bodies.

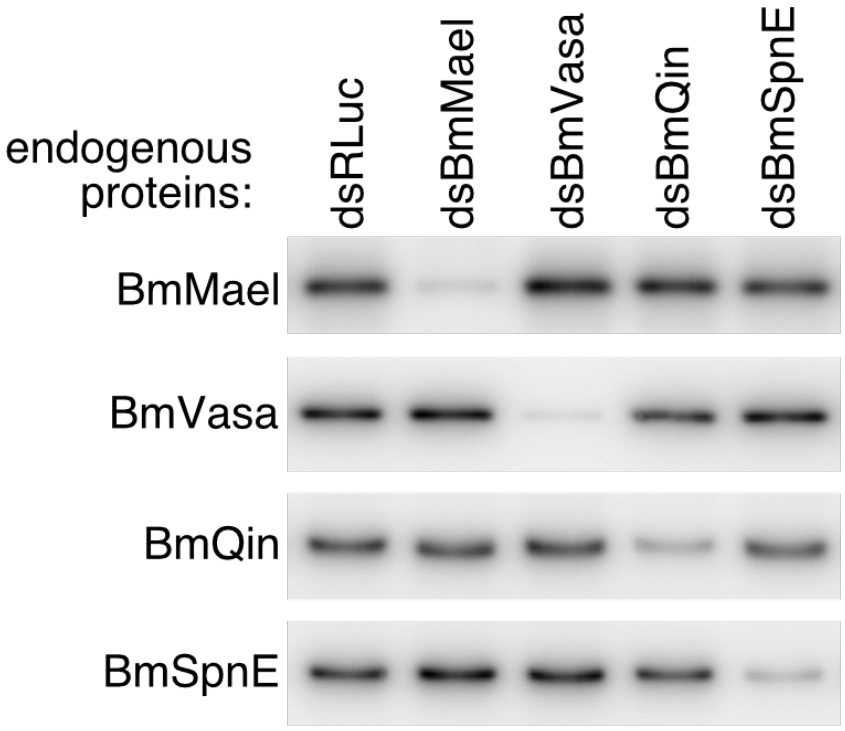

Figure 2-4-1. Western blotting of endogenous piRNA factors depleted by dsRNA-mediated knockdown

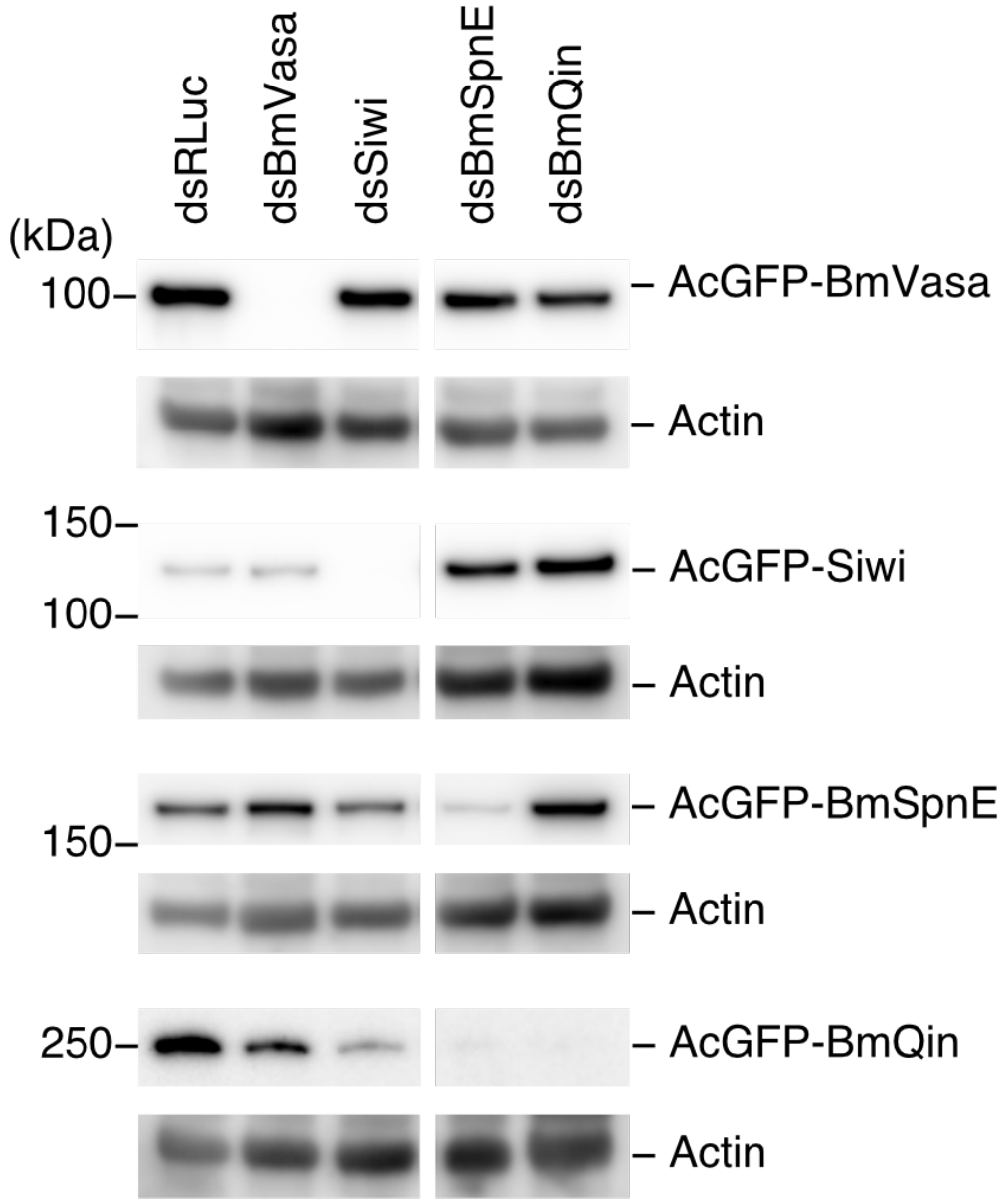

Figure 2-4-2. Western blotting of epitope-tagged piRNA factors depleted by dsRNA-mediated knockdown

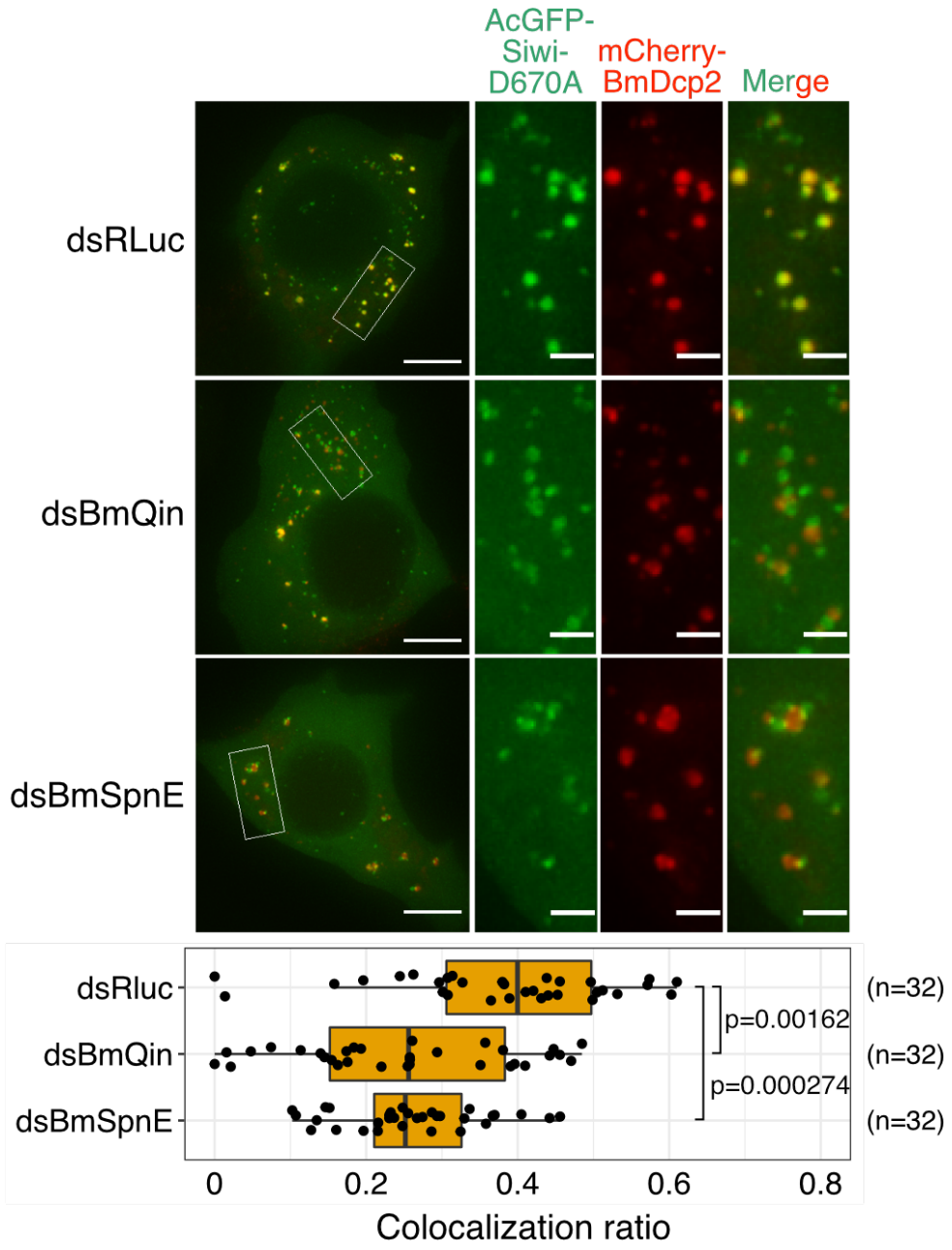

Figure 2-4-3. BmSpnE or BmQin knockdown causes segregation of Siwi-D670A from piP-bodies
(Top-left) Representative Z-projections (Maximum intensity). Scale bar 8 μm.
(Top-right) Enlarged area from the white box. Scale bar 2 μm.
(Bottom) Box plot showing that depletion of BmQin (n=32 cells) or BmSpnE (n=32 cells) reduces colocalization ratio between Siwi-D670A and BmDcp2, compared to control (dsRLuc, n=32 cells). Representative data from N = 3 independent experiments are shown. Bonferroni-corrected P-values were calculated by Asymptotic Wilcoxon rank sum test.

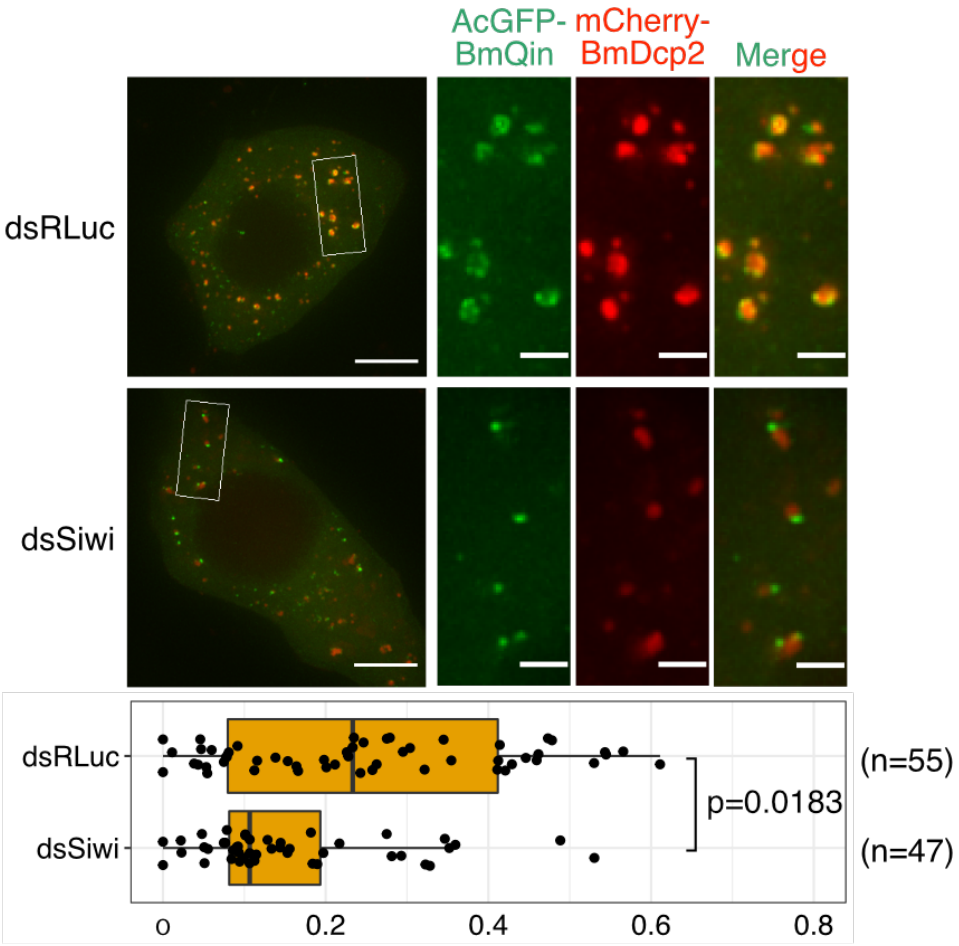

Figure 2-4-4. Siwi knockdown causes segregation of BmQin from piP-bodies
(Top-left) Representative Z-projections (Maximum intensity). Scale bar 8 μm.
(Top-right) Enlarged area from the white box. Scale bar 2 μm.
(Bottom) Box plot showing that depletion of Siwi (dsSiwi, n=47 cells) reduces colocalization ratio between BmQin and BmDcp2, compared to control (dsRLuc, n=55 cells). Representative data from N = 4 independent experiments are shown.

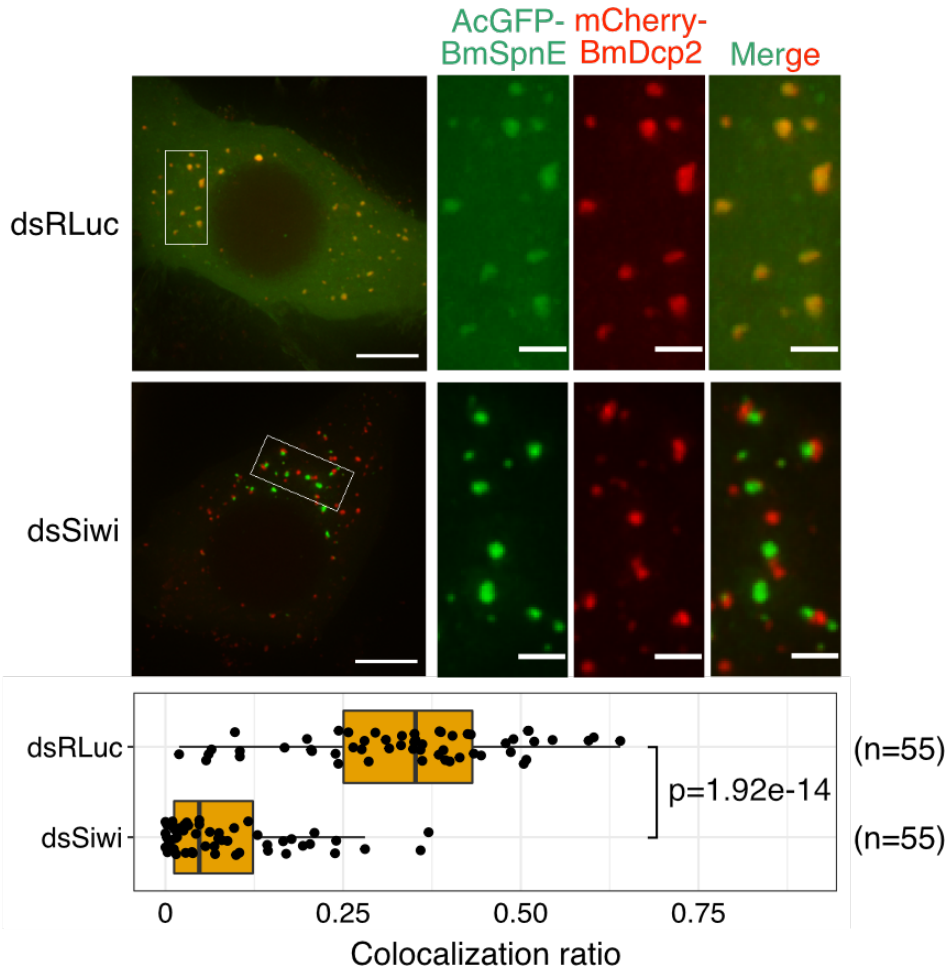

Figure 2-4-5. Siwi knockdown causes segregation of BmSpnE from piP-bodies
(Top-left) Representative Z-projections (Maximum intensity). Scale bar 8 μm.
(Top-right) Enlarged area from the white box. Scale bar 2 μm.
(Bottom) Box plot showing that depletion of Siwi (dsSiwi, n=55 cells) reduces colocalization ratio between BmSpnE and BmDcp2, compared to control (dsRLuc, n=55 cells). Representative data from N = 6 independent experiments are shown.

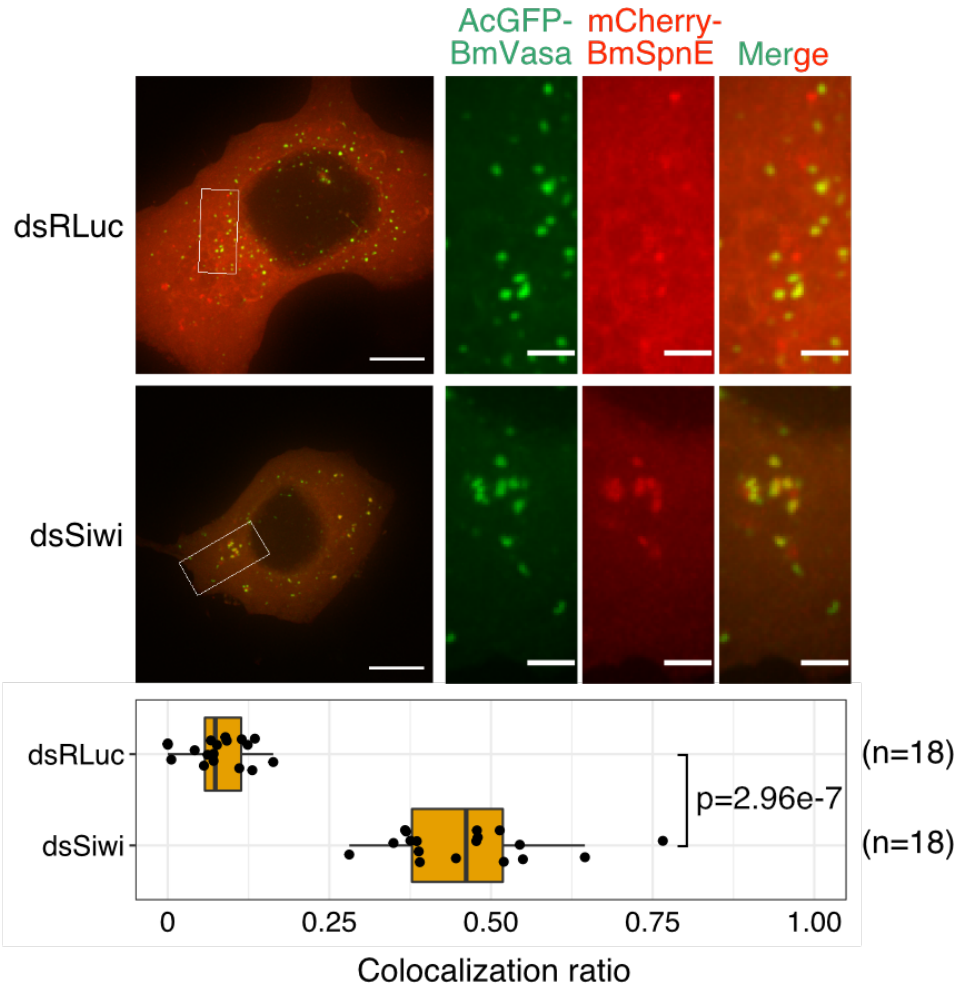

Figure 2-4-6. Siwi knockdown results in colocalization of BmSpnE and BmVasa
(Top-left) Representative Z-projections (Maximum intensity). Scale bar 8 μm.
(Top-right) Enlarged area from the white box. Scale bar 2 μm.
(Bottom) Box plot showing that depletion of Siwi (dsSiwi, n=18 cells) up-regulates colocalization ratio between BmSpnE and BmVasa, compared to control (dsRLuc, n=18 cells). Representative data from N = 3 independent experiments are shown.

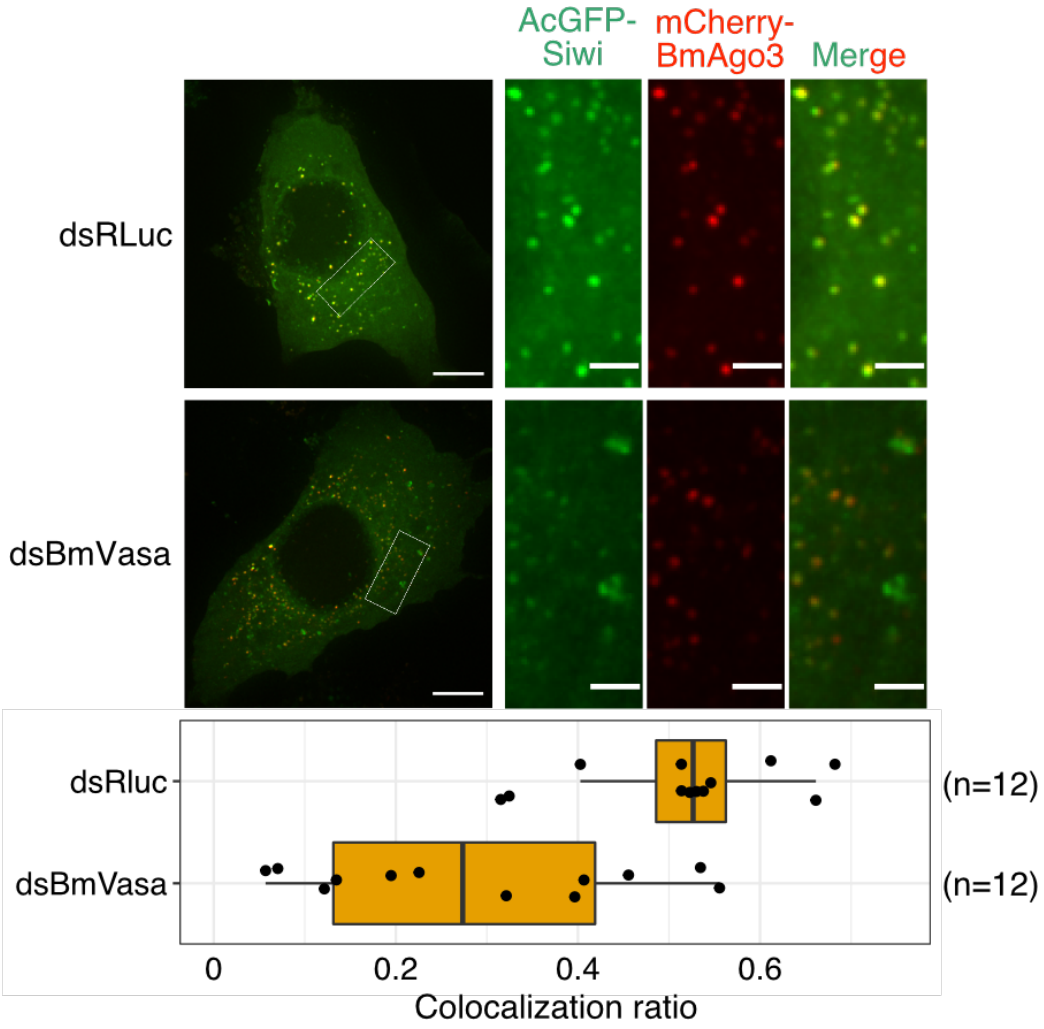

Figure 2-4-7. BmVasa knockdown causes segregation of Siwi from BmAgo3 foci
(Top-left) Representative Z-projections (Maximum intensity). Scale bar 8 μm.
(Top-right) Enlarged area from the white box. Scale bar 2 μm.
(Bottom) Box plot showing that depletion of BmVasa (dsBmVasa, n=12 cells) downregulates colocalization ratio between Siwi and BmAgo3, compared to control (dsRLuc, n=12 cells). Data points collected from N = 2 independent experiments are shown (statistical test is not performed for N < 3 data).

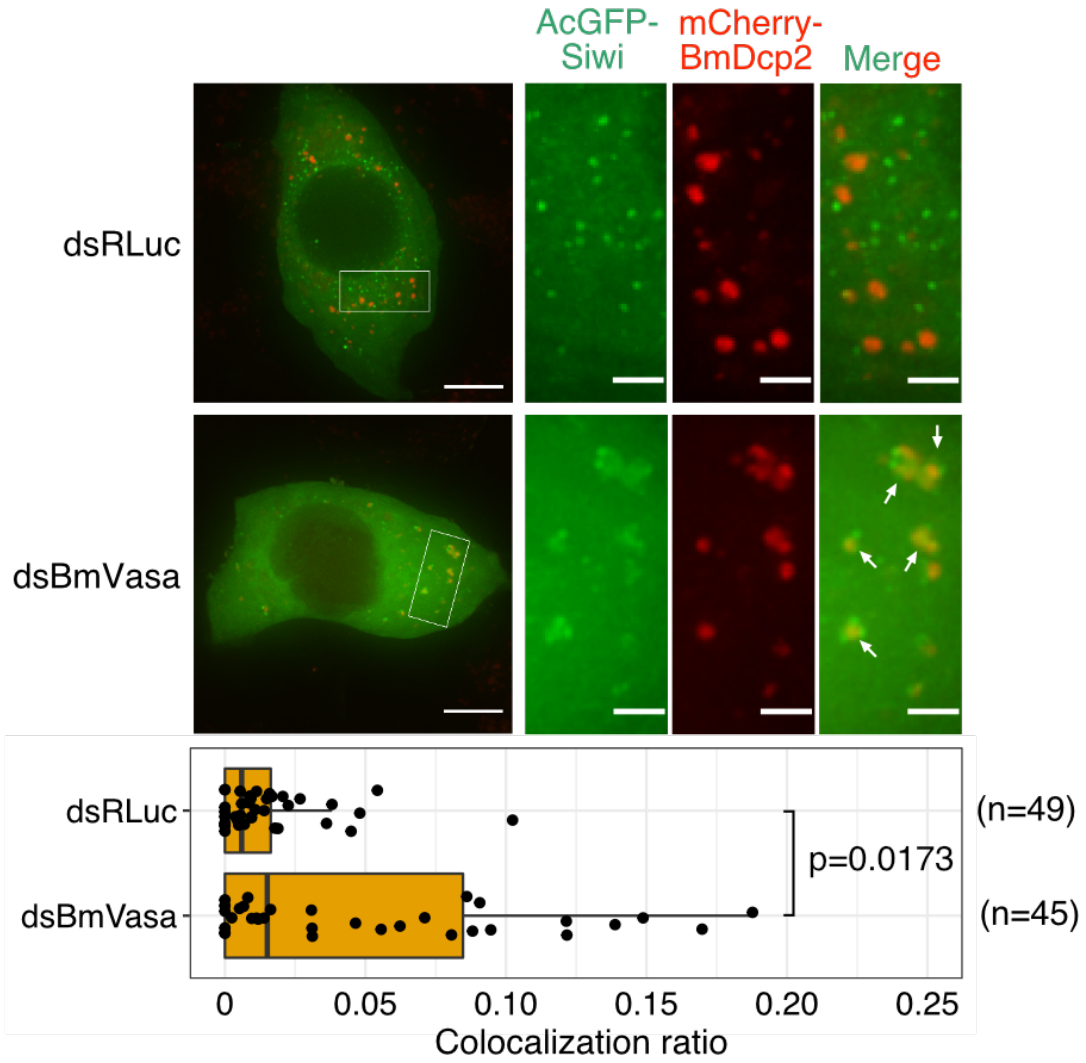

Figure 2-4-8. Depletion of BmVasa results in entanglement of Siwi at piP-bodies
(Top-left) Representative Z-projections (Maximum intensity). Scale bar 8 μm.
(Top-right) Enlarged area from the white box. Scale bar 2 μm. Interaction interfaces are indicated by white arrows.
(Bottom) Box plot showing that depletion of BmVasa (dsBmVasa, n=45 cells) mildly but significantly up-regulates colocalization ratio between Siwi and BmDcp2, compared to control (dsRLuc, n=49 cells). Representative data from N = 5 independent experiments are shown.

2.5. Siwi slicer and BmVasa ATPase activity regulates nuage/piP-body partitioning

It is still unclear why Siwi-D670A is not accumulated in nuage, given the fact that the nuage helicase BmVasa primarily binds Siwi-targets (Xiol *et al*, 2014). It was previously proposed that BmVasa may aid Siwi in liberating and hand overing its cleaved target to BmAgo3 (Xiol *et al*, 2014; Nishida *et al*, 2015). I reasoned that the same reaction may apply to Siwi-D670A regardless of a successful cleavage but the RNA clamping activity of BmVasa, which may explain why Siwi-D670A was dislodged from BmVasa-containing nuage **(Figure 2-2-2)**. If true, an ATPase mutant form of BmVasa could in theory disrupt the dissociation of Siwi-D670A from nuage.

Single mutation at a conserved glutamate residue in the Walker B motif of BmVasa abolished ATP hydrolysis activity by preventing the release of ADP and RNA, which traps BmAgo3, Siwi and BmQin at an enlarged nuage (Xiol *et al*, 2014; Nishida *et al*, 2015). To characterize the subcellular localization of the BmVasa ATPase mutant, I adopted and generated the FP-tagged version of this ATPase mutant (E339Q). FP-tagged BmVasa-E339Q was transfected alone or co-transfected with FP-fused BmVasa or BmDcp2 to check for its nuage or piP-body localization. The result suggested that FP-tagged BmVasa-E339Q was not colocalized with BmDcp2 in piP-bodies **(Figure 2-5-1)**. On the other hand, BmVasa was found partially co-localized with BmVasa-E339Q **(Figure 2-5-2)**, with most of the foci located in the non-perinuclear region. It is thus concluded that BmVasa ATPase mutant forms cytoplasmic foci distinct from naive nuage and piP-body, which is, most probably, an aberrant yet nuage-like RNP aggregate.

Next, I co-expressed FP-fused Siwi and Siwi-D670A with FP-fused BmVasa or BmVasa-E339Q to check whether BmVasa ATPase activity is required for the displacement of Siwi-D670A

from nuage to piP-body or not. Both BmVasa and BmVasa-E339Q colocalized with Siwi **(Figure 2-5-3)**, which is in line with previous studies (Xiol *et al*, 2014). Unexpectedly, co-expression of Siwi-D670A and BmVasa-E339Q led to the formation of significantly enlarged aggregates **(Figure 2-5-3, 2-5-4)**, which in some cases the aggregates can grow beyond 10 square micron – almost 10 times larger than a typical nuage **(Figure 2-5-5)**. This strongly suggested that the helicase activity of BmVasa is highly efficient in dissociating Siwi-D670A aggregates, which prevents the formation of larger aggregates. Conversely, Siwi slicer activity was also efficient enough to prevent Vasa-E339Q from such aggregation. Given that Siwi-D670A colocalizes with piP-body proteins and BmVasa-E339Q primarily colocalizes with nuage proteins such as the two wildtype PIWIs, I speculated that the co-expression of these two mutants disrupted the proper partition between nuage and piP-bodies. This suggests that both BmVasa ATPase and Siwi slicer activities have non-redundant roles in sorting RNP contents across the two foci **(Figure 2-5-6)**.

Although the current model suggests that BmVasa-E339Q traps Siwi on its target RNA, the aggregation of Siwi in BmVasa-E339Q aggregates has remained to be confirmed. To check whether Siwi trapped by BmVasa-E339Q was loaded with piRNA or not, I co-expressed the 5′ binding pocket mutant Siwi-Y607E with BmVasa-E339Q. In line with the model, Siwi-Y607E did not colocalize with BmVasa-E339Q, suggesting that the co-aggregation of Siwi and BmVasa-E339Q aggregates requires piRNA loading and target binding **(Figure 2-5-7)**.

The N-terminal disordered region of Vasa human homolog DDX4 can nucleate phase separation *in vitro* (Nott *et al*, 2015). Whether the same region contributes to nuage assembly as well as the observed piRNA-dependent aggregation is unknown. To address this question, I

repeated the experiment with N-terminal truncated BmVasa and BmVasa-E339Q. The truncated mutant, or BmVasa-DelN and BmVasa-DelN-E339Q in short, showed no significant difference from their non-truncated counterpart at the microscopic level as both co-localized with Siwi and Siwi-D670A respectively **(Figure 2-5-8)**. These results, despite failing to provide a molecular explanation for the aggregation nucleated by BmVasa-E339Q, agreed with previous reports that N-terminal domains of BmVasa are dispensable for the interaction with PIWIs (Xiol *et al*, 2014). It has to be noted that this is not enough to disapprove the involvement of LLPS in nuage assembly, because the endogenous BmVasa is remained untouched and the disordered region-containing proteins are redundant in nuage, including both PIWIs. Instead, this finding suggests that the co-aggregation between BmVasa-E339Q and Siwi-D670A is not merely the result of the increased disordered protein regions but is likely to involve piRNA-RNA interactions.

To summarize, I found that both ATPase activity of BmVasa and slicer activity of Siwi are required for the RNP remodeling in nuage. In cases where one of the two wildtype counterparts is expressed, the size of aggregation was similar to those observed with naive nuage and piP-bodies. The aggregation only enlarges when both BmVasa ATPase mutant and Siwi slicer mutant are co-expressed, suggesting that both catalytic activities have non-redundant roles in enforcing proper partition of RNP contents into their respective condensates. This partition mechanism most likely involves RNA, as suggested by the Siwi-Y607E experiment and previous studies on BmVasa helicase activities (Xiol *et al*, 2014; Nishida *et al*, 2015).

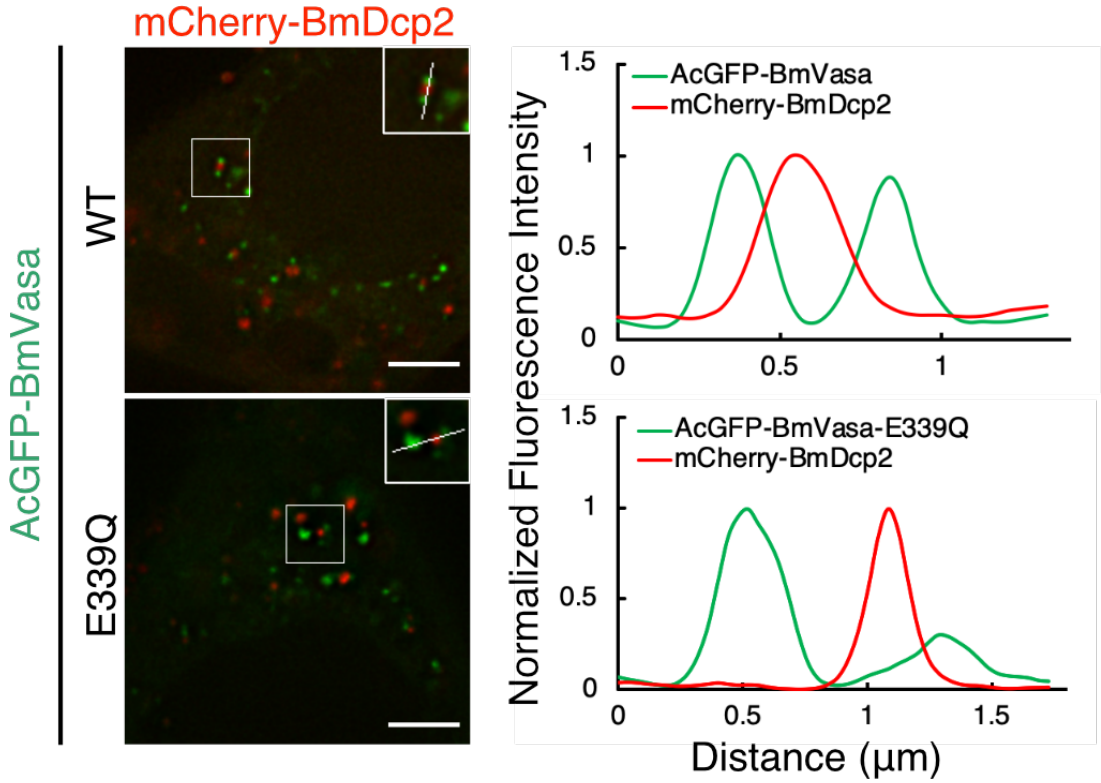

Figure 2-5-1. Localization of mCherry-BmDcp2 and AcGFP-BmVasa in BmN4 cells
BmDcp2 do not colocalize with BmVasa and BmVasa-E339Q. Line scans were normalized to the highest value. Scale bar 4 μm.

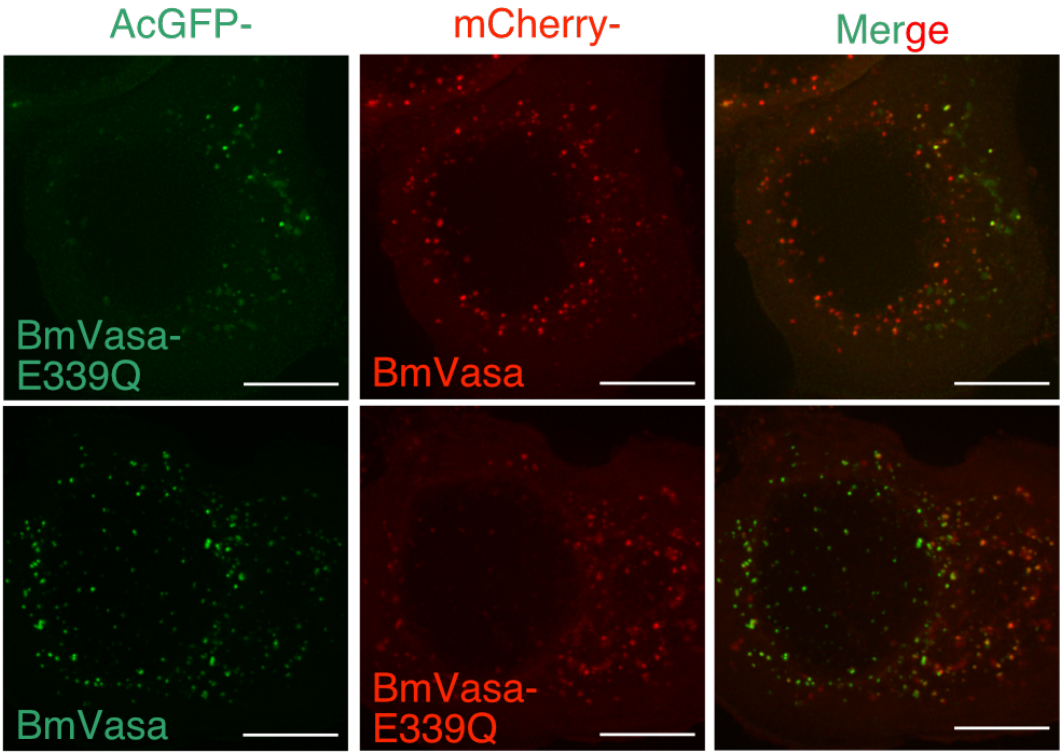

Figure 2-5-2. Localization of mCherry- and AcGFP-BmVasa-E339Q with wild-type BmVasa

Representative maximum intensity projections of wild-type BmVasa localized in perinuclear region and BmVasa-E339Q localized in non-perinuclear regions. BmVasa-E339Q partially colocalized with BmVasa. Scale bar 8 μm.

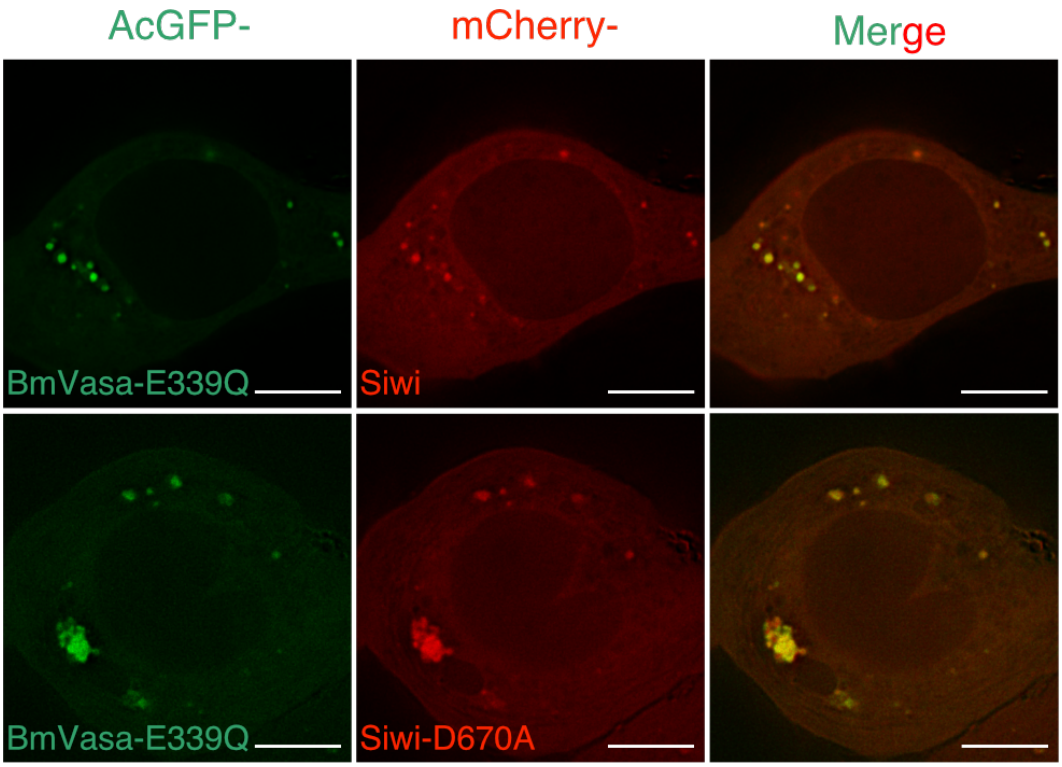

Figure 2-5-3. Co-aggregation of Siwi-D670A and BmVasa-E339Q in enormous cytoplasmic aggregates

Co-expression of BmVasa-E339Q and Siwi-D670A results in enormous aggregates with both mutants trapped. Wildtype Siwi does not cause any aggregation of comparable size. Scale bar 8 μm.

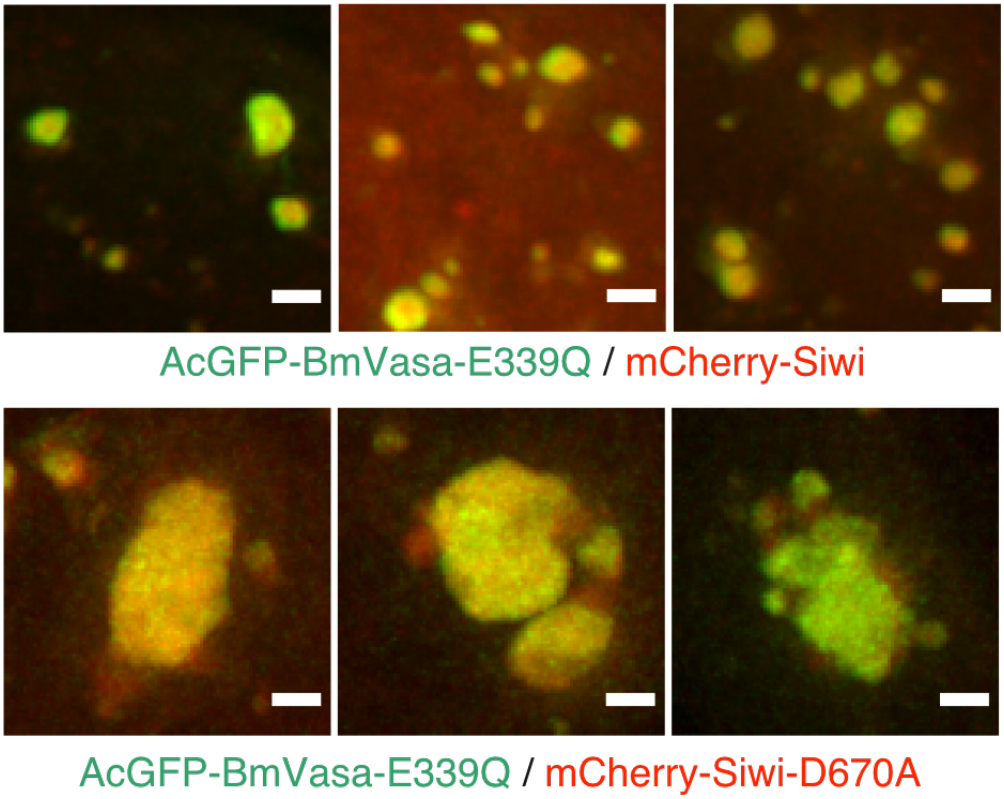

Figure 2-5-4. Co-expression of Siwi-D670A and BmVasa-E339Q results in aggregates with larger sizes

Representative maximum intensity projections of the Siwi-D670A and BmVasa-E339Q double mutant aggregates. Scale bar 1 μm.

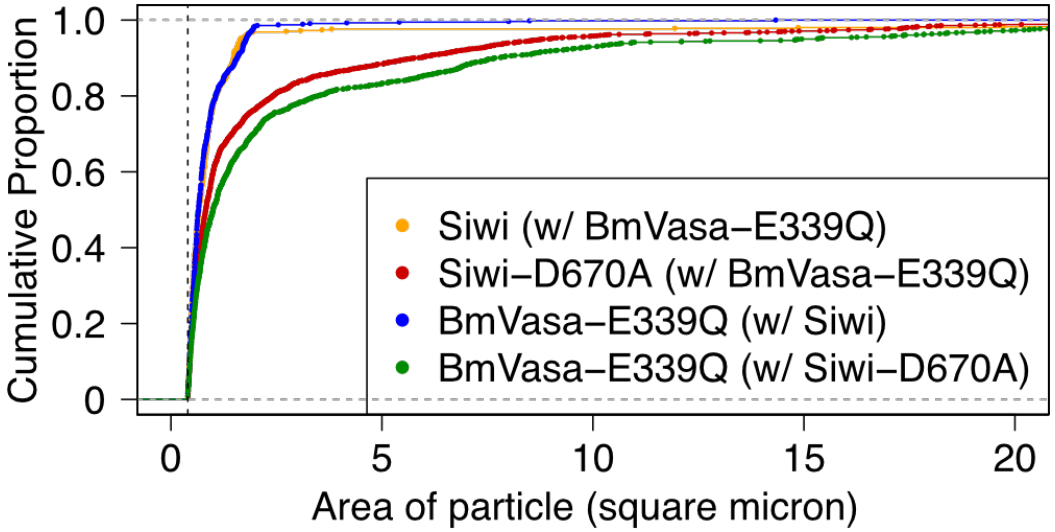

Figure 2-5-5. Cumulative proportion of the Siwi-D670A/BmVasa-E339Q aggregate area
More than 60% of the double-mutant aggregates have an increased sizes when compared to single-mutant aggregate.

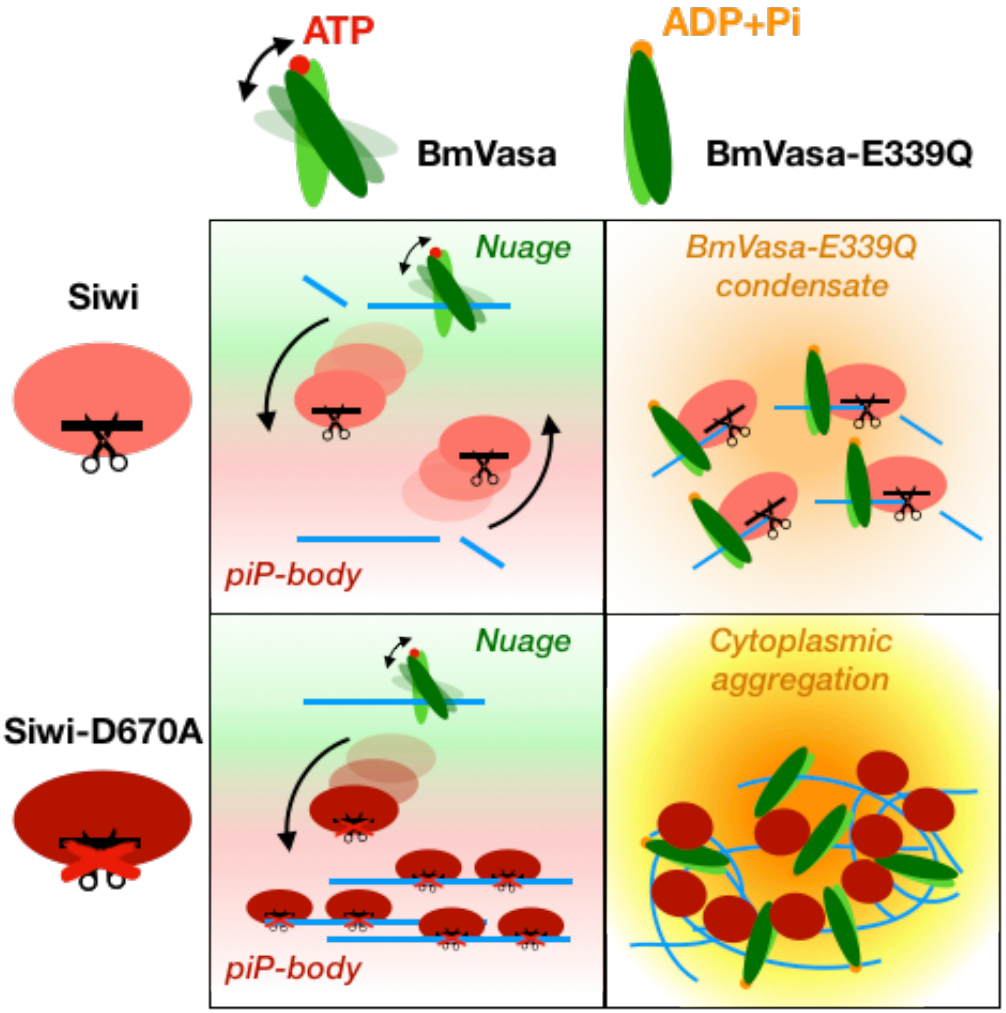

Figure 2-5-6. Siwi shuttles between nuage and piP-bodies
At steady state, wild-type Siwi is enriched in nuage but required for the piP-bodies assembly by physically interacting with BmSpnE and BmQin. Therefore, Siwi is likely to shuttle between nuage and piP-bodies in a transient manner. Siwi shuttling can be visualized by introducing D670A mutation to halt slicing, which causes the protein to retain in piP-bodies. Co-expressing Siwi-D670A and BmVasa-E339Q leads to the formation of enormous cytoplasmic aggregates, suggesting that BmVasa ATPase actively remodels RNP complexes and repel Siwi from nuage. Therefore, both BmVasa ATPase and Siwi slicer are required for Siwi shuttling.

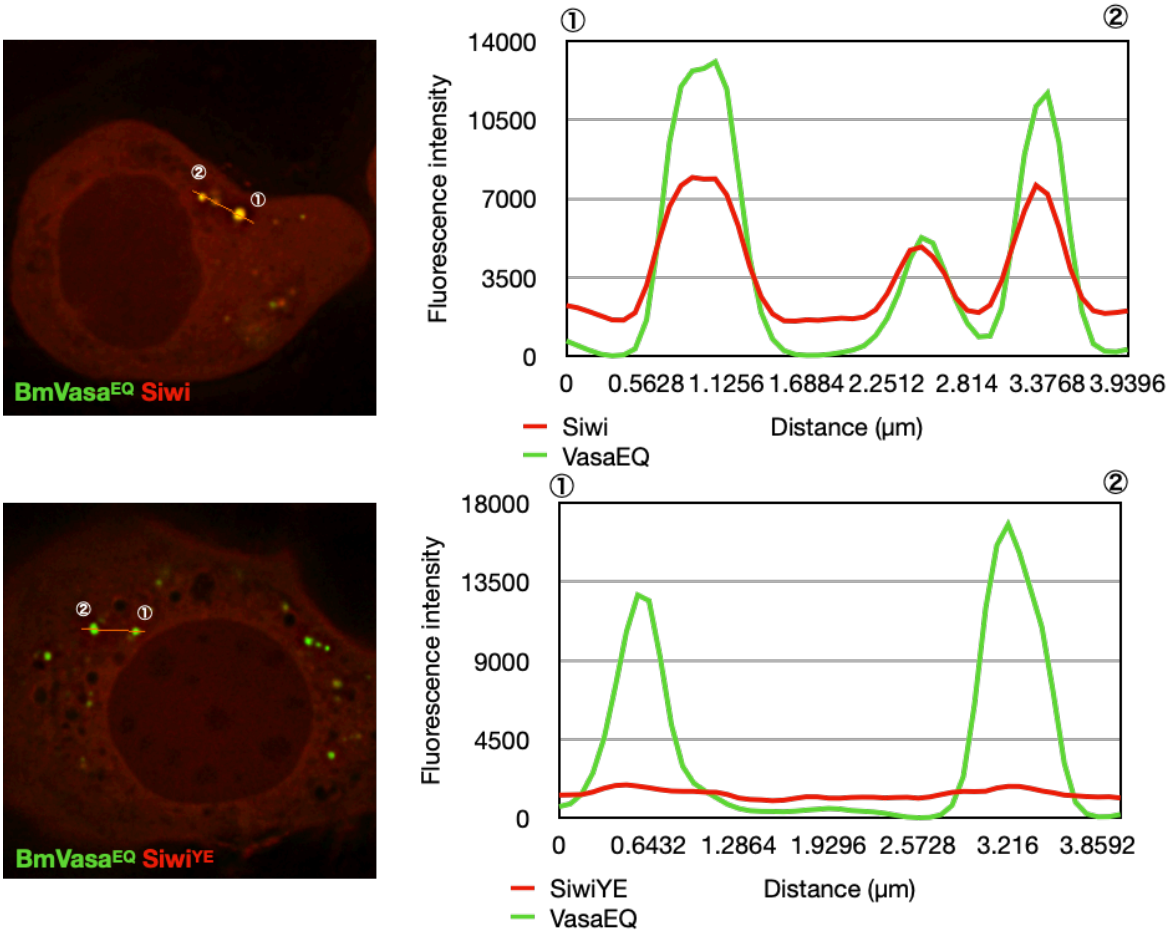

Figure 2-5-7. Colocalization between BmVasa-E339Q and Siwi impaired by piRNA loading mutation Y607E

Line scans (performed along the white line shown in the enlarged region) show that Siwi-Y607E lost its colocalization with BmVasa-E339Q. Line scan values were normalized to the highest value.

(a)

(b)

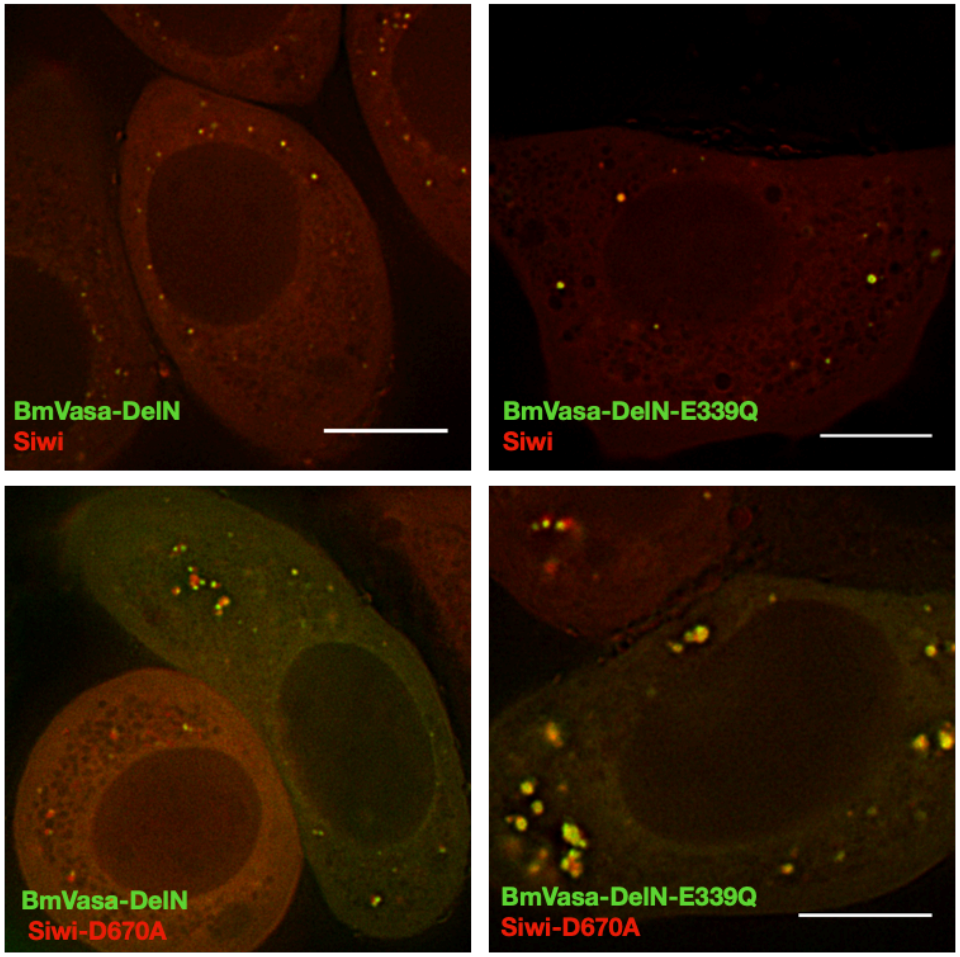

Figure 2-5-8. N-terminal domain of BmVasa is dispensible for its colocalization with Siwi
(a) Schematic diagram showing the truncated region (1-134 residues) of BmVasa. The same mutant was characterized by Xiol *et al* in 2014.
(b) Deconvolution microscopy of BmN4 co-expressing AcGFP-tagged BmVasa or BmVasa-DelN with mCherry-tagged Siwi or Siwi-D670A. NTD truncation has no effect on BmVasa-Siwi interaction and the aberrant aggregations observed. Scale bar 10 μm.

2.6. Disrupted nuage/piP-body partitioning causes mis-production of mRNA-derived piRNAs

The subcellular compartmentalization of the silkworm piRNA pathway in BmN4 cells coordinates the partition of piRNA factors into distinct RNP condensates. It is likely that the two condensates are the reaction site for different stages of the ping-pong cycle, given that PIWI proteins like Siwi shuttles between the compartments. However, the role of piP-body in piRNA biogenesis is still unclear. After all, the subcellular compartmentalization could mean little to piRNA biogenesis, similar to what has been observed with P-bodies and mRNA decay pathway (Eulalio *et al*, 2007; Stoecklin *et al*, 2006). Therefore, to study the significance of the nuage/piP-body subcellular compartmentalization, I performed small RNA sequencing (small RNA-seq) on BmN4 cells overexpressing Siwi-D670A and/or BmVasa-E339Q – both of which localizes to a piRNA condensate and are capable to disrupt local piRNA complexes.

I first checked the total piRNA levels in Siwi-D670A and/or BmVasa-E339Q overexpressed cells, after normalizing the total read-per-million (RPM) value to a few most abundant miRNAs (Izumi *et al*, 2016). The denatured gel electrophoresis and sequencing results both suggest that total piRNA level and peak length were not affected by the mutants **(Figure 2-6-1, 2-6-2)**. Since this is an overexpression experiment and the endogenous piRNA factors are not manipulated, it is reasonable that the mutant overexpression has minimal effects on the endogenous piRNAs, most of which are already bound by the endogenous PIWIs. Moreover, microscopy experiments suggested that BmVasa seems to repel BmVasa-E339Q **(Figure 2-5-2)** and Siwi-D670A **(Figure 2-2-2)** from nuage. It is possible that this activity may also reduce the negative effect on the ping-pong cycle.

To further explore the effect of Siwi-D670A/BmVasa-E339Q overexpression on the piRNA profile, I categorized the predicted silkworm genes into 3 groups – transposons (TEs), putative transposons (potential TEs) and non-transposon genes (non-TEs). The categorization was done by cross aligning the Silkbase Transposon Databases and Silkbase Gene Model (See also Materials and Methods). Potential TEs were first defined as a subgroup of non-TEs with mean piRNA RPM over 2^4 **(Figure 2-6-3)** and were further confirmed as potential TEs, as the mapped piRNAs largely distribute evenly on both sense and antisense of these genes – a feature not found in most other non-TE mRNAs **(Figure 2-6-4)**. It soon becomes clear that non-transposon-derived piRNAs were significantly upregulated by the presence of Siwi-D670A **(Figure 2-6-5)**. In contrast, TE-derived piRNAs and potential TE-derived piRNAs were not upregulated in Siwi-D670A expressing cells **(Figure 2-6-5)**. Intriguingly, the expression of non-TE-derived piRNAs was slightly reduced in BmVasa overexpressed cells, while modestly upregulated in BmVasa-E339Q overexpressed cells **(Figure 2-6-6)**. As a control, both BmAgo3 and BmAgo3 slicer mutant overexpressed cells displayed no significant changes in the level of TE- and non-TE-derived piRNAs **(Figure 2-6-6)**.

Next, I picked a few representative genes from each category and checked the piRNA coverage on the CDS of these genes. The result shows that non-TE piRNAs were increased throughout the CDS of constitutive genes like ribosomal protein S9 and eIF4E-1 **(Figure 2-6-7)** and were mapped only to the sense strand of the genes **(Figure 2-6-7, 2-6-4)**. In contrast, TE- and potential TE-derived piRNAs were mapped to both strands, suggesting that these piRNAs were generated through the ping-pong cycle **(Figure 2-6-7, 2-6-4)**. Previous studies have reported a

species of piRNA derived from 3′ UTRs of mRNAs (Robine *et al*, 2009). In the case of Siwi-D670A expressing cells, the upregulation of non-TE piRNAs was recorded in both UTRs and CDS **(Figure 2-6-8)**. In addition, non-TE piRNAs mostly arise from exon but not introns nor intergenic regions **(Figure 2-6-9)**, pointing to a cytoplasmic mRNA origin. In summary, Siwi-D670A induced non-TE piRNAs were promiscuously processed from mature, highly expressed cytoplasmic mRNAs without any bias towards the UTRs. While it is unlikely that these non-TE piRNAs were produced through the ping-pong cycle due to the sole strand directionality, it is unclear whether these piRNAs were produced by the primary pathway which requires BmZuc and BmArmi. To note, BmArmi co-aggregated with Siwi-D670A in piP-bodies when co-expressed **(Figure 2-2-10)**, which could possibly participate in the promiscuous production of non-TE piRNA directly in piP-bodies.

It is possible that these non-TE mapped "piRNAs" are in fact mRNA fragments due to mRNA degradation. To confirm whether the non-TE piRNAs were genuine piRNAs, I set out to check their length profile, 5′ nucleotide preference and the 2′-*O*-methylation. The upregulated non-TE piRNAs have a comparable length profile with the TE-derived piRNAs, with a single peak at 28-nt and weakly favor 5′ uracil – a hallmark of Siwi-loaded piRNAs **(Figure 2-6-10, 2-6-11)**. I next checked their status of 2′-*O*-methylation by treating input RNAs with sodium periodate ($NaIO_4$), which oxidizes all RNAs that are not protected at 3′-end and omits them from the small RNA library preparation steps. Resequencing results successfully reproduced the upregulation of non-TE-derived piRNAs by Siwi-D670A **(Figure 2-6-12)**. Importantly, the upregulated non-TE-derived piRNAs were resistant to $NaIO_4$ treatment, suggesting that they are *bona fide* 2′-*O*-methylated piRNAs **(Figure 2-6-12, 2-6-13)**.

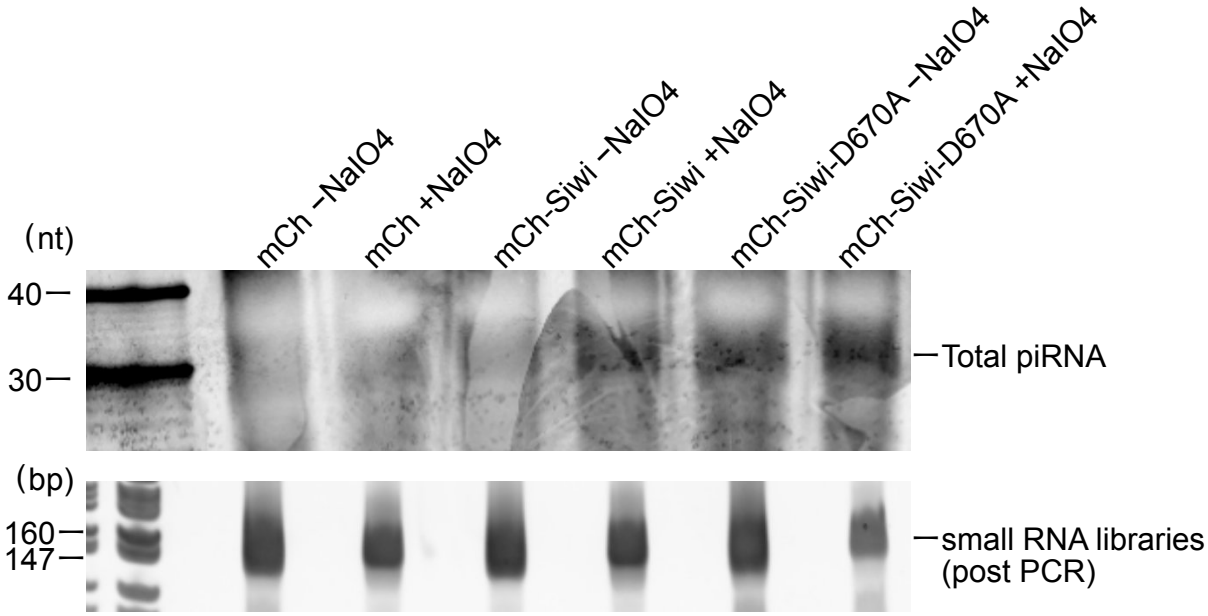

Figure 2-6-1. Gel analysis of pre-sequencing small RNA samples
(Top) Denatured polyacrylamide gel electrophoresis of BmN4 total RNAs.
(Bottom) TBE-PAGE of PCR-amplified small RNA libraries.

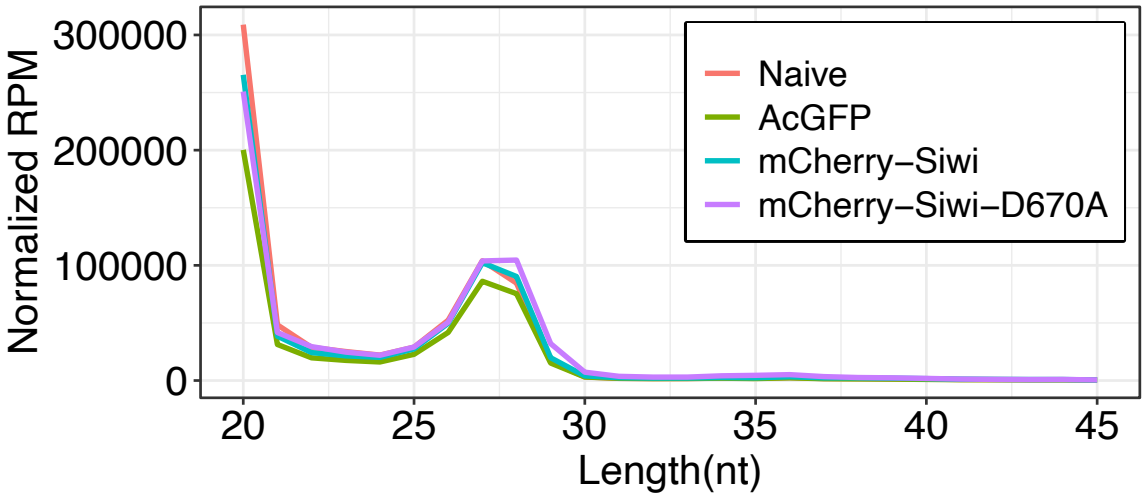

Figure 2-6-2. Length distribution of total small RNAs in BmN4 cells overexpressing AcGFP, mCherry-Siwi or mCherry-Siwi-D670A

The two peaks (20-nt and 27-nt) correspond to siRNA/miRNA and piRNA, respectively.

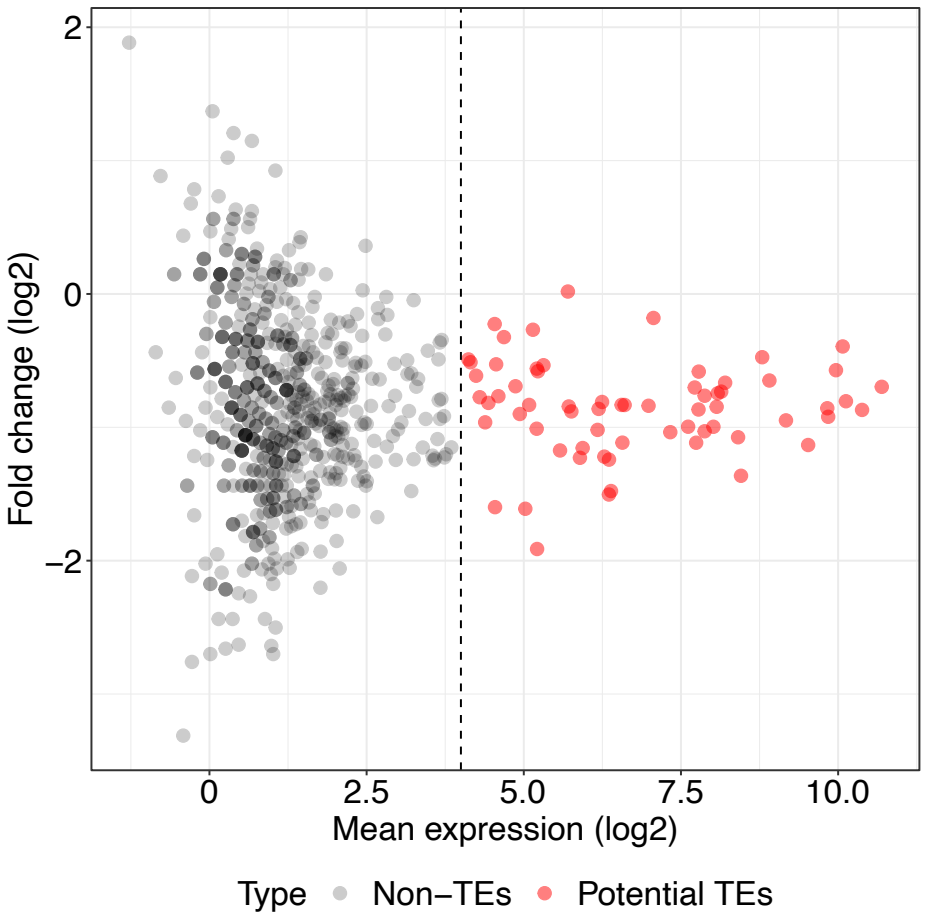

Figure 2-6-3. Differential piRNA expression analysis of the two naive small RNA libraries
Small RNA reads over 25-nt are mapped to genes (Silkbase GeneModel) that do not have a BLAST (tblastx) hit with transposons (Silkbase Transposon Database). A gene with an RPM higher than 2^4 is defined as potential transposon genes (potential TEs).

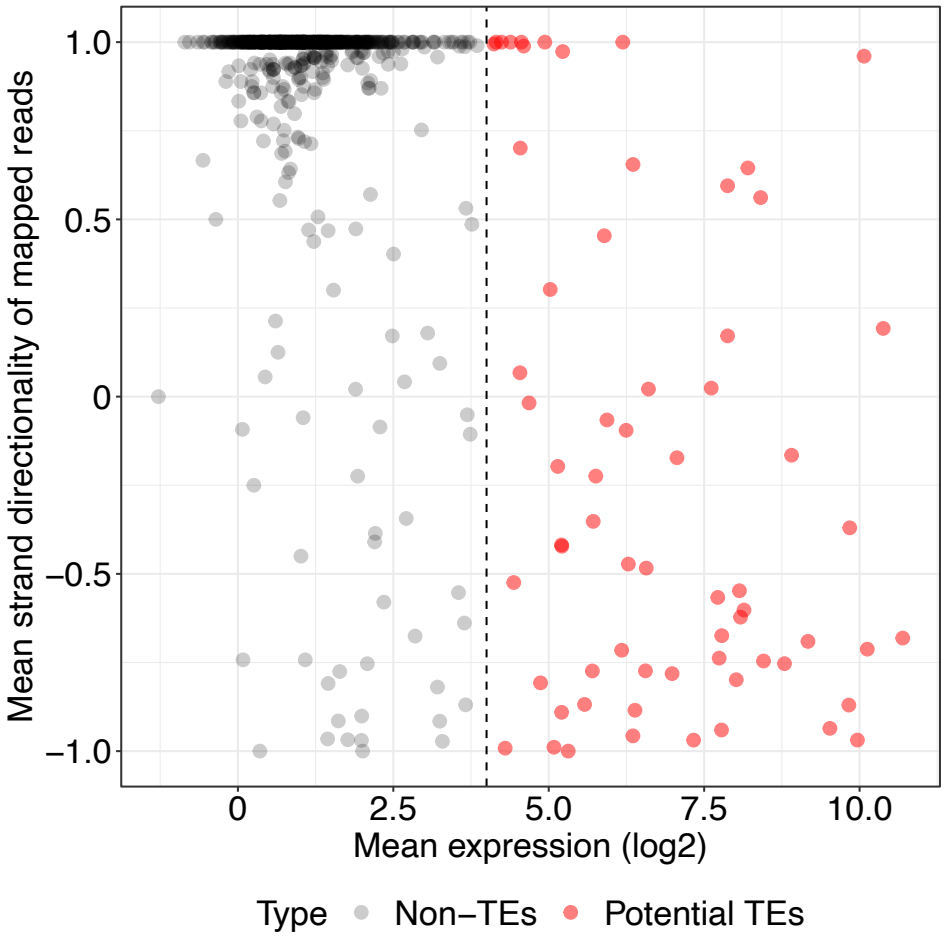

Figure 2-6-4. Analysis of the strand directionality of mapped piRNA reads
Strand directionality of piRNA reads is calculated by dividing sense reads over antisense reads. The mean directionality is calculated from the 2 naive libraries. Sense read mapped to a gene will have a 1.0 directionality value, while antisense reads will have a -1.0 value. Potential TEs are mapped with piRNA reads from both directions, suggesting that these piRNA are likely to be ping-pong piRNAs. Dashed line: expression threshold value (2^4 RPM) for the definition of potential TE genes.

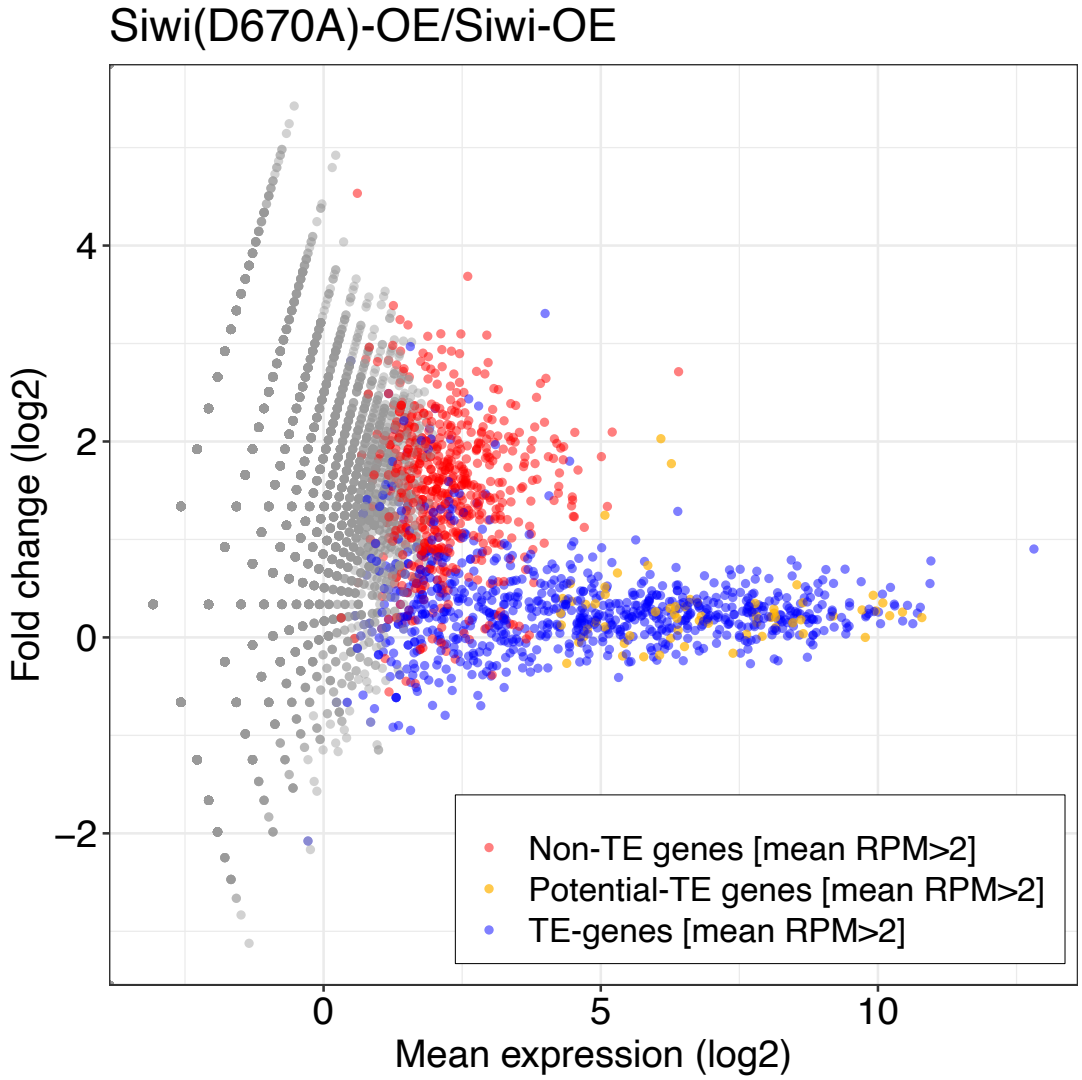

Figure 2-6-5. Differential piRNA expression analysis between Siwi-D670A and Siwi overexpressed BmN4 cells

Predicted CDSs were categorized into non-TE genes (red), potential-TE genes (orange), and TEs (blue). Each dot represents mapped piRNAs (> 25-nt) on a predicted silkworm gene. Siwi-D670A upregulates non-TE-derived piRNAs, while TE-derived piRNAs are not affected.

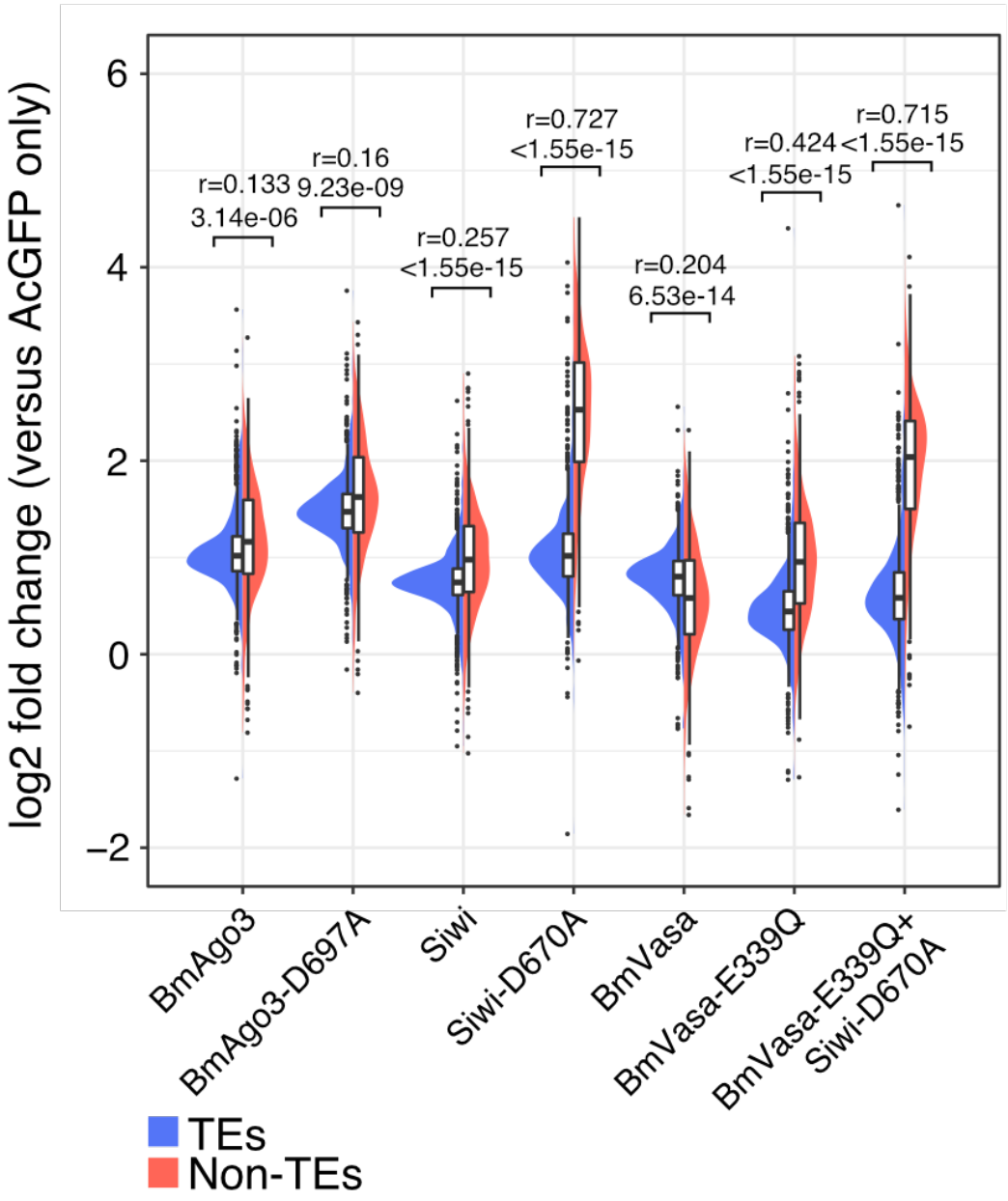

Figure 2-6-6. Split violin plots of piRNA expression fold change between AcGFP and piRNA factor(s) overexpressed BmN4 cells

Overexpression of Siwi-D670A, BmVasa-E339Q or both increases non-TE piRNA without altering the expression profile of TE-derived piRNA. Bonferroni-corrected P-values and the effect sizes (r) were calculated by asymptotic Wilcoxon rank sum test.

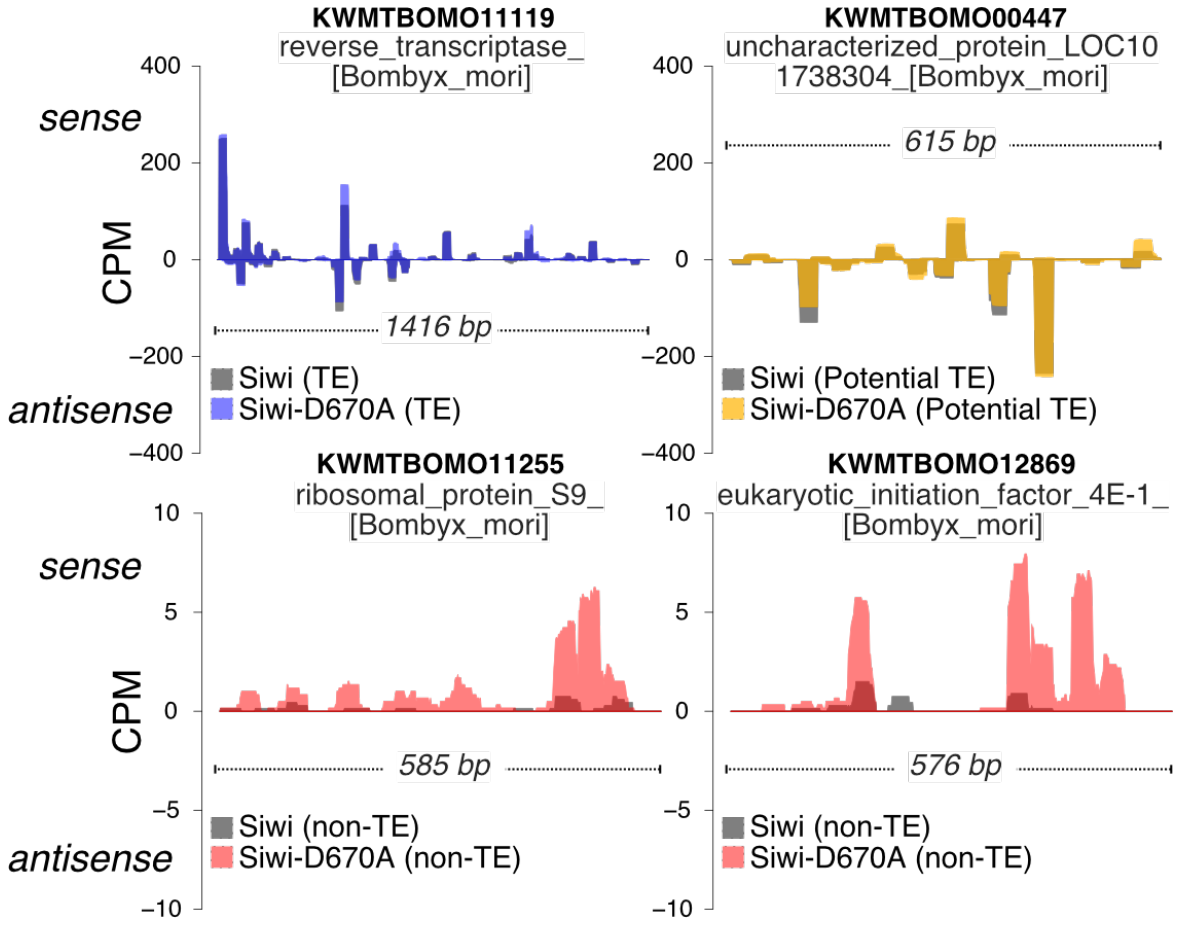

Figure 2-6-7. Normalized coverage per million (CPM) of piRNA mapped to the CDS sequence of 4 representative genes

(Top) Coverage of piRNA reads mapped to a TE gene (putative reverse transcriptase) and a potential TE gene (uncharacterized protein).

(Bottom) Coverage of piRNA reads mapped to 2 non-TE genes (ribosomal protein S9 and eIF4E-1) with elevated read counts in the Siwi-D670A library. No antisense non-TE piRNAs were observed in these examples.

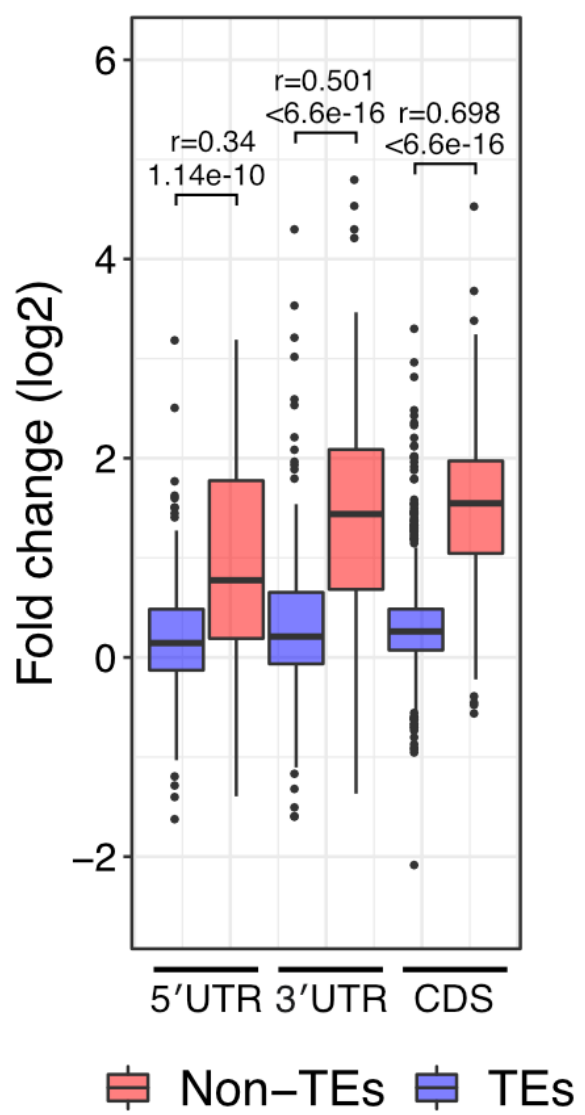

Figure 2-6-8. Fold change of piRNAs mapped to the UTRs and CDSs between Siwi-D670A and Siwi overexpressed libraries

Non-TE-derived piRNAs are similarly upregulated in 5′ UTR, CDS and 3′ UTR. Bonferroni-corrected P-values and the effect sizes (r) were calculated by asymptotic Wilcoxon rank sum test.

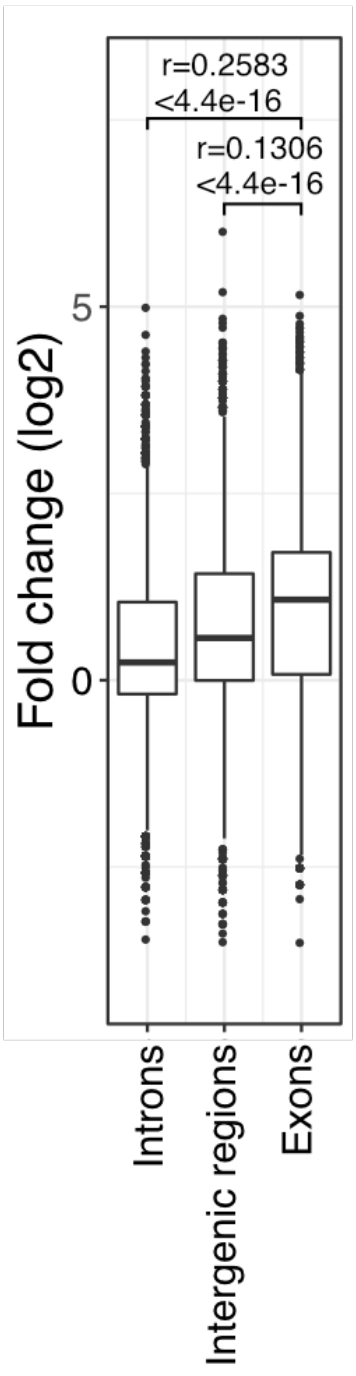

Figure 2-6-9. Fold change of piRNAs mapped to introns, intergenic regions, and exons between Siwi-D670A and Siwi overexpressed libraries
piRNAs upregulated by Siwi-D670A overexpression are mostly exonic. Bonferroni-corrected P-values and the effect sizes (r) were calculated by asymptotic Wilcoxon rank sum test.

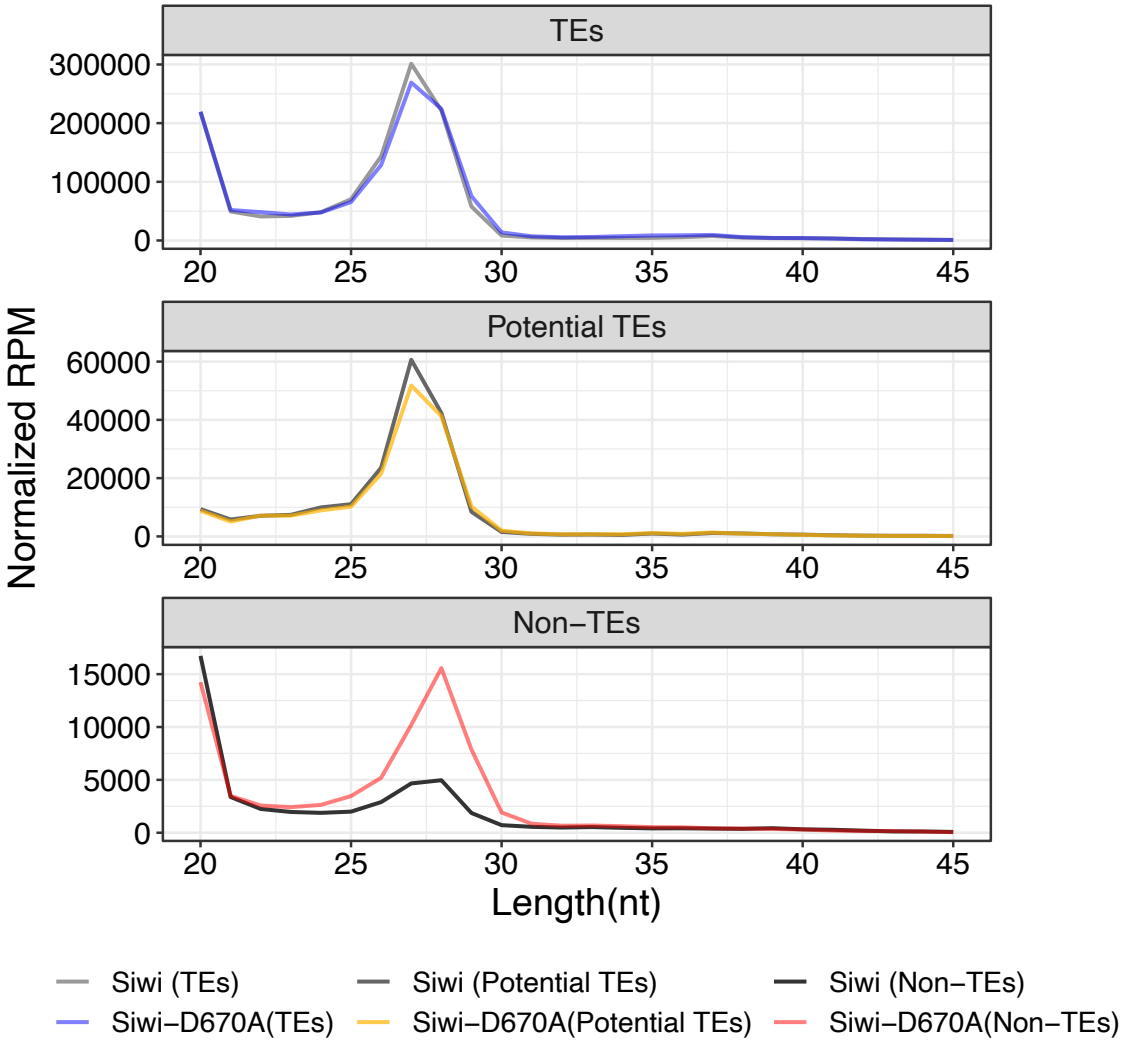

Figure 2-6-10. Length distribution of piRNA mapped to different groups of silkworm genes
For TEs and potential TEs, peak length of their mapped piRNA are both 27-nt, while peak length of piRNAs mapped to non-TEs is 28-nt. Siwi-D670A overexpression specifically upregulates 28-nt piRNAs but not 20-nt small RNAs.

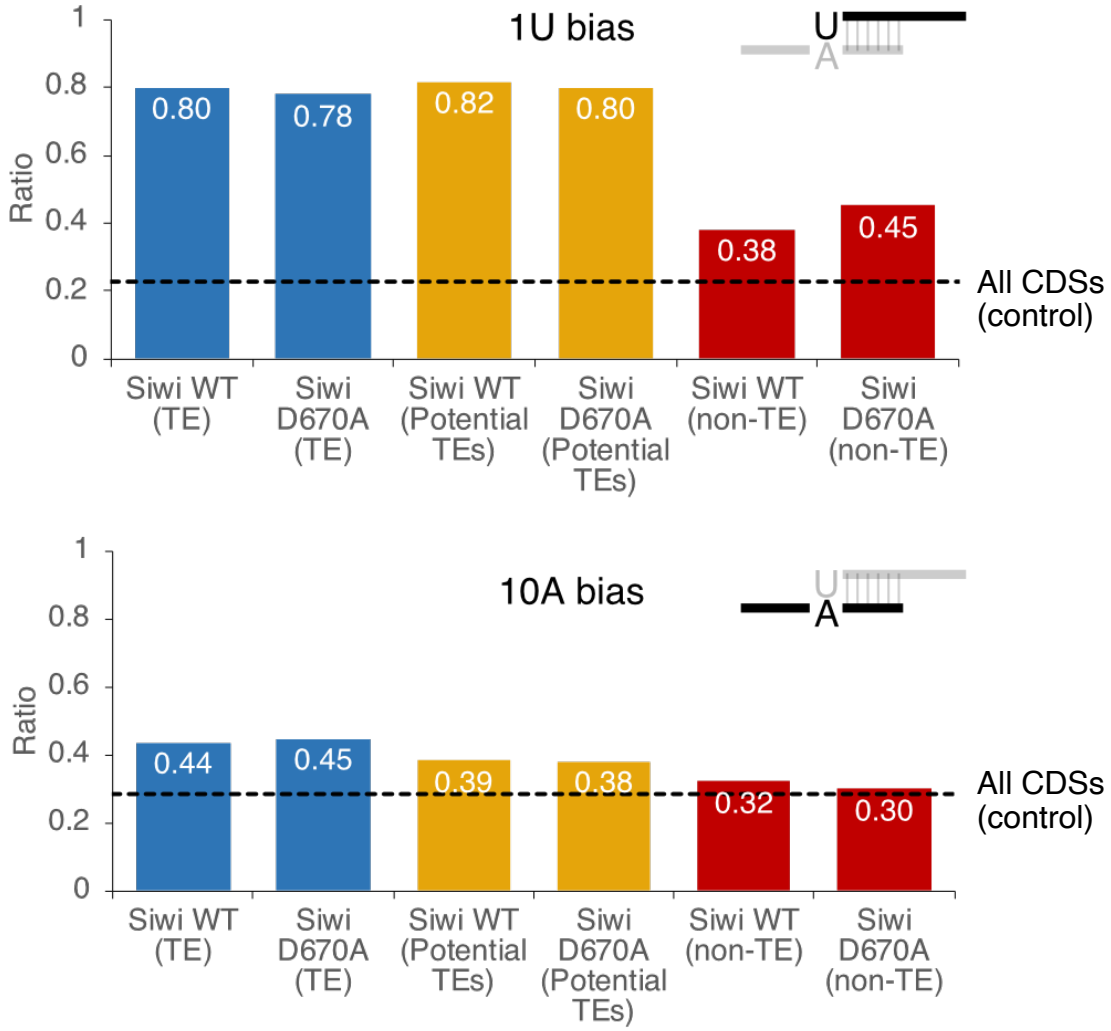

Figure 2-6-11. Non-TE-derived piRNAs in Siwi and Siwi-D670A libraries retained 1U but not 10A bias

(Top) Ratios of uracil forming the first nucleotide of piRNAs in TEs and potential TEs are roughly 80% in both libraries (1U bias). Such 1U bias is retained at 38% in Siwi-WT library and 45% in Siwi-D670A library in non-TE piRNAs, which is above the control (the frequency of uracil in all CDSs, 23%, black dotted line), suggesting the mapped reads contain 1U-biased bona fide piRNAs.

(Bottom) Ratios of adenine at the 10th nucleotide which usually found in ping-pong piRNAs (10A bias). The 10th nucleotides of TE piRNAs (~ 44%) and potential TE piRNAs (~ 38%) are mildly favor adenine and are significantly higher when compared with the control (frequency of adenine in all CDSs, 29%, black dotted line). Non-TE-derived piRNAs have a similar 10A ratio with the control (~ 30%, similar to the control), suggesting that non-TE-derived piRNAs are not produced by the ping-pong cycle.

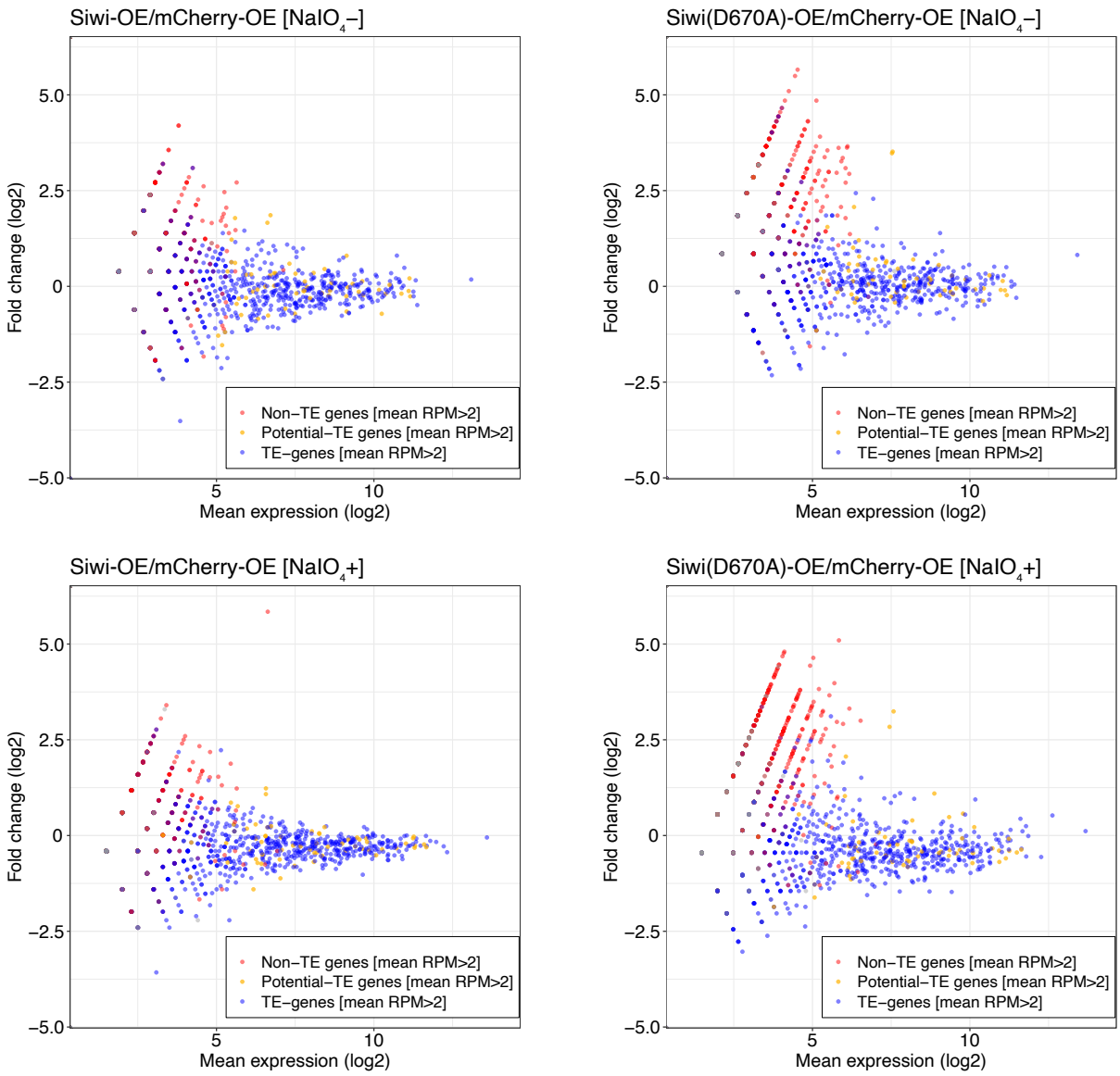

Figure 2-6-12. Differential piRNA expression analysis of Siwi/Siwi-D670A-overexpressed (OE) BmN4 cells against mCherry-OE cells

piRNA reads from Siwi-OE or Siwi-D670A-OE libraries that are longer than 25-nt are mapped to silkworm CDSs (Silkbase GeneModel). Non-TE piRNA reads are upregulated only in Siwi-D670A-OE cells. $NaIO_4$ treatment did not deplete non-TE piRNA reads, suggesting that these reads are protected at their 3′-end, likely by 2′-OMe modification same as the other piRNAs.

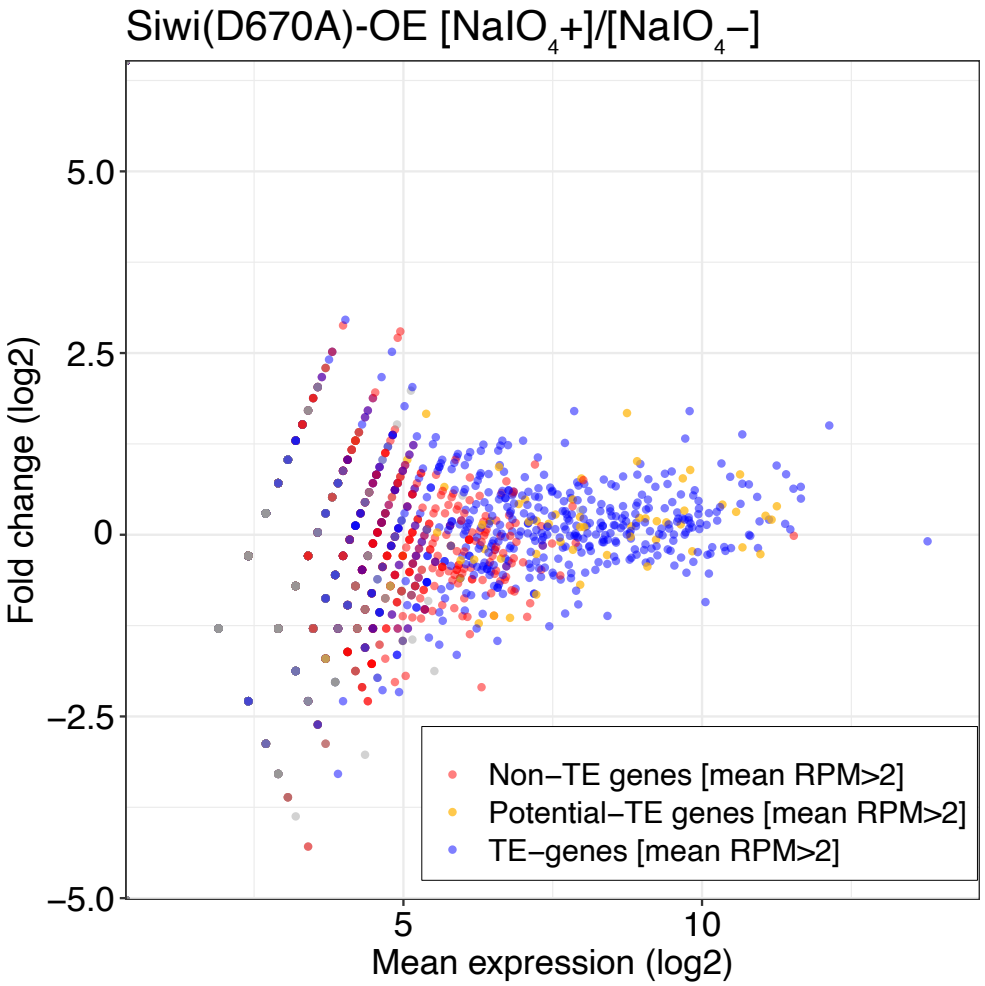

Figure 2-6-13. MA plot of $NaIO_4$ + against $NaIO_4$ – small RNA libraries from Siwi-D670A-OE cells

$NaIO_4$ treatment did not deplete non-TE piRNAs, despite that a mild depletion of the less abundant piRNAs is observed similarly with TE, potential TE and non-TE piRNAs.

2.7. BmSpnE ATPase activity is required for proper Siwi-associated piRNA biogenesis

If the nuage RNA helicase BmVasa repelled Siwi-D670A from nuage by remodeling RNP complexes, then why the piP-body RNA helicase BmSpnE would not? SpnE homolog in mice (TDRD9) is known to facilitate transposon silencing but dispensable in piRNA production (Shoji *et al*, 2009; Wenda *et al*, 2017). However, in fruit fly and silkworms, SpnE is required for piRNA production through an unknown pathway (Malone *et al*, 2009; Czech *et al*, 2013; Nishida *et al*, 2015). While multiple models have been proposed (Shoji *et al*, 2009; Wenda *et al*, 2017; Andress *et al*, 2016; Nishida *et al*, 2015), the biological function of SpnE is seemingly not conserved and is often loosely defined.

In the BmN4 context, BmSpnE is a piP-body protein that complexes with BmQin and strongly co-accumulates with Siwi-D670A. BmSpnE is sometimes enriched in a few granule-like puncta but remains largely dispersed **(Figure 2-1-1)**, which is similar to Siwi. Given that BmSpnE can be readily co-purified with Siwi (Nishida *et al*, 2015), BmSpnE is likely to interact physically with Siwi in the vast cytoplasm and in the piP-bodies. It is therefore tempting to ask whether the ATP-dependent helicase activity of BmSpnE facilitates the cytoplasmic relocation of Siwi or not. To study the function of BmSpnE ATPase, I mutated the conserved DExD-box helicase domain of BmSpnE in a similar way to BmVasa-E339Q. This resulted in the BmSpnE-E251Q mutant, an RNA binding mutant that does not bind with BmQin (Nishida *et al*, 2015).

By expressing the FP-tagged version of BmSpnE-E251Q, I found that the localization of BmSpnE was sharply changed by E251Q mutation **(Figure 2-7-1)**. Instead of largely dispersed, the foci of the mutant appear to be some sharp yet irregular aggregates in the cytoplasm. To test

whether BmSpnE-E251Q resides in P-body, I performed a colocalization test with BmQin and BmDcp2. It was found that both FP-tagged BmSpnE and BmSpnE-E251Q were colocalizing with BmDcp2 and BmQin **(Figure 2-7-2)**. This conflicts with a previous study as the authors reported that the BmSpnE-E251Q mutation impairs the proteins' interaction with BmQin (Nishida *et al*, 2015). Nevertheless, it is important to note that the colocalization is not enough to prove the physical interaction between two proteins, as indirect interaction via other components in the same complex can also result in colocalization. In line with the above observation, E251Q mutation did not abolish the colocalization between BmSpnE and Siwi-D670A **(Figure 2-7-3)**. Instead, BmSpnE-E251Q mutant was found explicitly colocalized with wildtype Siwi **(Figure 2-7-3)**, which was not the case when co-expressed with wildtype BmSpnE **(Figure 2-2-3)**. Therefore, expression of the ATPase mutant form of BmSpnE results in trapping wildtype Siwi in cytoplasmic aggregates without disturbing the piP-bodies.

In the case of BmVasa-E339Q, the ATPase mutant formed non-perinuclear aggregates with wildtype Siwi, Siwi-D670A and other nuage proteins which are in the non-perinuclear region **(Figure 2-5-2)**. For piP-body, such change will not be visible if the condensate by default localizes in the non-perinuclear region of the cytoplasm. Therefore, to study the effect of BmSpnE ATPase mutant on piP-bodies, I performed immunoprecipitation experiments with cells co-expressing piP-body piRNA factors (BmSpnE, BmSpnE-E251Q, BmQin and BmMael) and traditional P-body markers. For the P-body markers, in addition to BmDcp2, I also included BmMe31B, which is the silkworm homolog of human DDX6 (also known as rck/p54), a core P-body DEAD-box helicase that is required for P-body assembly (Serman *et al*, 2007; Minshall *et al*, 2009). In contrast to the colocalization analyses, immunoprecipitation suggests that most piP-body factors – except

BmMael – did not co-purify with BmDcp2 or BmMe31B **(Figure 2-7-4)**. Strikingly, I found that BmSpnE-E251Q but not wildtype BmSpnE strongly co-purified with BmMe31B **(Figure 2-7-4)**. This suggests that BmSpnE ATPase is regulating interactions between piRNA factors and constitutive P-body factors.

In order to investigate the importance of BmSpnE ATPase activity on piRNA biogenesis, I performed piRNA sequencing (piRNA-seq) on BmN4 cells overexpressed with wildtype BmSpnE or BmSpnE-E251Q. While mature piRNA with a length distribution peaked at 28-nt was not altered by BmSpnE-E251Q expression, I found a subtle increase in piRNA precursor reads ranging from 32−42-nt long **(Figure 2-7-5)**. To check whether these piRNA precursors are Siwi-specific or BmAgo3-specific, I divided the silkworm piRNA database used in Izumi *et al*., 2016 into 10 groups by comparing their amount recovered from Siwi-IP and BmAgo3-IP **(Figure 2-7-6)**. The result shows that these precursors were mostly consisted of Siwi-specific piRNA precursors (Group 1-6) **(Figure 2-7-7)**, suggesting that BmSpnE ATPase activity is required for the maturation of Siwi-piRNA precursors. In contrast, overexpression of BmSpnE alone did not cause the accumulation of Siwi-piRNA precursors. To take a closer look at the function of BmSpnE, I analyzed two piRNA loci from the silkworm piRNA database, piRNA-1289 and piRNA-1059, which are Siwi-specific (Group 4) and BmAgo3-specific (Group 8) piRNA locus respectively. Both loci have a double-peak length distribution, with a mature piRNA peak at 27 or 28-nt and a precursor piRNA peak at 36-nt. For the Siwi-specific piRNA-1289, both BmSpnE-E251Q overexpression and BmSpnE knockdown caused an increase at the 36-nt precursor piRNA peak **(Figure 2-7-8, 2-7-9)**. In contrast, BmAgo3-specific piRNA-1059 was not affected **(Figure 2-7-8, 2-7-9)**. Analysis of BmAgo3-IP and Siwi-IP libraries shows that piRNA-1289 was

specifically accumulated in immunopurified BmAgo3 as a 36-nt long piRNA precursor (pre-piRNA-1289) **(Figure 2-7-10)**. These results argue for the role of BmSpnE ATPase in facilitating Siwi piRNA production at the BmAgo3-to-Siwi axis of the ping-pong cycle.

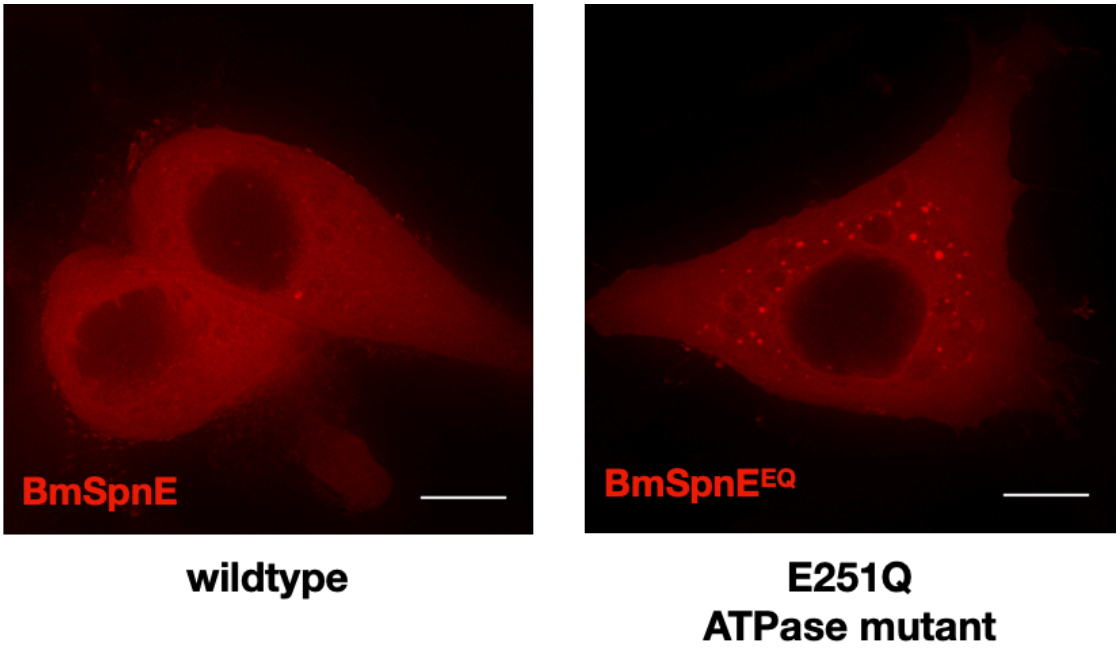

Figure 2-7-1. Subcellular localization of wildtype BmSpnE and the E251Q mutant
Representative Z-stacks of BmN4 cells expressing mCherry-tagged BmSpnE or the E251Q ATPase mutant. Images acquired from Z-stacks with 0.2μm spacing. The E251Q mutation caused aggregation in cytoplasm. Scale bar 10 μm.

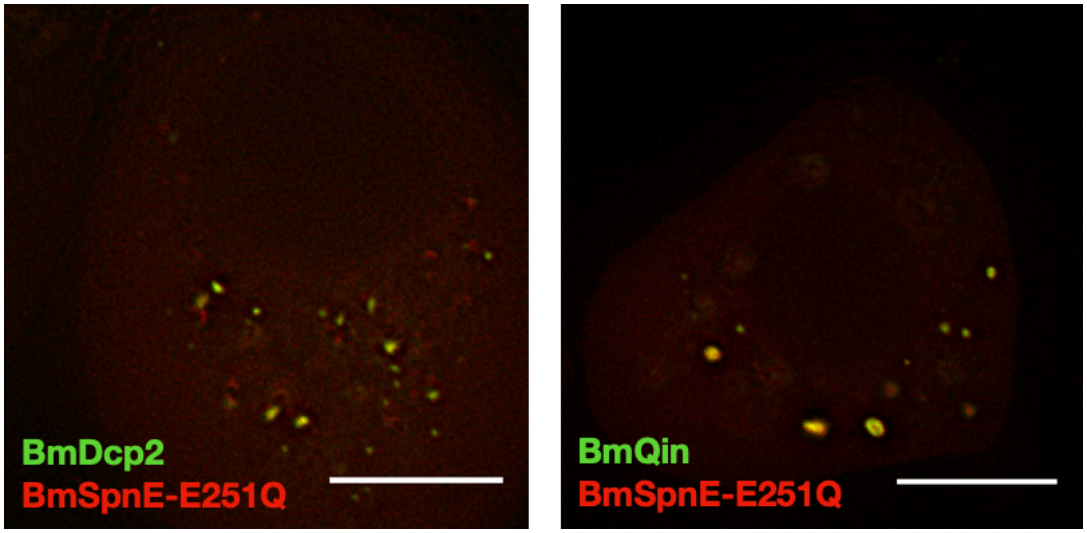

Figure 2-7-2. Co-localization of BmSpnE-E251Q mutant to BmDcp2 and BmQin
Deconvolution microscopy of BmN4 cells expressing mCherry-tagged BmSpnE-E251Q and piP-body proteins. The mutant co-localized with BmQin and BmDcp2 but also found in other non-P-body foci. Scale bar 10 μm.

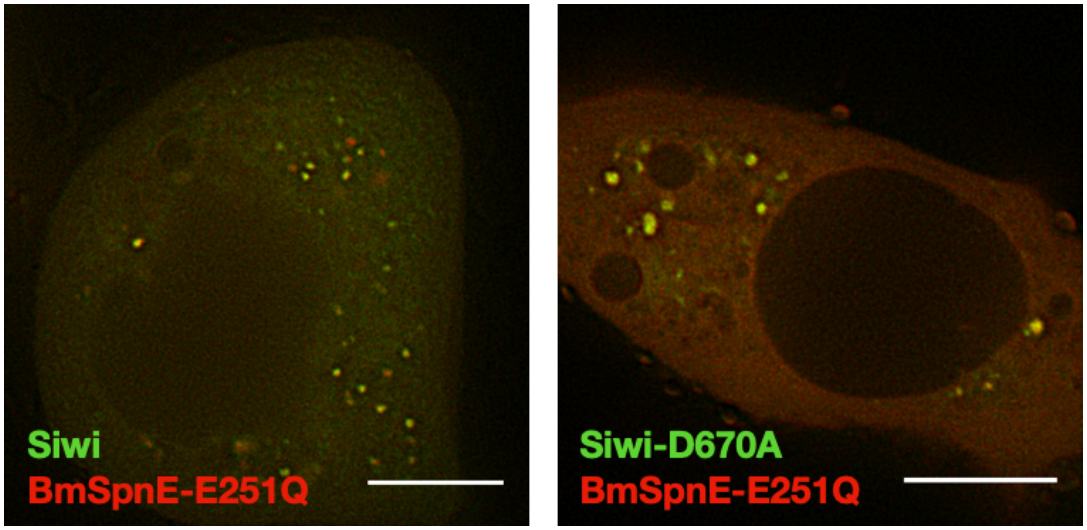

Figure 2-7-3. Co-localization of BmSpnE-E251Q mutants with Siwi and Siwi-D670A
Deconvolution microscopy of BmN4 cells co-expressing mCherry-tagged BmSpnE E251Q with AcGFP-tagged Siwi or Siwi-D670A. Scale bar 10μm.

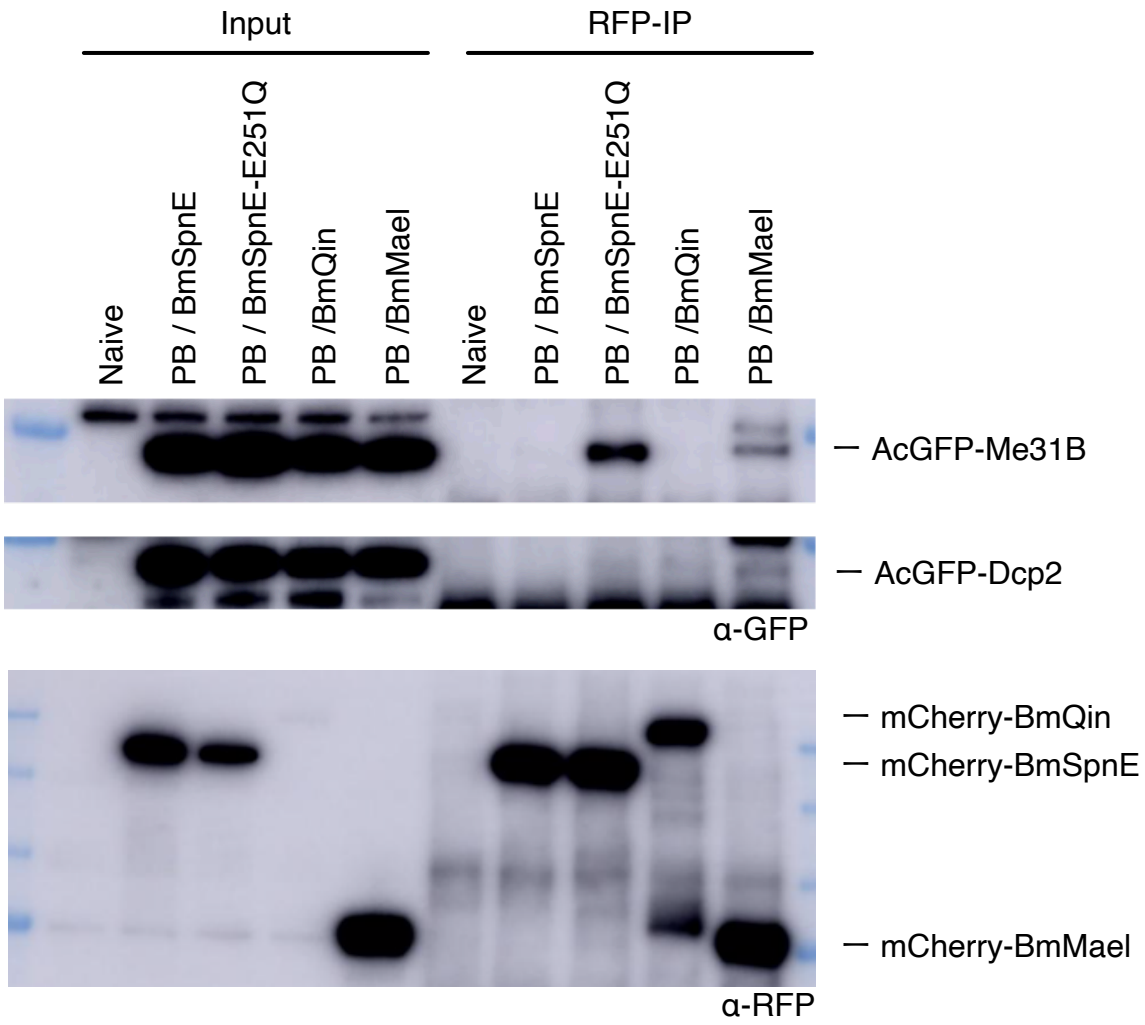

Figure 2-7-4. Immunoprecipitation of piP-body factors revealed physical association with constitutive P-body factors

RFP-immunoprecipitation of mCherry-BmQin, BmSpnE or BmMael revealed that most piP-body proteins except BmMael did not co-purified with constitutive P-body factors. Mutation of BmSpnE ATPase causes the mutant to bind physically to BmMe31B, the core P-body helicase.

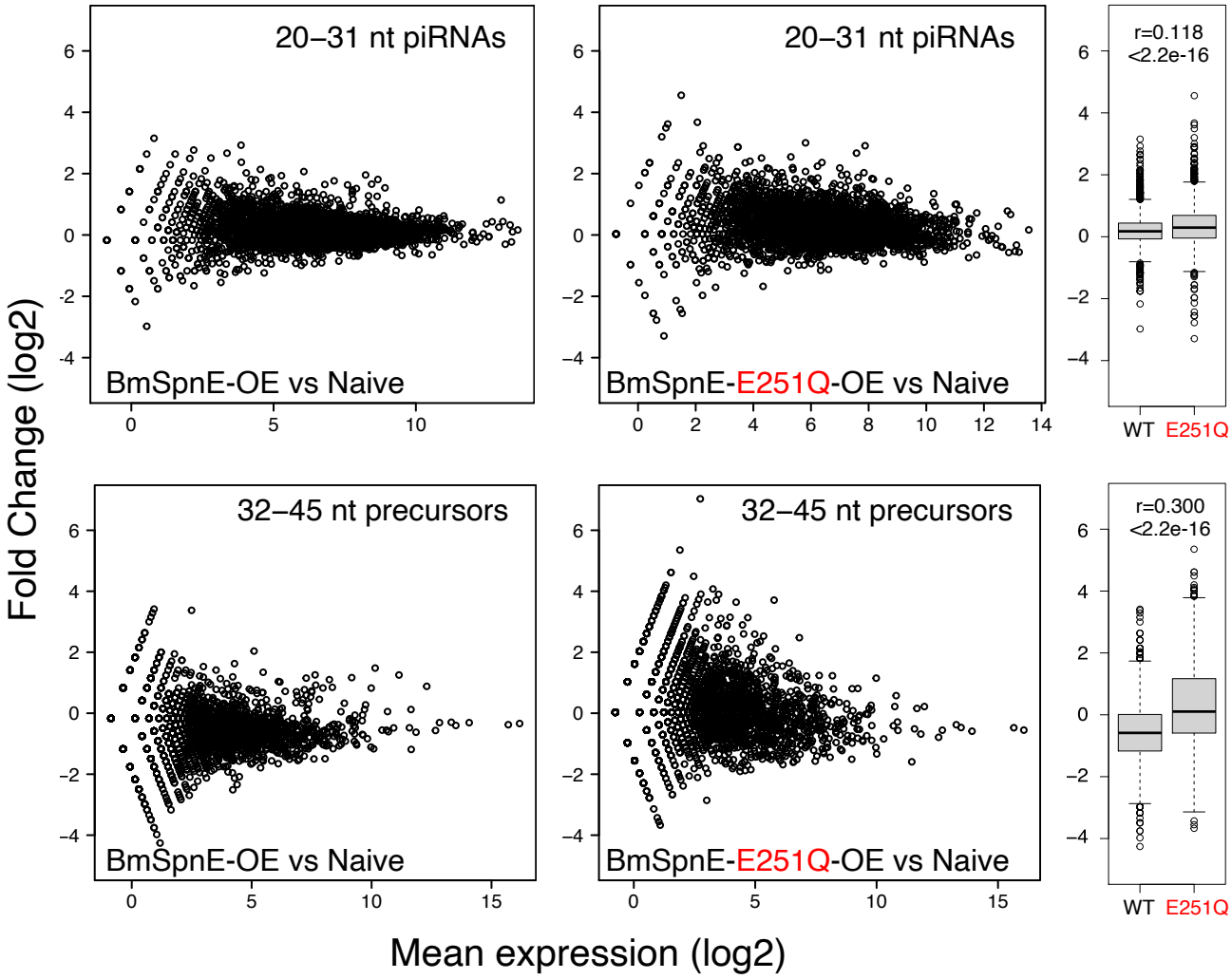

Figure 2-7-5. piRNA precursors accumulate in BmSpnE-E251Q expressing BmN4 cells
(Left) Fold change of piRNAs (20 to 31-nt) and piRNA precursors (32 to 45-nt) reads between BmSpnE-overexpressed (OE) and BmSpnE-E251Q-OE cells. Overexpression of BmSpnE-E251Q did not affect mature piRNA level (top), but instead causes a subtle accumulation of piRNA precuror when compared to wildtype BmSpnE-OE (bottom).
(Right) Boxplots depicting the total population of all data points in the scatter plots at left. Bonferroni-corrected P-values and the effect sizes (r) were calculated by asymptotic Wilcoxon rank sum test.

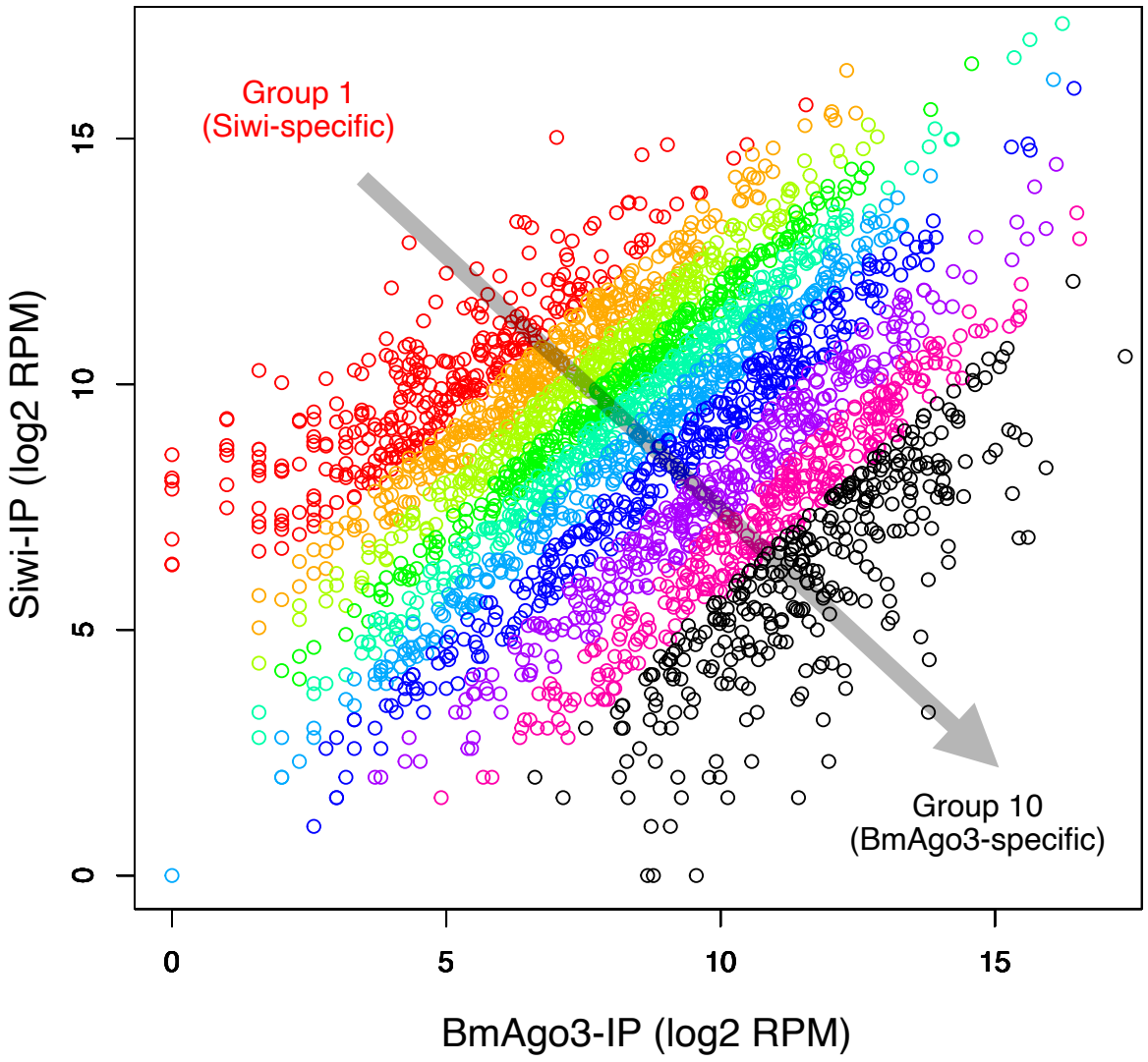

Figure 2-7-6. Definition of Siwi/BmAgo3-specific piRNAs
To define Siwi-specific piRNAs and BmAgo3-specific piRNAs, piRNAs co-purified from Siwi-immunoprecipiation (IP) and BmAgo3-IP were sequenced and mapped against silkworm piRNA database in described in Izumi *et al* 2016. These piRNA loci were than divided into 10 groups, with Group 1 containing Siwi-specific piRNAs and Group 10 containing BmAgo3-specific piRNAs.

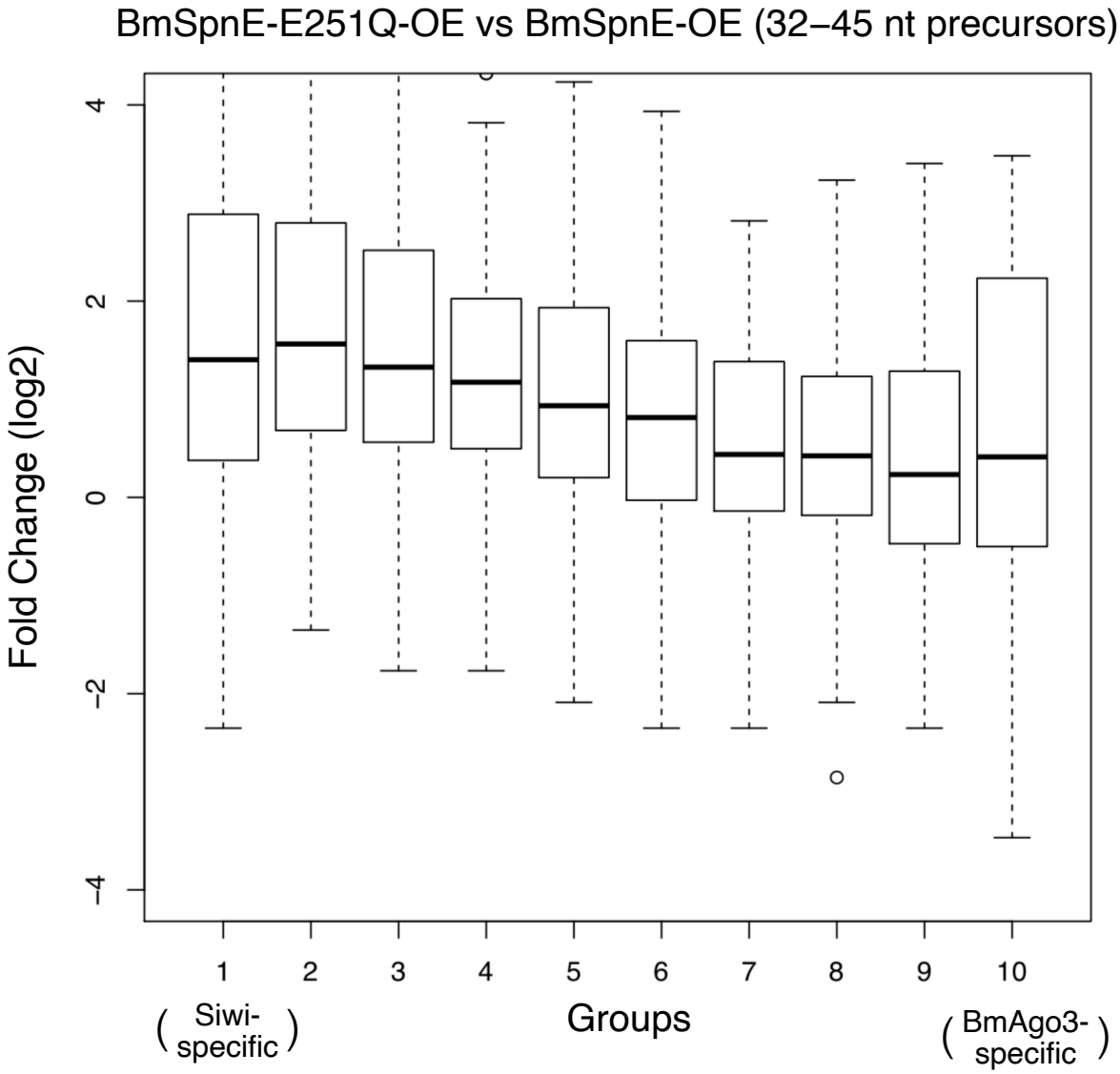

Figure 2-7-7. Accumulated piRNA precursors in BmSpnE-E251Q expressing cells are Siwi-dominant pre-piRNA

Fold change of pre-piRNA (32 to 45-nt) expression in BmSpnE-E251Q-OE cells was calculated by comparing to wildtype BmSpnE-OE cells. Applying the piRNA groups defined in Figure 2-7-6 revealed a clear tendency where Siwi-specific pre-piRNAs were specifically upregulated by BmSpnE-E251Q-OE.

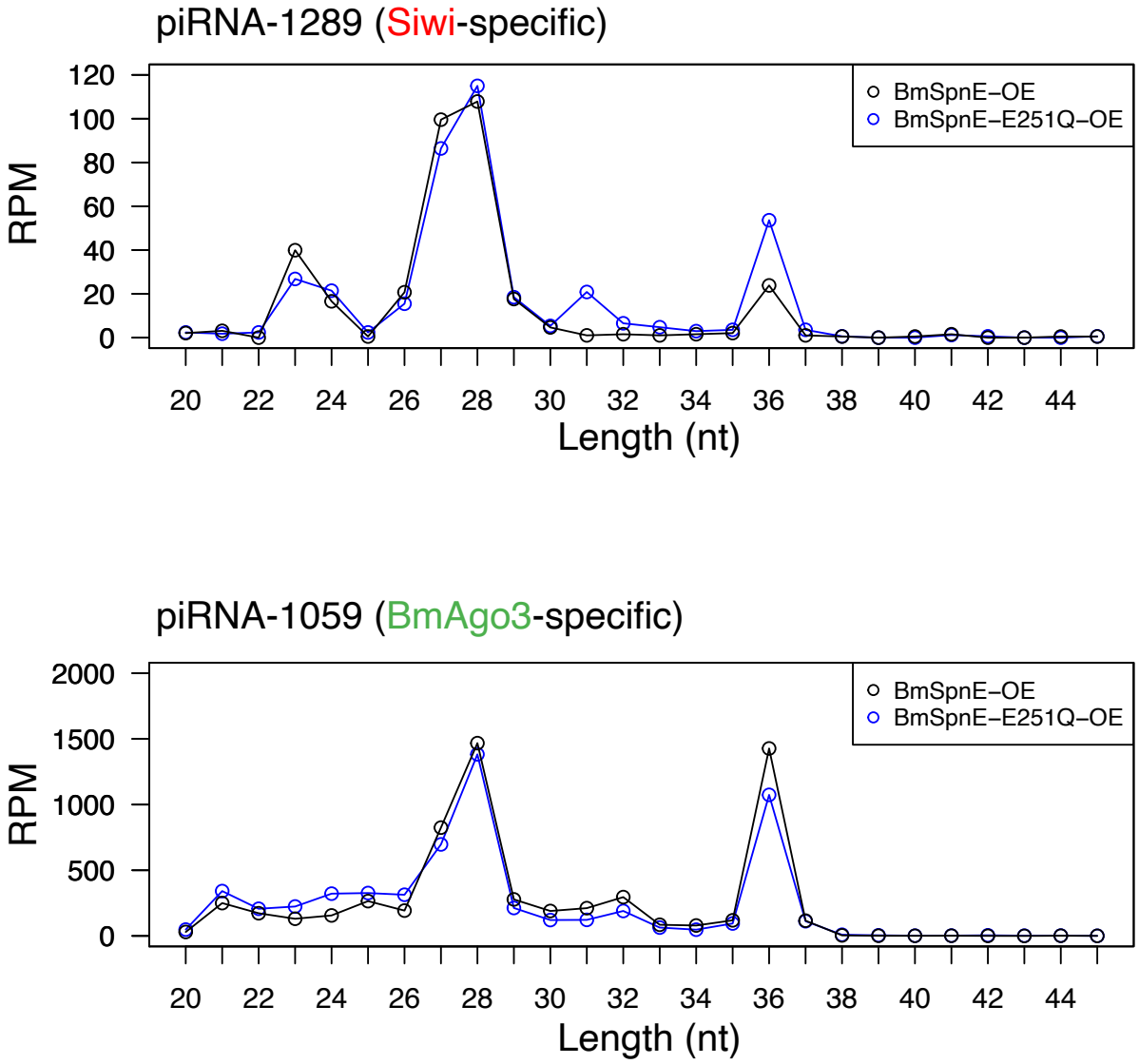

Figure 2-7-8. BmSpnE-E251Q upregulated the 36-nt long precusor of a Siwi-specific piRNA

While both Siwi-specific piRNA-1289 and BmAgo3-specific piRNA-1059 are peaked at 28-nt and 36-nt, only the precursor peak of piRNA-1289 was upregulated by BmSpnE-E251Q mutant overexpression.

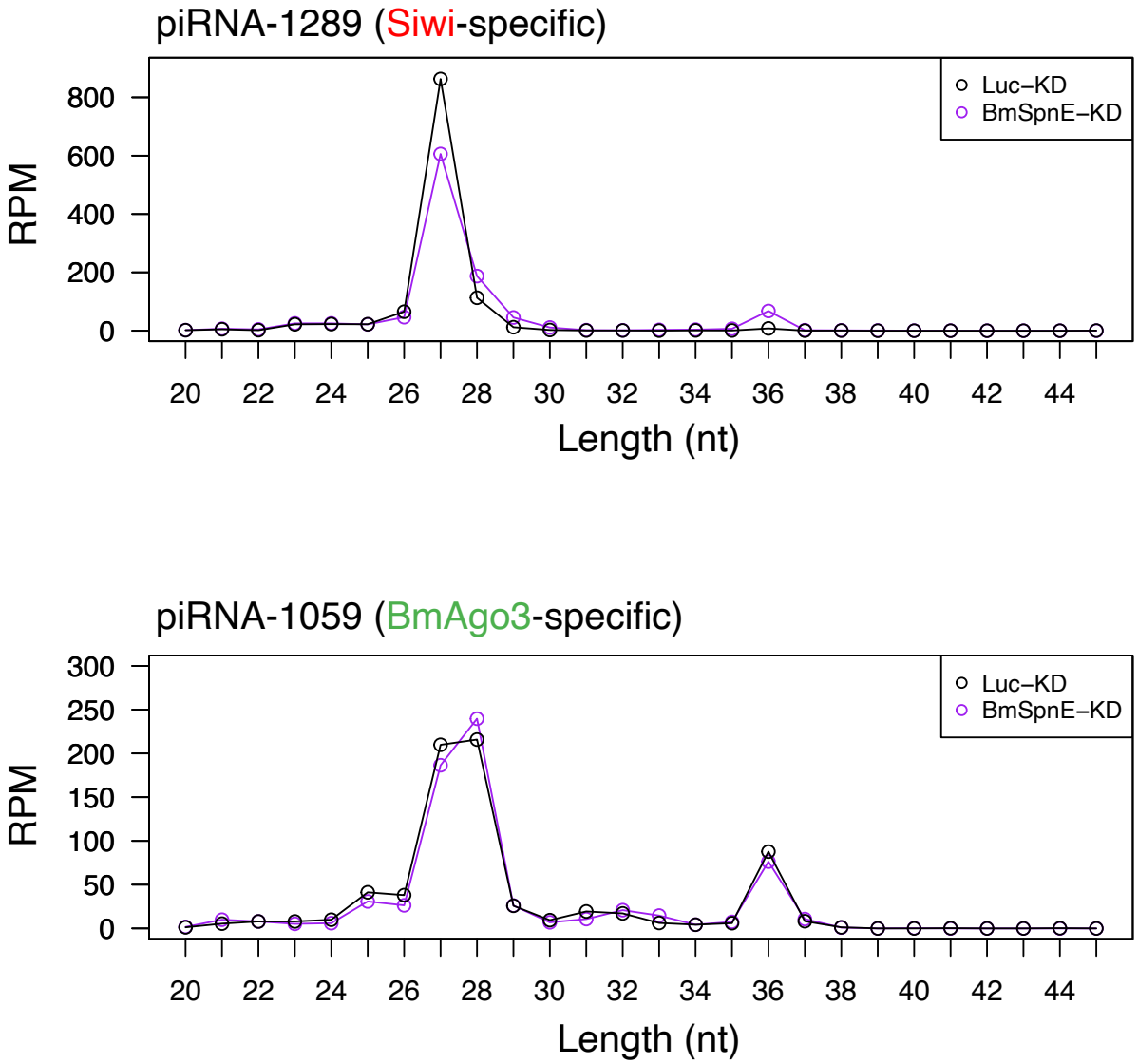

Figure 2-7-9. BmSpnE knockdown upregulated the 36-nt long precusor of a Siwi-specific piRNA

While both Siwi-specific piRNA-1289 and BmAgo3-specific piRNA-1059 are peaked at 28-nt and 36-nt, only the precursor peak of piRNA-1289 was upregulated by BmSpnE depletion.

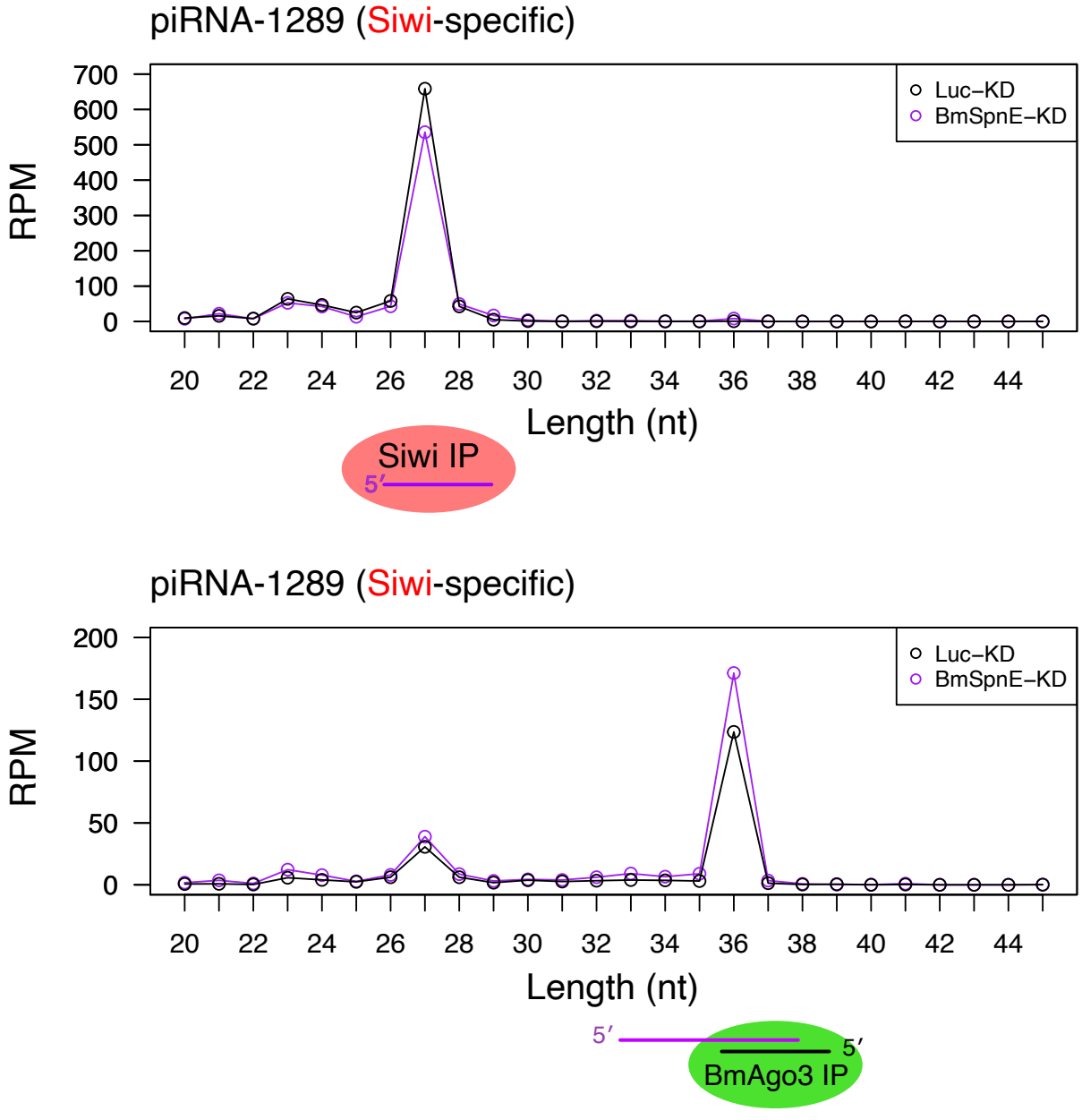

Figure 2-7-10. BmSpnE depletion leads to retainment of of Siwi piRNA precursor in immunopurified BmAgo3

While BmSpnE knockdown (KD) did little to mature piRNA-1289 bound by Siwi (top), piRNA-1289 was found specifically accumulated in immunopurified BmAgo3 as 36-nt long precursors (purple strand bound by the BmAgo3).

3. Discussion

3.1. Proposed model for nuage/piP-body compartmentalization

In this study, I quantitatively characterized the dynamic spatial regulation of core piRNA factors in silkworm BmN4 cells by taking advantage of live cell imaging and ectopic expression of protein mutants. I found that besides nuage and outer mitochondrial surface, key piRNA factors like BmSpnE and BmQin were also found in piP-bodies, the P-body-like condensate but harbors piRNA factors **(Figure 2-2-3)**. A slicer defective version of Siwi was found to mis-localize to these piP-bodies, while the same mutation did not affect the localization of BmAgo3 **(Figure 2-2-2)**. These results suggest that Siwi can interact with both nuage and piP-body proteins by shuttling between the two piRNA condensates, which is essential for the proper partition of piRNA factors into nuage and piP-bodies.

In line with the current BmVasa action model (Xiol *et al*, 2014), my findings supported a function of BmVasa in remodeling Siwi-D670A complexes in nuage. This activity releases the mutant from irreversible-bound RNAs and results in the diminishing nuage localization of Siwi-D670A. Instead, Siwi-D670A at some point may reach piP-body, the condensate where a number of piRNA factors – but not BmVasa – were found to localize. The lack of BmVasa in piP-body renders Siwi-D670A unable to escape from the target RNA but only to co-aggregates with BmSpnE and BmQin. In normal cells, wildtype Siwi can cleave the target RNA and release itself to the cytoplasm, thus allowing Siwi to change its interactors and shuttle between nuage and piP-bodies.

Noteworthy, the Siwi-D670A foci no longer behave like liquid but instead behave like solid aggregates **(Figure 2-3-1, 2-3-2)**. Such aggregation appears to concentrate piRNA factors like BmSpnE, BmQin, BmMael and BmArmi, causing a sharp rise in their granule-to-cell ratio **(Figure 2-2-9, 2-2-10, 2-3-3)**. In these circumstances, BmN4 cells started producing mRNA-derived piRNAs (non-TE piRNAs) promiscuously, while transposon-derived ping-pong piRNAs were largely unaffected **(Figure 2-6-5)**. These non-TE piRNAs are mostly, if not all, sense to the template mRNAs, suggesting that they were not produced by the ping-pong machinery **(Figure 2-6-4, 2-6-6)**.

One possible way that causes the mis-production is that the co-aggregation of piRNA factors such as BmSpnE, BmQin, BmMael and BmArmi triggered the production of non-TE piRNAs by processing non-translating mRNAs that are stored in P-bodies (Hubstenberger *et al*, 2017). Apo-PIWIs that stop by the aggregates could then mistakenly loads the non-TE pre-piRNAs, which will be processed by Trimmer in mitochondria and methylated by BmHen1 subsequently. However, as Siwi-D670A had a markedly reduced subcellular diffusion rate within the foci **(Figure 2-3-1)**, it is likely that these factors will be co-trapped in the irreversible RNA-Siwi pre-cleavage complexes. Alternatively, it is also possible that a yet-discovered fidelity-ensuring factor in nuage or elsewhere was trapped in Siwi-D670A pre-cleavage complex, hindering it from performing its normal functions and thus upregulates non-TE piRNA production at the nuage-mitochondria interface **(Figure 3)**.

The candidates for the proposed fidelity determining factor(s) may include BmQin, BmArmi and BmVret. The first candidate, BmQin, has the ability to both docks to BmVasa-E339Q

aggregate (Xiol *et al*, 2014) and to Siwi-D670A aggregate in piP-bodies **(Figure 2-2-4)**. It is possible that BmQin may have mutual roles in piP-body assemblies and in concentrating piRNA-targeted transcripts in corresponding condensates. In fact, a previous study reported that in mice, loss of Qin homolog reactivates the ping-pong cycle in meiotic cells and causes upregulation of non-TE sense piRNA from 3′ UTR of protein-coding genes (Wasik *et al*, 2015). It is however not clear that this function is conserved in silkworm or not.

The second candidate BmArmi is known for its essential role in phased piRNA production (Olivieri *et al*, 2010; Saito *et al*, 2010; Haase *et al*, 2010; Ge *et al*, 2019; Ishizu *et al*, 2019), a pathway that could, in theory, produces non-TE piRNAs directly from the mRNAs. Importantly, *Drosophila* Armi ATPase is responsible to select piRNA precursor transcripts over the other mRNAs (Ge *et al*, 2019; Ishizu *et al*, 2019). It is possible that Siwi-D670A or BmVasa-E339Q may inhibit such activity by trapping a significant amount of BmArmi in aggregates **(Figure 2-2-10)**, leading to the promiscuous production of non-TE piRNAs.

The mouse homolog of the third candidate, TDRD1, was linked to the aberrant production of 3′ UTR-derived exonic piRNAs (Reuter *et al*, 2009), although the exact molecular mechanism is still unknown. In silkworm, BmVret (homolog of TDRD1) was recently reported to facilitate Siwi-piRNA production by interconnecting BmAgo3 and unloaded Siwi (Nishida *et al*, 2020). If Siwi-D670A traps BmVret in piP-bodies, it may actively recruit unloaded Siwi to piP-bodies, causing the misloading of non-TE RNA fragments. These misloaded fragments can then be trimmed by some random exonucleases in piP-bodies or by Trimmer at the piP-body/mitochondria interface, resulting in the 28-nt length profile of the non-TE piRNAs.

Steady state:

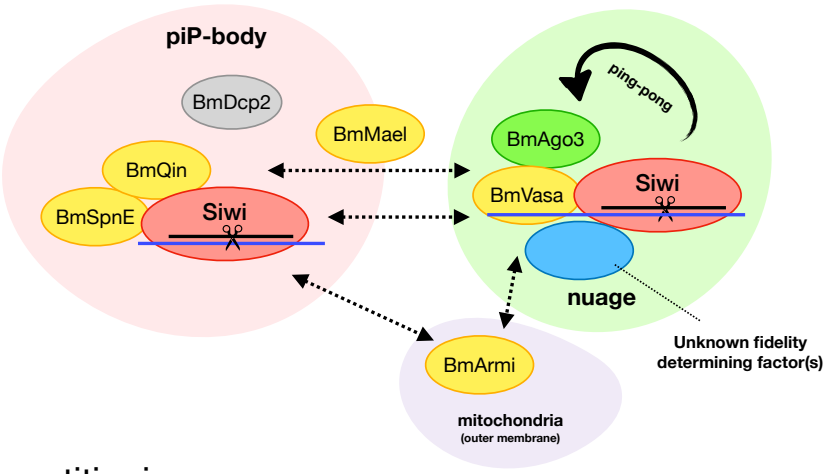

Impaired partitioning:

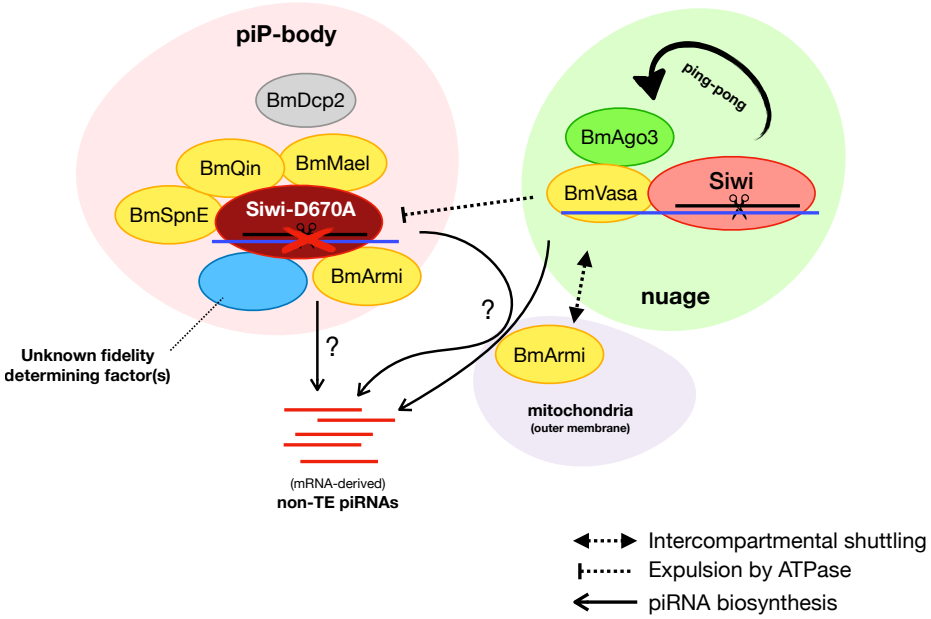

Figure 3. Proposed model for nuage/piP-body partitioning in BmN4 cells
At steady state, piRNA factors localize to nuage and piP-body stably or in a transient manner. For example, Siwi appears to enrich in nuage but can transiently enters piP-body to interacts with BmSpnE and BmQin. The shuttling of Siwi requires its own slicer activity, where BmVasa helps by remodeling RNP interaction using its ATPase activity. A few Siwi-interacting factors such as BmMael and BmArmi are likely to enter the compartments where Siwi is present. When Siwi-D670A is present, the mutant is expelled from nuage by BmVasa and is trapped in piP-body and co-aggregates with piP-body factors as well as those shuttling between compartments. In such case, it will not be surprising if a hypothetic fidelity determining factor could be similarly trapped in piP-body, which may explain the upregulation of 28-nt non-TE piRNAs. It is also possible that non-TE piRNA is directly generated from piP-body, where a number of piRNA biosynthesis factors are enriched.

3.2. Biological implications of nuage/piP-body subcellular compartmentalization

This study represents the first report of the association of piP-body with the silkworm piRNA pathway (Chung *et al*, 2021). In other model animals, especially mouse and fruit flies, the interplay between P-body proteins and piRNA pathway components was described in more detail.

In fly ovaries, nuage is found in the perinuclear region of differentiating germ cells (Eddy, 1975). Researchers predicted that nuage may further form a sponge-like condensate named sponge bodies by intermingling with P-body-like granules in nurse cells (Wilsch-Bräuninger *et al*, 1997; Voronina *et al*, 2011). Sponge bodies mostly contain constitutive P-body proteins like Dcp2 and Me31B (Snee & Macdonald, 2009). In addition, Vasa-negative sponge bodies are often found in contact with Vasa-positive nuage (Wilsch-Bräuninger *et al*, 1997), while changing their composition in a highly dynamic manner (Snee & Macdonald, 2004). It is unclear whether these granules are functionally linked to each other or not. Meanwhile, it was reported that non-perinuclear nuage sometimes overlaps with P-body proteins and transposon RNAs in *Drosophila* ovaries (Lim *et al*, 2009). These foci may include Spn-E, Aubergine (Siwi homolog), Dcp2 and Me31B. The best guess of the function of these non-perinuclear nuage was to direct piRNA-targeted transposon for decay, given that their formation seems to be piRNA dependent (Lim *et al*, 2009). In contrast to the subcellular compartmentalization in silkworms, these foci shared some common piRNA factors with perinuclear nuage in *Drosophila* ovaries (Lim *et al*, 2009). These studies demonstrated that nuage and P-bodies not only co-exist but may interact or even merge at different stages of development in *Drosophila* germ cells. It is, however, technically challenging to resolve the details of these rapidly remodeling germ granules, due to the continuous changes that happen along with the epigenomic and genomic remodeling during germ cell development.

The merging of nuage and P-body proteins was also well-documented in mice. The mouse piP-bodies were found in gonocytes but not in later stages when the expression of MIWI2 comes to an end (Meikar *et al*, 2011). In round spermatids, a single, compact condensate named chromatoid body (CB) forms instead (reviewed in Kotaja & Sassone-Corsi, 2007). At this stage, CBs harbor both piRNAs and miRNAs, as well as their major components that require for their actions and biogenesis (Meikar *et al*, 2010; Kotaja *et al*, 2006; Meikar *et al*, 2014). These include MVH (Vasa homolog), PIWIs (MIWI and MILI), TDRDs, splicing factors, RNA decay factors, miRNA-related proteins and more (Meikar *et al*, 2014). Given the diversity of the CB proteome, it is likely that CBs are implicated in multiple RNA processing machinery, with more interests focused on the piRNAs. These piRNAs, also known as pachytene piRNAs, were proposed to execute a massive mRNA elimination event by physically interacting with mRNA deadenylase CAF1, instead of targeting transposons during late spermiogenesis (Gou *et al*, 2014). Remarkably, MVH was found physically interacting with Dicer proteins, the processing factor required for the biogenesis of siRNA and miRNAs (Kotaja *et al*, 2006). It is therefore plausible that piRNA factors in CBs dynamically interact with miRNA factors as well as key components in the mRNA degradation pathway to facilitate the transition from the meiotic phase to the later phases. Despite the intense interplay and colocalization, it was found that the formation of CB is not required for piRNA biogenesis in spermatids (Tanaka *et al*, 2011). In fact, pachytene piRNA can be found in meiotic cells (Aravin *et al*, 2006), which is prior to the emergence of CBs.

In my study, I used the silkworm ovary-derived cell line BmN4 as a study model. It is not clear from which stage of the oogenesis the cell line was isolated, since the establishment uses

whole ovaries and was transformed into a cell line that well adopts the laboratory condition (Grace, 1967). While both sponge bodies and CBs were previously well-studied in different models, it is to note that there has been no evidence that an active ping-pong cycle may occur in these condensates. Indeed, mouse gonocyte is the only model that reported to have a partition of piRNA factors across nuage and P-bodies while having an active ping-pong cycle at the same time (Aravin *et al*, 2009). The silkworm compartmentalization, however, distinct from the one in mouse gonocytes in the following ways: (1) in silkworm, the localization of PIWI in piP-bodies was not visible until the slicer domain is mutated; (2) the slicer activity of the piP-body localizing MIWI2 is dispensable for MILI-piRNA amplification in mouse gonocyte (Fazio *et al*, 2011), while the slicer activity of Siwi participated in both ping-pong and phased piRNA production (Izumi *et al*, 2020). Importantly, I found that when such subcellular compartmentalization was disrupted without depleting endogenous piRNA factors, aberrant piRNAs derived from exonic mRNAs were promiscuously produced. This study is therefore especially meaningful to the piRNA fields as it revealed a valuable entry point to intercept the highly dynamic piRNA pathway and to study the fidelity determining mechanism at the stage of precursor acquisition.

It is fascinating, though equally bizarre, that such a nuage/piP-body compartmentalization conserved in silkworms and mice but not in fruit flies, given that fruit flies are the closer relatives to silkworms than mice. It is of note that, despite both belong to the class insecta, the piRNA pathways in silkworms and fruit flies are largely different from each other. In fruit fly ovaries, there are three PIWIs (Piwi, Aub and Ago3) instead of two in silkworms (Siwi and BmAgo3). The *Drosophila* Piwi is a nuclear PIWI protein that help establish DNA or histone methylation marks on transposons, where in *Bombyx mori* the presence of such a nuclear PIWI was not reported. In

mice, a total number of three PIWIs (MILI, MIWI, MIWI2) exist, but at most two of them may co-exist at any given timepoint. The MIWI2 is largely considered as the nuclear PIWI counterpart which mediates chromatin/DNA methylation, yet still distinct from the *Drosophila* Piwi by actively participating in the ping-pong cycle with an active slicer domain (Siomi *et al*, 2011). Furthermore, 3′-definition of piRNAs in *Drosophila* is either performed directly by Zucchini or Nibbler, an exonuclease. In contrast, both silkworms and mice require the exonuclease Trimmer/PNDLC1 for 3′-end maturation. These together suggest that all three model animals have each of them a highly differentiated piRNA pathway, and that even both silkworm and fruit flies are in the same class, their piRNA pathways can have different number of PIWIs and a distinct maturation mechanism. Since we are still struggling to understand the degree as well as the rules of the conservation of piRNA pathway across these models, it is permissible that the nuage/piP-body compartmentalization is somewhat conserved between mice and silkworm but not in fruit flies. As previously mentioned, *Drosophila* P-body factors may interact with piRNA factors in condensates such as cytoplasmic nuage and sponge bodies. It will be insightful to check if these piRNA-related P-body-like condensates contribute to the substrate specificity of the piRNA pathways or not.

3.3. Tracking down the functions of RNA helicases in silkworm piRNA pathway

In my study, I confirmed that BmVasa with an active ATPase did not co-accumulate with slicer defective Siwi. Instead, it is only when the BmVasa ATPase is mutated, the two proteins finally co-aggregated. This agrees with the previous model which hypothesizes that BmVasa remodels Siwi-RNA complexes and helps in transferring the 3′ cleavage product to BmAgo3 (Xiol *et al*, 2014; Nishida *et al*, 2015). Besides resolving Siwi-D670A aggregation in nuage, BmVasa is required for proper localization of Siwi as well as the dissociation from piP-bodies **(Figure 2-4-7, 2-4-8)**. Noteworthy, the lack of BmVasa did not render piP-body proteins localize in nuage. Instead, depletion of Siwi causes BmSpnE to colocalize with BmVasa **(Figure 2-4-6)**, suggesting Siwi-RNA complexes are the primary target of BmVasa activity.

Considering all data, I hypothesized that BmVasa ATPase releases Siwi-D670A from irreversibly bound-RNA, which prohibits Siwi-D670A from accumulating in perinuclear nuage. According to this hypothesis, BmVasa knockdown should lead to overrepresentation of Siwi-D670A in perinuclear nuage-like particles. Instead, I observed that when BmVasa was depleted, Siwi-D670A remained in non-perinuclear condensates, colocalizing with BmDcp2 **(Figure 2-4-8)**. This could be reasoned by the inability to assembly nuage due to the loss of BmVasa. In *Drosophila*, Vasa appears to be the protein that has the most upstream position in the hierarchical assembly of the nuage (Lim & Kai, 2007). It is therefore more likely that upon BmVasa depletion, nuage proteins would relocate to piP-bodies in non-perinuclear region, but not in the opposite way. Therefore, in addition to the roles in facilitating Siwi-to-BmAgo3 handover, my study suggests that BmVasa can remodel Siwi-RNA interactions, recruits key piRNA factors to nuage and may inhibit promiscuous piRNA production by its ATPase activity.

The findings with BmSpnE-E251Q and knockdown assay together suggested that BmSpnE ATPase participated in the BmAgo3-to-Siwi axis of the ping-pong cycle by maintaining the proper cytoplasmic localization of Siwi. Notably, another DEAD-box helicase BmDDX43 was proposed as the counterpart of BmVasa – a piRNA factor to release BmAgo3-bound Siwi precursor piRNA and facilitate the handover of precursor to Siwi (Murakami *et al*, 2021). BmSpnE was excluded from the candidate due to a previous report where BmSpnE depletion causes loss of both Siwi- and BmAgo3-associated piRNAs (Nishida *et al*, 2015; Murakami *et al*, 2021). It is unclear why in our system BmSpnE knockdown did not result in the total loss of piRNA but only the accumulation of Siwi precursor piRNAs. Given that BmDDX43 colocalizes with BmAgo3 in nuage (Murakami *et al*, 2021), it is possible that BmSpnE knockdown or BmSpnE-E251Q expression refrained Siwi from entering nuage, and hence impairs piRNA precursor handover with BmDDX43-bounded BmAgo3. It was also reported that BmSpnE specifically interacts with unloaded Siwi (Nishida *et al*, 2015), which further strengthens the proposed model. Still, the exact role of BmSpnE in the piRNA pathway remains unclear. Future studies on the BmSpnE-interacting RNA and proteins – especially those located in the newly defined piP-body – are expected to provide more hints on the production of Siwi-associated piRNAs.

3.4 Limitation and future prospective

In this study, most of the microscopic experiments were performed by inducing overexpression of FP-tagged piRNA factors, which is enough to alter the localization of these proteins. Ideally, editing the endogenous gene by homologous recombination combined with programmed double-strand breaks (by CRISPR-Cas9 system, for example) will reduce these possible artifacts to the minimum. However, while CRISPR-Cas9 mediated gene knockout has been successfully demonstrated in BmN4 cells, nucleotide editing or gene knock-in has been technically challenging for this cell line. Furthermore, a prolonged culture period that is required to establish a knock-in cell line of Siwi mutants may risk the complete loss of piRNA and secondary effects that may complicate downstream analysis. In fact, I and my colleague Dr. Keisuke Shoji attempted to establish a Siwi-D670A stable cell line but failed due to cell death (unpublished data). These failures suggest that the Siwi-D670A mutant may be toxic to BmN4 cells, and therefore transient expression of the mutant with reduced expression level will be the best and only method for now. To reduce the protein expression level, I replaced the OpIE2 baculovirus promoter with a Tet-On inducible promoter and achieved a 30-folds cut of the FP-tagged protein level in BmN4 cells **(Figure 2-2-7)**. With an expression level far lower than the endogenous counterparts, I validated a few key colocalization pairs that demonstrated the piP-body enrichment of Siwi-D670A, BmSpnE and BmQin **(Figure 2-2-8)**. Since the observed colocalization patterns are identical between OpIE2 and Tet-On systems, I therefore concluded that instead of the protein level, it is the catalytic activity that causes the localization shift.

The small RNA sequencing experiment performed in cells overexpressing Siwi and/or BmVasa mutants demonstrated a possible role of subcellular compartmentalization in maintaining

the self-nonself discrimination of piRNA biosynthesis. The observation of which both Siwi-D670A and BmVasa-E339Q upregulate non-TE piRNAs suggested that the effect cannot be solely associated with the dominant-negative effect of interrupting either one of the two key catalytic activities. However, it remains unclear how exactly these non-TE piRNAs arose. The apparent lack of ping-pong signature and antisense non-TE piRNAs argue against the involvement of the ping-pong cycle in non-TE piRNA production, but those may not necessarily be generated by the primary piRNA pathway. Alternatively, it will be extremely difficult to track down the production mechanism of non-TE piRNAs if PIWIs randomly acquire RNA degradation products that are short enough to fit into the protein. Moreover, sense-orientated non-TE piRNAs do not appear to have an immediate effect on the transcriptome, as it is highly unlikely that a self, exonic mRNA will have an antisense strand which has physiological functions. Of note, non-TE piRNAs are not only found in Siwi-D670A expression cells but also in naive BmN4 cells, albeit to a lesser extent. Since it is favorable to the cell if it can put all cytoplasmic mRNAs under surveillance to prepare for a sudden-activated transposon, it is possible that the non-productive non-TE piRNA production is a part of the transcriptome surveillance system in germ cells.

Future studies on the nuage/piP-body proteome and interactome should provide clues to the self-nonself determining as well as the precursor acquisition mechanism of the silkworm piRNA pathway. The recent advance in a method named Fluorescence-Activated Particle Sorting (Hubstenberger *et al*, 2017) is one of the best candidates to elucidate nuage/piP-body proteome. It succeeded in purifying human P-bodies with a condensate-optimized cell sorter, which allows downstream analysis using mass spectrometry (Hubstenberger *et al*, 2017). An alternative way to survey RNP contents in piRNA condensates would be Proximity Labeling. While an array of

molecular tools are currently available, these tools generally allow *in situ* biotinylation of proteins in proximity to the bait protein that was tagged with an engineered biotin ligase named BirA (Roux *et al*, 2012). The biotin-labeled proteins then can be pulled down and analyzed with mass spectrometry. The short labeling radius of the BirA mutant allows detection of proteins at the core or transiently localized to an RNP condensate, and has demonstrated promising results with human P-bodies (Youn *et al*, 2018). Moreover, an alternative method named APEX-seq can label RNA content in proximity to the bait protein (Fazal *et al*, 2019; Padrón *et al*, 2019), which could be particularly useful in detecting RNA contents in RNP condensates – an important aspect in nuage/piP-body assembly and the subcellular compartmentalization processes.

To conclude, my study reported a new layer of regulation on the fidelity of piRNA biogenesis. First, I found that multiple piRNA factors localized in a distinct cytoplasmic condensate (piP-bodies) which resembles P-bodies and harbor the P-body maker BmDcp2. Disabling the slicer activity of Siwi causes the protein to exit nuage and enter piP-bodies, while the same mutation did not affect the other silkworm PIWI, BmAgo3. Siwi slicer mutant (Siwi-D670A) co-aggregates with multiple piRNA factors in piP-bodies, which leads to an unexpected elevation in exonic piRNAs from non-TE genes. I also found that two RNA helicases, BmVasa and BmSpnE, utilize their ATPase activities to aid the correct localization of Siwi. When present, BmVasa ATPase mutant triggers the aggregation of Siwi and Siwi-D670A at cytoplasm, while the BmSpnE ATPase mutant traps Siwi at piP-bodies, likely through the physical association with the canonical P-body helicase BmDDX6. These results together demonstrated the complexity and dynamics of the subcellular spatial organization of piRNA factors and suggested a direct involvement of Siwi, BmVasa, BmSpnE catalytic activities in regulating their fellow piRNA

factors to ensure the fidelity of piRNA biogenesis. Lastly, this new layer of regulation ensures germ cells are enriched with transposon piRNAs but not exonic piRNAs that originates from non-transposon transcripts, which is essentially important for the genome stability and the proper development of germ cell.

4. Materials and methods

Cell culture and transfection

BmN4 cells were cultured in IPL-41 medium (Applichem) supplemented by 10% heat-inactivated Fetal Bovine Serum (FBS) at 28 °C. For transfection, 5 x 10^4 BmN4 cells/well in 350 µL IPL-41 (with 10% FBS) were mounted to non-coated 8-well (24.5mm × 53.9mm) glass chamber (Matsunami Glass) prior to transfection. X-tremeGENE HP (Roche) was used at a concentration of 2 µL per 1 µg DNA in 150 µL IPL-41. For transfection experiments, a total of 150 ng of DNA was transfected to one well and incubated for 4 days. For small RNA sequencing, overexpression was performed by repeating the transfection at Day 4 and incubate the cells for an extra 3 days before RNA extraction. For 1,6-Hexanediol treatment, 5% (w/v) 1,6-Hexanediol (Sigma-Aldrich) dissolved in PBS was added to the wells 30 min prior to the experiment. For pTet transfection, 100 ng/mL Doxycycline (MP Biomedicals) was added to the medium 24 hours after transfection.

Plasmid construction

Generation of pIZ-FP-Siwi and pIZ-FP-BmAgo3

Coding sequence of fluorescence proteins (FPs; AcGFP and mCherry) were amplified from pAcGFP1 or pmCherry (Takara Clontech) by PCR and cloned into pIZ-FLAG6H-Siwi and pIZ-FLAG6H-BmAgo3 (Kawaoka *et al*, 2009) using primers #1–9. See also Table 1 for primer sequences.

Cloning of BmDcp2, BmVasa, BmSpnE and BmQin

pIZ-AcGFP-BmAgo3 or pIZ-mCherry-BmAgo3 were digested with NotI (NEB) and BamHI (NEB) restriction enzymes. Coding sequences of AcGFP and mCherry were amplified by PCR using primers #2, #6, and #10. The coding sequences of BmSpnE, BmQin, and BmDcp2 were amplified by RT–PCR, with the cDNA generated using SuperScript III Reverse Transcriptase (Thermo Fisher/Invitrogen) and PCR performed with primers #11–19. Coding sequence of BmVasa was amplified from a KAIKO cDNA clone [from National BioResource Project (Silk-worm)] using primers #20–22. FP (AcGFP/mCherry) coding sequences were then mixed with BmVasa, BmSpnE, BmQin, and BmDcp2 fragments and ligated to the enzyme digested pIZ vectors by using NEBuilder Hifi DNA Assembly kit (NEB). See also Table 1 for primer sequences.

Generation of BmAgo3-D697A, Siwi-D670A, Siwi-Y607E, and BmVasa-E339Q

PCR site-directed mutagenesis using primers #40–50 and #2 combined with NEBuilder Hifi DNA Assembly kit (NEB) were used to generate BmAgo3-D697A, Siwi-D670A, Siwi-Y607E, BmVasa-E339Q, BmVasa-DelN and BmSpnE-E251Q mutants. See also Table 1 for primer sequences.

Generation of pTet-constructs

To generate pTet-AcGFP, multiple DNA fragments were amplified by PCR from pMK243 (a gift from T. Natsume) with primer pairs (#23 & #25, #24 & 25, #26 & #27, #28 & #29) and from pIZ-AcGFP with primer pairs (#30 & #31, #32 & #33) and were ligated with NEBuilder Hifi DNA Assembly kit (NEB). Cloning of CDSs of piRNA factors into pTet-AcGFP was then performed with primers #2, #34– 39 using PCR and NEBuilder Hifi DNA Assembly kit (NEB).

dsRNA synthesis and transfection

For dsRNA synthesis, in vitro transcription template DNAs were prepared by using PCR primers containing T7 promoters (primers #51–62). All dsRNAs were transcribed using T7-Scribe Standard RNA IVT kit (CELLSCRIPT) and were purified by ethanol precipitation and ammonium acetate precipitation. For transfection, dsRNAs (300 ng per well) were transfected twice on day 0 and day 4 and cells were observed on day 7 post-transfection. pIZ constructs were co-transfected with the dsRNAs on day 4 post-transfection. See also Table 1 for primer sequences.

Extraction of total RNA and $NaIO_4$ treatment

Total RNA of BmN4 was extracted from 1mL 80% confluence BmN4 cells centrifuged at 1,500 *g* for 3 minutes and washed with PBS. Cell pellet was directly treated with 1mL ice-cold TRI reagent (MRC) and incubated at room temperature for 5 minutes. 200 μL chloroform (Wako) was added to the solution and mixed by vigorous shaking. 2 minutes incubation at room temperature was followed by centrifugation at 12,000 *g* at 4 ℃ for 15 minutes. Aqueous layer was extracted by pipetting and added to 500 μL ice-cold isopropanol (nacalai tesque) and incubated at room temperature for 5 minutes. The mixture was then centrifuged at 12,000 *g* at 4 ℃ for 8 minutes. Supernatant was aspirated and the pellet containing total RNA was washed by 99% ethanol (nacalai tesque) and resuspended in appropriate amount of Milli-Q water. $NaIO_4$-mediated oxidation was performed as described previously (Kawaoka *et al*, 2011).

Generation of cDNA

cDNA was generated by using SuperScript III (Invitrogen) following instruction provided by the manufacturer. In brief, 3 μg total RNA from BmN4 was incubated with 50 μM oligo(dT)20 and

10 mM dNTPs at 65 ℃ for 5 minutes to unfold RNA secondary structure. The mixture was then placed on ice for more than 1 minute and then added to the reaction mix containing 1 × First strand buffer, 0.1 M DTT, 25 mM $MgCl_2$, 40 U RNasin (Promega) and 200 U SuperScript III RT. The reaction mix was incubated in 50 ℃ for 60 minutes and then 85 ℃ for 5 minutes to stop the reaction. It was then treated with 2U E. Coli RNase H and incubated at 37 ℃ for 20 minutes. For each PCR reaction, 40 ng was used as template.

Lysate preparation and Western blotting

Cells were washed twice with ice-cold PBS and then lysed with 1 × lysis buffer (30 mM HEPES-KOH (pH 7.4), 100 mM potassium acetate, 2 mM magne- sium acetate) with 0.2% Triton X-100 (Wako). The cell lysates were then cleared by centrifugation at 17,000 *g* at 4 ℃ for 20 minutes and the supernatants were collected. Primary antibodies used for western blotting includes anti-GFP (B- 2) (Santa Cruz), anti-RFP (MBL), anti-actin (Santa Cruz, sc-1616), anti-Siwi (Izumi *et al*, 2020), anti-BmVasa (Nishida *et al*, 2015), anti-BmSpnE (Nishida *et al*, 2015), anti-BmQin (Nishida *et al*, 2015), and anti-BmMael [affinity-purified rabbit polyclonal antibody generated by immunizing N-terminally His-tagged recombinant BmMael (Scrum)]. Secondary antibodies include anti-mouse IgG-HRP (MBL), anti-rabbit IgG-HRP (MBL), and anti-goat IgG-HRP (Jackson ImmunoResearch).

Flow cytometry

BmN4 cells were first treated with 500 ng propidium iodide (Nacalai Tesque) 5 minutes before loading to a CytoFLEX S system (Beckman Coulter) equipped with 488-nm and 561-nm lasers.

Deconvolution microscopy

DeltaVision Elite (GE Healthcare Life Sciences) was used for all microscopic experiment except for Figure 2-2-9 and 2-2-10. Cells mounted to a glass chamber were magnified with a PLAPON 60XO/1.42 oil-immersion objective (Olympus) and directed with Solid-state light (Insight SSL) from LED light source at wavelength 475/28 for FITC (AcGFP) and 542/27 for TRITC (mCherry). Emission filters "Standard" set was used, with wavelengths including 525/48 for FITC (AcGFP), 597/45 for TRITC (mCherry) and 435/48 for DAPI (Hoechst). Data was acquired by a sCMOS camera and analyzed on the microscope regulation software softWoRx. For Z-sections, 10.00 μm was scanned with 0.2 μm thickness for each cell unless specified otherwise. For time-lapses, samples were incubated in 28 ℃ throughout the experiment. Images were acquired at 1 frame per second. All images were processed by deconvolution algorithm in softWoRx with settings listed below: Enhanced Ratio (aggressive), 10 cycles, Noise Filtering: Medium. FRAP experiments were performed as photokinetic assay (PKA) experiments on the DeltaVision Elite system following manufacturers' instructions.

Immunofluorescence

BmN4 cells were fixed with 4% paraformaldehyde for 10 min at RT and subsequently permeabilized with 0.3% Triton X-100 for 5 min at RT. Blocking was performed with 1% BSA/0.1% Triton X-100 for 1 h at RT and stained with anti-BmMael and Alexa Fluor 488 donkey anti-rabbit IgG antibody (Thermo Fisher/Invitrogen).

Image processing and quantification

For line profiling performed to quantify local co-localization, 3-independent unstacked 16bit grayscale images were manually checked for the co-localization between two channels and the representative dots were selected. ImageJ (NIH) function "Plot Profile" was used to quantify pixel intensity. Data was replotted by spreadsheet application Number and replaced to the figure file directly.

For quantification of co-localization with ComDet v0.3.6.1 (ImageJ/Fiji plugin), unstacked 16-bit grayscale images with multi-channels were directly quantified. Detection parameters were set as below: Include larger particles ticked (detect in both channels independently). Approximate particle size: 3.00 pix. Sensitivity: SNR=20. ch1 shared the same setting with ch2. Max distance between colocalized spot: pix 2.00. Data set was summarized and the mean co-localization ratio (number of co-localized dot ÷ total number of dots, collected from both channels) was used for quantification. P-values were calculated using “wilcox_test” function of R package Coin (version 1.3-1) in R (version 3.5.3).

For calculation of granule-to-cell intensity ratio, auto-thresholding performed in Fiji using “Default” and “MaxEntropy Dark” was used to generate whole-cell and granule masks for intensity quantification. The background fluorescence intensity was quantified by inverting whole-cell mask and was subtracted from the whole-cell and granule intensity. For the foci area, auto-thresholding (“MaxEntropy Dark”) was used for masking and “Analyze Particles” was used for area measurement.

Library preparation and Small RNA sequencing

Small RNA libraries were prepared by using NEBNext Multiplex Small RNA Library Prep Set for Illumina (NEB) according to the manufacturers' instructions. After sequencing on an Illumina HiSeq 4000 platform or on an Illumina MiniSeq Sequencing System, adapter sequences removal was performed by cutadapt. 20–45-nt reads were mapped to (i) Silkbase Transposon libraries (BmTE and 121TEs) (Osanai-Futahashi *et al*, 2008) and (ii) Silkbase GeneModel library (Kawamoto *et al*, 2019) with Bowtie allowing zero mismatches. Sequencing data were normalized with both highly abundant miRNAs and total mapping reads (as performed in Izumi *et al*, 2016). UTR sequences were obtained with function "gffread" from GFF Ultilities. P-values and effect size (r) were calculated using "wilcox_test" function of R package Coin (version 1.3-1). Subgroups of genes were defined by performing BLAST (tblastx) Silkbase transposon databases (a total of 1,811 TE genes) and GeneModel database and thresholding the genes with an e-value of 1e-10 and a mean expression threshold > 2 piRNA reads per gene. UTR sequences were extracted from Silkbase Gene model GFF3 files (Kawamoto *et al*, 2019) with function "gffread" from GFF Ultilities (Pertea & Pertea, 2020).

5. Acknowledgements

I would like to express my deepest appreciation to my advisor Prof. Yukihide Tomari for the guidance and continuous support, for his patience, immense knowledge and encouragement. I would never have managed to make the sharp turn into studying piRNA granules without his endorsement and motivation.

My sincere thanks also go to Dr. Natsuko Izumi and Dr. Keisuke Shoji for their insightful discussion and kind comments that always helped me. It would not be possible to conduct this research and finish writing this thesis without their precious help and support. Dr. Natsuko Izumi also provided data for the following figures: Figures 2-2-5, 2-2-9, 2-2-10 and 2-4-1.

I thank all current members in Tomari Laboratory for their brilliant suggestion and advice. I must also express my gratitude and appreciation to my family for letting me through all the difficulties I encountered.

6. Bibliography

Alberti S, Gladfelter A & Mittag T (2019) Considerations and challenges in studying liquid-liquid phase separation and biomolecular condensates. *Cell* 176: 419–434

Andress A, Bei Y, Fonslow BR, Giri R, Wu Y, Yates JR III & Carthew RW (2016) Spindle-E cycling between nuage and cytoplasm is controlled by Qin and PIWI proteins. *J Cell Biol* 213: 201–211

Aravin A, Gaidatzis D, Pfeffer S, Lagos-Quintana M, Landgraf P, Iovino N, Morris P, Brownstein MJ, Kuramochi-Miyagawa S, Nakano T, *et al* (2006) A novel class of small RNAs bind to MILI protein in mouse testes. *Nature* 442: 203–207

Aravin AA, van der Heijden GW, Castañeda J, Vagin VV, Hannon GJ & Bortvin A (2009) Cytoplasmic compartmentalization of the fetal piRNA pathway in mice. *PLoS Genet* 5: e1000764

Aravin AA, Sachidanandam R, Bourc'his D, Schaefer C, Pezic D, Toth KF, Bestor T & Hannon GJ (2008) A piRNA pathway primed by individual transposons is linked to de novo DNA methylation in mice. *Mol Cell* 31: 785–799

Boswell RE & Mahowald AP (1985) tudor, a gene required for assembly of the germ plasm in Drosophila melanogaster. *Cell* 43: 97–104

Brangwynne CP, Eckmann CR, Courson DS, Rybarska A, Hoege C, Gharakhani J, Jülicher F & Hyman AA (2009) Germline P granules are liquid droplets that localize by controlled dissolution/condensation. *Science* 324: 1729–1732

Brennecke J, Aravin AA, Stark A, Dus M, Kellis M, Sachidanandam R & Hannon GJ (2007) Discrete small RNA-generating loci as master regulators of transposon activity in Drosophila. *Cell* 128: 1089–1103

Burke KA, Janke AM, Rhine CL & Fawzi NL (2015) Residue-by-Residue View of In Vitro FUS Granules that Bind the C-Terminal Domain of RNA Polymerase II. *Mol Cell* 60: 231–241

Carmell MA, Girard A, van de Kant HJG, Bourc'his D, Bestor TH, de Rooij DG & Hannon GJ (2007) MIWI2 is essential for spermatogenesis and repression of transposons in the mouse male germline. *Dev Cell* 12: 503–514

Chen C, Jin J, James DA, Adams-Cioaba MA, Park JG, Guo Y, Tenaglia E, Xu C, Gish G, Min J, *et al* (2009) Mouse Piwi interactome identifies binding mechanism of Tdrkh Tudor domain to arginine methylated Miwi. *Proc Natl Acad Sci* 106: 20336–20341

Chung PY, Shoji K, Izumi N & Tomari Y (2021) Dynamic subcellular compartmentalization ensures fidelity of piRNA biogenesis in silkworms. *EMBO Rep*: e51342

Cook HA, Koppetsch BS, Wu J & Theurkauf WE (2004) The Drosophila SDE3 Homolog armitage Is Required for oskar mRNA Silencing and Embryonic Axis Specification. *Cell* 116: 817–829

Counce SJ (1963) Developmental morphology of polar granules in Drosophila. Including observations on pole cell behavior and distribution during embryogenesis. *J Morphol* 112: 129–145

Czech B & Hannon GJ (2016) One Loop to Rule Them All: The Ping-Pong Cycle and piRNA-Guided Silencing. *Trends Biochem Sci* 41: 324–337

Czech B, Preall JB, McGinn J & Hannon GJ (2013) A Transcriptome-wide RNAi Screen in the Drosophila Ovary Reveals Factors of the Germline piRNA Pathway. *Mol Cell* 50: 749–761

Das PP, Bagijn MP, Goldstein LD, Woolford JR, Lehrbach NJ, Sapetschnig A, Buhecha HR, Gilchrist MJ, Howe KL, Stark R, *et al* (2008) Piwi and piRNAs act upstream of an endogenous siRNA pathway to suppress Tc3 transposon mobility in the Caenorhabditis elegans germline. *Mol Cell* 31: 79–90

Ding D, Liu J, Dong K, Midic U, Hess RA, Xie H, Demireva EY & Chen C (2017) PNLDC1 is essential for piRNA 3' end trimming and transposon silencing during spermatogenesis in mice. *Nat Commun* 8: 819

Dodson AE & Kennedy S (2020) Phase Separation in Germ Cells and Development. *Dev Cell* 55: 4–17

Eddy EM (1975) Germ plasm and the differentiation of the germ cell line. *Int Rev Cytol* 43: 229–280

Elbaum-Garfinkle S, Kim Y, Szczepaniak K, Chen CC-H, Eckmann CR, Myong S & Brangwynne CP (2015) The disordered P granule protein LAF-1 drives phase separation into droplets with tunable viscosity and dynamics. *Proc Natl Acad Sci U S A* 112: 7189–7194

Eulalio A, Behm-Ansmant I, Schweizer D & Izaurralde E (2007) P-body formation is a consequence, not the cause, of RNA-mediated gene silencing. *Mol Cell Biol* 27: 3970–3981

Fazal FM, Han S, Parker KR, Kaewsapsak P, Xu J, Boettiger AN, Chang HY & Ting AY (2019) Atlas of Subcellular RNA Localization Revealed by APEX-Seq. *Cell* 178: 473-490.e26

Fazio SD, Bartonicek N, Giacomo MD, Abreu-Goodger C, Sankar A, Funaya C, Antony C, Moreira PN, Enright AJ & O'Carroll D (2011) The endonuclease activity of Mili fuels piRNA amplification that silences LINE1 elements. *Nature* 480: 259–263

Franks TM & Lykke-Andersen J (2008) The Control of mRNA Decapping and P-Body Formation. *Mol Cell* 32: 605–615

Fujita K, Sagisaka A, Tomimoto K, Ishibashi J, Imanishi S, Yamakawa M & Tanaka H (2009) DNA vector-based RNA interference in cell lines derived from Bombyx mori. *Biosci Biotechnol Biochem* 73: 2026–2031

Gainetdinov I, Colpan C, Arif A, Cecchini K & Zamore PD (2018) A Single Mechanism of Biogenesis, Initiated and Directed by PIWI Proteins, Explains piRNA Production in Most Animals. *Mol Cell* 71: 775-790.e5

Ge DT, Wang W, Tipping C, Gainetdinov I, Weng Z & Zamore PD (2019) The RNA-Binding ATPase, Armitage, Couples piRNA Amplification in Nuage to Phased piRNA Production on Mitochondria. *Mol Cell* 74: 982–995

Gossen M & Bujard H (1992) Tight control of gene expression in mammalian cells by tetracycline-responsive promoters. *Proc Natl Acad Sci* 89: 5547–5551

Gou L-T, Dai P, Yang J-H, Xue Y, Hu Y-P, Zhou Y, Kang J-Y, Wang X, Li H, Hua M-M, *et al* (2014) Pachytene piRNAs instruct massive mRNA elimination during late spermiogenesis. *Cell Res* 24: 680–700

Grace TDC (1967) Establishment of a Line of Cells from the Silkworm Bombyx mori. *Nature* 216: 613–613

Grivna ST, Beyret E, Wang Z & Lin H (2006) A novel class of small RNAs in mouse spermatogenic cells. *Genes Dev* 20: 1709–1714

Gunawardane LS, Saito K, Nishida KM, Miyoshi K, Kawamura Y, Nagami T, Siomi H & Siomi MC (2007) A slicer-mediated mechanism for repeat-associated siRNA 5' end formation in Drosophila. *Science* 315: 1587–1590

Haase AD, Fenoglio S, Muerdter F, Guzzardo PM, Czech B, Pappin DJ, Chen C, Gordon A & Hannon GJ (2010) Probing the initiation and effector phases of the somatic piRNA pathway in Drosophila. *Genes Dev* 24: 2499–2504

Han BW, Wang W, Li C, Weng Z & Zamore PD (2015) piRNA-guided transposon cleavage initiates Zucchini-dependent, phased piRNA production. *Science* 348: 817–821

Handler D, Meixner K, Pizka M, Lauss K, Schmied C, Gruber FS & Brennecke J (2013) The genetic makeup of the Drosophila piRNA pathway. *Mol Cell* 50: 762–777

Harris AN & Macdonald PM (2001) Aubergine encodes a Drosophila polar granule component required for pole cell formation and related to eIF2C. *Dev Camb Engl* 128: 2823–2832

Hay B, Ackerman L, Barbel S, Jan LY & Jan YN (1988a) Identification of a component of Drosophila polar granules. *Dev Camb Engl* 103: 625–640

Hay B, Jan LY & Jan YN (1988b) A protein component of Drosophila polar granules is encoded by vasa and has extensive sequence similarity to ATP-dependent helicases. *Cell* 55: 577–587

Hegner RW (1912) The History of the Germ Cells in the Pædogenetic Larva of Miastor. *Science* 36: 124–126

Honda S, Kirino Y, Maragkakis M, Alexiou P, Ohtaki A, Murali R, Mourelatos Z & Kirino Y (2013) Mitochondrial protein BmPAPI modulates the length of mature piRNAs. *RNA N Y N* 19: 1405–1418

Houwing S, Berezikov E & Ketting RF (2008) Zili is required for germ cell differentiation and meiosis in zebrafish. *EMBO J* 27: 2702–2711

Houwing S, Kamminga LM, Berezikov E, Cronembold D, Girard A, van den Elst H, Filippov DV, Blaser H, Raz E, Moens CB, *et al* (2007) A role for Piwi and piRNAs in germ cell maintenance and transposon silencing in Zebrafish. *Cell* 129: 69–82

Hubstenberger A, Courel M, Bénard M, Souquere S, Ernoult-Lange M, Chouaib R, Yi Z, Morlot J-B, Munier A, Fradet M, *et al* (2017) P-Body Purification Reveals the Condensation of Repressed mRNA Regulons. *Mol Cell* 68: 144–157

Huettner AF (1923) The origin of the germ cells in Drosophila melanogaster. *J Morphol* 37: 385–423

Hutvagner G & Simard MJ (2008) Argonaute proteins: key players in RNA silencing. *Nat Rev Mol Cell Biol* 9: 22–32

Ipsaro JJ, Haase AD, Knott SR, Joshua-Tor L & Hannon GJ (2012) The structural biochemistry of Zucchini implicates it as a nuclease in piRNA biogenesis. *Nature* 491: 279–283

Ishizu H, Kinoshita T, Hirakata S, Komatsuzaki C & Siomi MC (2019) Distinct and Collaborative Functions of Yb and Armitage in Transposon-Targeting piRNA Biogenesis. *Cell Rep* 27: 1822-1835.e8

Ishizu H, Siomi H & Siomi MC (2012) Biology of PIWI-interacting RNAs: new insights into biogenesis and function inside and outside of germlines. *Genes Dev* 26: 2361–2373

Izumi N, Shoji K, Sakaguchi Y, Honda S, Kirino Y, Suzuki T, Katsuma S & Tomari Y (2016) Identification and functional analysis of the pre-piRNA 3′ Trimmer in silkworms. *Cell* 164: 962–973

Izumi N, Shoji K, Suzuki Y, Katsuma S & Tomari Y (2020) Zucchini consensus motifs determine the mechanism of pre-piRNA production. *Nature* 578: 311–316

Kalmykova AI, Klenov MS & Gvozdev VA (2005) Argonaute protein PIWI controls mobilization of retrotransposons in the Drosophila male germline. *Nucleic Acids Res* 33: 2052–2059

Kawamoto M, Jouraku A, Toyoda A, Yokoi K, Minakuchi Y, Katsuma S, Fujiyama A, Kiuchi T, Yamamoto K & Shimada T (2019) High-quality genome assembly of the silkworm, Bombyx mori. *Insect Biochem Mol Biol* 107: 53–62

Kawaoka S, Hayashi N, Suzuki Y, Abe H, Sugano S, Tomari Y, Shimada T & Katsuma S (2009) The Bombyx ovary-derived cell line endogenously expresses PIWI/PIWI-interacting RNA complexes. *RNA* 15: 1258–1264

Kawaoka S, Izumi N, Katsuma S & Tomari Y (2011) 3′ End Formation of PIWI-Interacting RNAs In Vitro. *Mol Cell* 43: 1015–1022

Khurana JS & Theurkauf W (2010) piRNAs, transposon silencing, and Drosophila germline development. *J Cell Biol* 191: 905–913

Kirino Y, Kim N, de Planell-Saguer M, Khandros E, Chiorean S, Klein PS, Rigoutsos I, Jongens TA & Mourelatos Z (2009) Arginine methylation of Piwi proteins catalysed by dPRMT5 is required for Ago3 and Aub stability. *Nat Cell Biol* 11: 652–658

Kirino Y, Vourekas A, Kim N, de Lima Alves F, Rappsilber J, Klein PS, Jongens TA & Mourelatos Z (2010) Arginine methylation of vasa protein is conserved across phyla. *J Biol Chem* 285: 8148–8154

Klattenhoff C, Xi H, Li C, Lee S, Xu J, Khurana JS, Zhang F, Schultz N, Koppetsch BS, Nowosielska A, *et al* (2009) The Drosophila HP1 homolog Rhino is required for transposon silencing and piRNA production by dual-strand clusters. *Cell* 138: 1137–1149

Kotaja N, Bhattacharyya SN, Jaskiewicz L, Kimmins S, Parvinen M, Filipowicz W & Sassone-Corsi P (2006) The chromatoid body of male germ cells: Similarity with processing bodies and presence of Dicer and microRNA pathway components. *Proc Natl Acad Sci* 103: 2647–2652

Kotaja N & Sassone-Corsi P (2007) The chromatoid body: a germ-cell-specific RNA-processing centre. *Nat Rev Mol Cell Biol* 8: 85–90

Kroschwald S, Maharana S, Mateju D, Malinovska L, Nüske E, Poser I, Richter D & Alberti S (2015) Promiscuous interactions and protein disaggregases determine the material state of stress-inducible RNP granules. *eLife* 4: e06807

Kroschwald S, Maharana S & Simon A (2017) Hexanediol: a chemical probe to investigate the material properties of membrane-less compartments. *Matters* 3: e201702000010

Lander ES, Linton LM, Birren B, Nusbaum C, Zody MC, Baldwin J, Devon K, Dewar K, Doyle M, FitzHugh W, *et al* (2001) Initial sequencing and analysis of the human genome. *Nature* 409: 860–921

Lasko P (2010) Tudor domain. *Curr Biol CB* 20: R666-667

Lasko PF & Ashburner M (1988) The product of the Drosophila gene vasa is very similar to eukaryotic initiation factor-4A. *Nature* 335: 611–617

Lau NC, Seto AG, Kim J, Kuramochi-Miyagawa S, Nakano T, Bartel DP & Kingston RE (2006) Characterization of the piRNA complex from rat testes. *Science* 313: 363–367

Lehmann R & Nüsslein-Volhard C (1986) Abdominal segmentation, pole cell formation, and embryonic polarity require the localized activity of oskar, a maternal gene in Drosophila. *Cell* 47: 141–152

Liang L, Diehl-Jones W & Lasko P (1994) Localization of vasa protein to the Drosophila pole plasm is independent of its RNA-binding and helicase activities. *Dev Camb Engl* 120: 1201–1211

Lim AK & Kai T (2007) Unique germ-line organelle, nuage, functions to repress selfish genetic elements in Drosophila melanogaster. *Proc Natl Acad Sci U S A* 104: 6714–6719

Lim AK, Tao L & Kai T (2009) piRNAs mediate posttranscriptional retroelement silencing and localization to pi-bodies in the Drosophila germline. *J Cell Biol* 186: 333–342

Lin H & Spradling AC (1997) A novel group of pumilio mutations affects the asymmetric division of germline stem cells in the Drosophila ovary. *Dev Camb Engl* 124: 2463–2476

Liu L, Qi H, Wang J & Lin H (2011) PAPI, a novel TUDOR-domain protein, complexes with AGO3, ME31B and TRAL in the nuage to silence transposition. *Dev Camb Engl* 138: 1863–1873

Ma L, Buchold GM, Greenbaum MP, Roy A, Burns KH, Zhu H, Han DY, Harris RA, Coarfa C, Gunaratne PH, *et al* (2009) GASZ is essential for male meiosis and suppression of retrotransposon expression in the male germline. *PLoS Genet* 5: e1000635

Mahowald AP (1962) Fine structure of pole cells and polar granules in Drosophila melanogaster. *J Exp Zool* 151: 201–215

Mahowald AP (1968) Polar granules of Drosophila. II. Ultrastructural changes during early embryogenesis. *J Exp Zool* 167: 237–261

Mahowald AP (1971) Polar granules of Drosophila. III. The continuity of polar granules during the life cycle of Drosophila. *J Exp Zool* 176: 329–343

Malone CD, Brennecke J, Dus M, Stark A, McCombie WR, Sachidanandam R & Hannon GJ (2009) Specialized piRNA pathways act in germline and somatic tissues of the Drosophila ovary. *Cell* 137: 522–535

Malone CD & Hannon GJ (2009) Small RNAs as guardians of the genome. *Cell* 136: 656–668

Matsumoto N, Nishimasu H, Sakakibara K, Nishida KM, Hirano T, Ishitani R, Siomi H, Siomi MC & Nureki O (2016) Crystal Structure of Silkworm PIWI-Clade Argonaute Siwi Bound to piRNA. *Cell* 167: 484–497

Meikar O, Da Ros M, Liljenbäck H, Toppari J & Kotaja N (2010) Accumulation of piRNAs in the chromatoid bodies purified by a novel isolation protocol. *Exp Cell Res* 316: 1567–1575

Meikar O, Ros MD, Korhonen H & Kotaja N (2011) Chromatoid body and small RNAs in male germ cells. *Reproduction* 142: 195–209

Meikar O, Vagin VV, Chalmel F, Sõstar K, Lardenois A, Hammell M, Jin Y, Ros MD, Wasik KA, Toppari J, *et al* (2014) An atlas of chromatoid body components. *RNA* 20: 483–495

Minshall N, Kress M, Weil D & Standart N (2009) Role of p54 RNA Helicase Activity and Its C-terminal Domain in Translational Repression, P-body Localization and Assembly. *Mol Biol Cell* 20: 2464–2472

Mohn F, Handler D & Brennecke J (2015) piRNA-guided slicing specifies transcripts for Zucchini-dependent, phased piRNA biogenesis. *Science* 348: 812–817

Mohn F, Sienski G, Handler D & Brennecke J (2014) The rhino-deadlock-cutoff complex licenses noncanonical transcription of dual-strand piRNA clusters in Drosophila. *Cell* 157: 1364–1379

Molliex A, Temirov J, Lee J, Coughlin M, Kanagaraj AP, Kim HJ, Mittag T & Taylor JP (2015) Phase separation by low complexity domains promotes stress granule assembly and drives pathological fibrillization. *Cell* 163: 123–133

Murakami R, Sumiyoshi T, Negishi L & Siomi MC (2021) DEAD-box polypeptide 43 facilitates piRNA amplification by actively liberating RNA from Ago3-piRISC. *EMBO Rep* 22: e51313

Nagao I, Aoki Y, Tanaka M & Kinjo M (2008) Analysis of the molecular dynamics of medaka nuage proteins by fluorescence correlation spectroscopy and fluorescence recovery after photobleaching. *FEBS J* 275: 341–349

Nishida KM, Iwasaki YW, Murota Y, Nagao A, Mannen T, Kato Y, Siomi H & Siomi MC (2015) Respective Functions of Two Distinct Siwi Complexes Assembled during PIWI-Interacting RNA Biogenesis in Bombyx Germ Cells. *Cell Rep* 10: 193–203

Nishida KM, Okada TN, Kawamura T, Mituyama T, Kawamura Y, Inagaki S, Huang H, Chen D, Kodama T, Siomi H, *et al* (2009) Functional involvement of Tudor and dPRMT5 in the piRNA processing pathway in Drosophila germlines. *EMBO J* 28: 3820–3831

Nishida KM, Sakakibara K, Sumiyoshi T, Yamazaki H, Mannen T, Kawamura T, Kodama T & Siomi MC (2020) Siwi levels reversibly regulate secondary piRISC biogenesis by affecting Ago3 body morphology in Bombyx mori. *EMBO J* 39: e105130

Nishimasu H, Ishizu H, Saito K, Fukuhara S, Kamatani MK, Bonnefond L, Matsumoto N, Nishizawa T, Nakanaga K, Aoki J, *et al* (2012) Structure and function of Zucchini endoribonuclease in piRNA biogenesis. *Nature* 491: 284–287

Nishimura T, Nagamori I, Nakatani T, Izumi N, Tomari Y, Kuramochi-Miyagawa S & Nakano T (2018) PNLDC1, mouse pre-piRNA Trimmer, is required for meiotic and post-meiotic male germ cell development. *EMBO Rep* 19: e44957

Nott TJ, Petsalaki E, Farber P, Jervis D, Fussner E, Plochowietz A, Craggs TD, Bazett-Jones DP, Pawson T, Forman-Kay JD, *et al* (2015) Phase Transition of a Disordered Nuage Protein Generates Environmentally Responsive Membraneless Organelles. *Mol Cell* 57: 936–947

Nüsslein-Volhard C, Frohnhöfer HG & Lehmann R (1987) Determination of anteroposterior polarity in Drosophila. *Science* 238: 1675–1681

Olivieri D, Sykora MM, Sachidanandam R, Mechtler K & Brennecke J (2010) An in vivo RNAi assay identifies major genetic and cellular requirements for primary piRNA biogenesis in Drosophila. *EMBO J* 29: 3301–3317

Osanai-Futahashi M, Suetsugu Y, Mita K & Fujiwara H (2008) Genome-wide screening and characterization of transposable elements and their distribution analysis in the silkworm, Bombyx mori. *Insect Biochem Mol Biol* 38: 1046–1057

Ozata DM, Gainetdinov I, Zoch A, O'Carroll D & Zamore PD (2019) PIWI-interacting RNAs: small RNAs with big functions. *Nat Rev Genet* 20: 89–108

Padrón A, Iwasaki S & Ingolia NT (2019) Proximity RNA Labeling by APEX-Seq Reveals the Organization of Translation Initiation Complexes and Repressive RNA Granules. *Mol Cell* 75: 875-887.e5

Pane A, Jiang P, Zhao DY, Singh M & Schüpbach T (2011) The Cutoff protein regulates piRNA cluster expression and piRNA production in the Drosophila germline. *EMBO J* 30: 4601–4615

Pane A, Wehr K & Schüpbach T (2007) zucchini and squash Encode Two Putative Nucleases Required for rasiRNA Production in the Drosophila Germline. *Dev Cell* 12: 851–862

Patel SS, Belmont BJ, Sante JM & Rexach MF (2007) Natively unfolded nucleoporins gate protein diffusion across the nuclear pore complex. *Cell* 129: 83–96

Pertea G & Pertea M (2020) GFF Utilities: GffRead and GffCompare. *F1000Research* 9: 304

Peskett TR, Rau F, O'Driscoll J, Patani R, Lowe AR & Saibil HR (2018) A Liquid to Solid Phase Transition Underlying Pathological Huntingtin Exon1 Aggregation. *Mol Cell* 70: 588-601.e6

Rabinowitz M (1941) Studies on the cytology and early embryology of the egg of Drosophila melanogaster. *J Morphol* 69: 1–49

Reuter M, Chuma S, Tanaka T, Franz T, Stark A & Pillai RS (2009) Loss of the Mili-interacting Tudor domain-containing protein-1 activates transposons and alters the Mili-associated small RNA profile. *Nat Struct Mol Biol* 16: 639–646

Robine N, Lau N, Balla S, Jin Z, Okamura K, Kuramochi-Miyagawa S, Blower MD & Lai EC (2009) A broadly conserved pathway generates 3' UTR-directed primary piRNAs. *Curr Biol CB* 19: 2066–2076

Roux KJ, Kim DI, Raida M & Burke B (2012) A promiscuous biotin ligase fusion protein identifies proximal and interacting proteins in mammalian cells. *J Cell Biol* 196: 801–810

Saito K, Ishizu H, Komai M, Kotani H, Kawamura Y, Nishida KM, Siomi H & Siomi MC (2010) Roles for the Yb body components Armitage and Yb in primary piRNA biogenesis in Drosophila. *Genes Dev* 24: 2493–2498

Saito K, Nishida KM, Mori T, Kawamura Y, Miyoshi K, Nagami T, Siomi H & Siomi MC (2006) Specific association of Piwi with rasiRNAs derived from retrotransposon and heterochromatic regions in the Drosophila genome. *Genes Dev* 20: 2214–2222

Serman A, Le Roy F, Aigueperse C, Kress M, Dautry F & Weil D (2007) GW body disassembly triggered by siRNAs independently of their silencing activity. *Nucleic Acids Res* 35: 4715–4727

Sheth U, Pitt J, Dennis S & Priess JR (2010) Perinuclear P granules are the principal sites of mRNA export in adult C. elegans germ cells. *Development* 137: 1305–1314

Shiromoto Y, Kuramochi-Miyagawa S, Daiba A, Chuma S, Katanaya A, Katsumata A, Nishimura K, Ohtaka M, Nakanishi M, Nakamura T, *et al* (2013) GPAT2, a mitochondrial outer membrane protein, in piRNA biogenesis in germline stem cells. *RNA N Y N* 19: 803–810

Shoji M, Tanaka T, Hosokawa M, Reuter M, Stark A, Kato Y, Kondoh G, Okawa K, Chujo T, Suzuki T, *et al* (2009) The TDRD9-MIWI2 complex is essential for piRNA-mediated retrotransposon silencing in the mouse male germline. *Dev Cell* 17: 775–787

Siomi MC, Mannen T & Siomi H (2010) How does the Royal Family of Tudor rule the PIWI-interacting RNA pathway? *Genes Dev* 24: 636–646

Siomi MC, Sato K, Pezic D & Aravin AA (2011) PIWI-interacting small RNAs: the vanguard of genome defence. *Nat Rev Mol Cell Biol* 12: 246–258

Slotkin RK & Martienssen R (2007) Transposable elements and the epigenetic regulation of the genome. *Nat Rev Genet* 8: 272–285

Snee MJ & Macdonald PM (2004) Live imaging of nuage and polar granules: evidence against a precursor-product relationship and a novel role for Oskar in stabilization of polar granule components. *J Cell Sci* 117: 2109–2120

Snee MJ & Macdonald PM (2009) Dynamic organization and plasticity of sponge bodies. *Dev Dyn Off Publ Am Assoc Anat* 238: 918–930

Stoecklin G, Mayo T & Anderson P (2006) ARE-mRNA degradation requires the 5′–3′ decay pathway. *EMBO Rep* 7: 72–77

Szakmary A, Reedy M, Qi H & Lin H (2009) The Yb protein defines a novel organelle and regulates male germline stem cell self-renewal in Drosophila melanogaster. *J Cell Biol* 185: 613–627

Tanaka H, Fujita K, Sagisaka A, Tomimoto K, Imanishi S & Yamakawa M (2009) shRNA Expression Plasmids Generated by a Novel Method Efficiently Induce Gene-Specific Knockdown in a Silkworm Cell Line. *Mol Biotechnol* 41: 173–179

Tanaka T, Hosokawa M, Vagin VV, Reuter M, Hayashi E, Mochizuki AL, Kitamura K, Yamanaka H, Kondoh G, Okawa K, *et al* (2011) Tudor domain containing 7 (Tdrd7) is essential for dynamic ribonucleoprotein (RNP) remodeling of chromatoid bodies during spermatogenesis. *Proc Natl Acad Sci* 108: 10579–10584

Tang W, Tu S, Lee H-C, Weng Z & Mello CC (2016) The RNase PARN-1 Trims piRNA 3′ Ends to Promote Transcriptome Surveillance in C. elegans. *Cell* 164: 974–984

Tolia NH & Joshua-Tor L (2007) Slicer and the argonautes. *Nat Chem Biol* 3: 36–43

Tomari Y, Du T, Haley B, Schwarz DS, Bennett R, Cook HA, Koppetsch BS, Theurkauf WE & Zamore PD (2004) RISC Assembly Defects in the Drosophila RNAi Mutant armitage. *Cell* 116: 831–841

Vagin VV, Sigova A, Li C, Seitz H, Gvozdev V & Zamore PD (2006) A distinct small RNA pathway silences selfish genetic elements in the germline. *Science* 313: 320–324

Vagin VV, Wohlschlegel J, Qu J, Jonsson Z, Huang X, Chuma S, Girard A, Sachidanandam R, Hannon GJ & Aravin AA (2009) Proteomic analysis of murine Piwi proteins reveals a role

for arginine methylation in specifying interaction with Tudor family members. *Genes Dev* 23: 1749–1762

Voronina E, Seydoux G, Sassone-Corsi P & Nagamori I (2011) RNA Granules in Germ Cells. *Cold Spring Harb Perspect Biol* 3: a002774–a002774

Wang J, Saxe JP, Tanaka T, Chuma S & Lin H (2009) Mili interacts with tudor domain-containing protein 1 in regulating spermatogenesis. *Curr Biol CB* 19: 640–644

Wang JT, Smith J, Chen B-C, Schmidt H, Rasoloson D, Paix A, Lambrus BG, Calidas D, Betzig E & Seydoux G (2014) Regulation of RNA granule dynamics by phosphorylation of serine-rich, intrinsically disordered proteins in C. elegans. *eLife* 3: e04591

Wasik KA, Tam OH, Knott SR, Falciatori I, Hammell M, Vagin VV & Hannon GJ (2015) RNF17 blocks promiscuous activity of PIWI proteins in mouse testes. *Genes Dev* 29: 1403–1415

Watanabe T, Chuma S, Yamamoto Y, Kuramochi-Miyagawa S, Totoki Y, Toyoda A, Hoki Y, Fujiyama A, Shibata T, Sado T, *et al* (2011) MITOPLD is a mitochondrial protein essential for nuage formation and piRNA biogenesis in the mouse germline. *Dev Cell* 20: 364–375

Watanabe T, Takeda A, Tsukiyama T, Mise K, Okuno T, Sasaki H, Minami N & Imai H (2006) Identification and characterization of two novel classes of small RNAs in the mouse germline: retrotransposon-derived siRNAs in oocytes and germline small RNAs in testes. *Genes Dev* 20: 1732–1743

Webster A, Li S, Hur JK, Wachsmuth M, Bois JS, Perkins EM, Patel DJ & Aravin AA (2015) Aub and Ago3 Are Recruited to Nuage through Two Mechanisms to Form a Ping-Pong Complex Assembled by Krimper. *Mol Cell* 59: 564–575

Weick E-M & Miska EA (2014) piRNAs: from biogenesis to function. *Dev Camb Engl* 141: 3458–3471

Wenda JM, Homolka D, Yang Z, Spinelli P, Sachidanandam R, Pandey RR & Pillai RS (2017) Distinct Roles of RNA Helicases MVH and TDRD9 in PIWI Slicing-Triggered Mammalian piRNA Biogenesis and Function. *Dev Cell* 41: 623-637.e9

Williams RW & Rubin GM (2002) ARGONAUTE1 is required for efficient RNA interference in Drosophila embryos. *Proc Natl Acad Sci U S A* 99: 6889–6894

Wilsch-Bräuninger M, Schwarz H & Nüsslein-Volhard C (1997) A Sponge-like Structure Involved in the Association and Transport of Maternal Products during Drosophila Oogenesis. *J Cell Biol* 139: 817–829

Wilson JE, Connell JE & Macdonald PM (1996) aubergine enhances oskar translation in the Drosophila ovary. *Dev Camb Engl* 122: 1631–1639

Xiol J, Spinelli P, Laussmann MA, Homolka D, Yang Z, Cora E, Couté Y, Conn S, Kadlec J, Sachidanandam R, *et al* (2014) RNA clamping by Vasa assembles a piRNA amplifier complex on transposon transcripts. *Cell* 157: 1698–1711

Youn J-Y, Dunham WH, Hong SJ, Knight JDR, Bashkurov M, Chen GI, Bagci H, Rathod B, MacLeod G, Eng SWM, *et al* (2018) High-Density Proximity Mapping Reveals the Subcellular Organization of mRNA-Associated Granules and Bodies. *Mol Cell* 69: 517-532.e11

Zhang H, Elbaum-Garfinkle S, Langdon EM, Taylor N, Occhipinti P, Bridges AA, Brangwynne CP & Gladfelter AS (2015) RNA Controls PolyQ Protein Phase Transitions. *Mol Cell* 60: 220–230

Zhang Y, Guo R, Cui Y, Zhu Z, Zhang Y, Wu H, Zheng B, Yue Q, Bai S, Zeng W, *et al* (2017) An essential role for PNLDC1 in piRNA 3' end trimming and male fertility in mice. *Cell Res* 27: 1392–1396

Zhang Z, Koppetsch BS, Wang J, Tipping C, Weng Z, Theurkauf WE & Zamore PD (2014) Antisense piRNA amplification, but not piRNA production or nuage assembly, requires the Tudor-domain protein Qin. *EMBO J* 33: 536–539

Zhu L, Masaki Y, Tatsuke T, Li Z, Mon H, Xu J, Lee JM & Kusakabe T (2013) A MC motif in silkworm Argonaute 1 is indispensible for translation repression. *Insect Mol Biol* 22: 320–330